NATIONAL ADVISORY COMMITTEE FOR AERONAUTICS

TECHNICAL NOTE 2212

THE EFFECT OF ICE FORMATIONS ON PROPELLER PERFORMANCE

By Carr B. Neel, Jr., and Loren G. Bright

Ames Aeronautical Laboratory
Moffett Field, Calif.

Washington
October 1950

NATIONAL ADVISORY COMMITTEE FOR AERONAUTICS

TECHNICAL NOTE 2212

THE EFFECT OF ICE FORMATIONS ON PROPELLER PERFORMANCE

By Carr B. Neel, Jr., and Loren G. Bright

SUMMARY

Measurements of propeller efficiency loss due to ice formation are supplemented by an analysis to establish the magnitude of efficiency losses to be anticipated during flight in icing conditions. The measurements were made during flight in natural icing conditions; whereas the analysis consisted of an investigation of changes in blade-section aerodynamic characteristics caused by ice formation and the resulting propeller efficiency changes. Agreement in the order of magnitude of efficiency losses to be expected is obtained between measured and analytical results. The results indicate that, in general, efficiency losses can be expected to be less than 10 percent; whereas maximum losses, which will be encountered only rarely, may be as high as 15 or 20 percent. Reported losses larger than 15 or 20 percent, based on reductions in airplane performance, probably are due to ice accretions on other parts of the airplane.

Blade-element theory is used in the analytical treatment, and calculations are made to show the degree to which the aerodynamic characteristics of a blade section must be altered to produce various propeller efficiency losses. The effects of ice accretions on airfoil-section characteristics at subcritical speeds and their influence on drag-divergence Mach number are examined, and the attendant maximum efficiency losses are computed. The effect of kinetic heating on the radial extent of ice formation is considered, and its influence on required length of blade heating shoes is discussed. It is demonstrated how the efficiency loss resulting from an icing encounter is influenced by the decisions of the pilot in adjusting the engine and propeller controls.

INTRODUCTION

It has long been recognized that one of the hazards of flight in icing conditions is the formation of ice on propellers. The presence of ice on propeller blades causes a decrease in the operating efficiency of the propeller and a corresponding decrease in the airplane performance. There has been much disagreement as to the actual magnitude of efficiency

losses experienced in icing conditions. Measurements have been made of propeller efficiency losses with simulated ice formations (references 1 and 2) and in natural icing conditions (reference 3). The measured losses were low when compared with those generally expected; however, reports of very large apparent losses, deduced from decrease in airplane performance, persisted. A review of the available data (references 1, 2, and 3) indicated that further efficiency-loss measurements supplemented by an analysis of the problem would be required before conclusive statements could be made regarding the order of magnitude of losses to be anticipated in icing conditions. The objectives of the present investigation, therefore, were to provide additional measurements of propeller efficiency loss resulting from ice formation, and to analyze the problem of efficiency loss in an attempt to provide a means for applying, generally, the existing data. Thus, additional data to determine efficiency loss were obtained in flight under natural icing conditions as part of a comprehensive investigation of aircraft icing by the NACA. Another phase of the program (reported in reference 4) was the investigation of the meteorological factors conducive to icing, therefore providing quantitative data on the severity of the icing conditions under which propeller-performance measurements were made.

The research was conducted by the Ames Aeronautical Laboratory. Data were obtained over most of the United States during the winters of 1946-47 and 1947-48. Measurements made during the winter of 1946-47 are included in reference 3. The results of the 1947-48 winter season are presented in this report.

Appreciation is extended to United Air Lines, Inc., the United States Weather Bureau, and the Air Materiel Command of the U. S. Air Force for aid and cooperation in the research.

DESCRIPTION OF EQUIPMENT

The flight tests were conducted with the twin-engine airplane shown in figure 1. Modifications had been made to provide thermal ice-prevention equipment for the wings, tail, and windshield. A description of the thermal system is given in reference 5. The right engine and propeller were utilized for the purposes of the research, and standard commercial electrically heated blade shoes were installed on the left propeller for ice protection.

The test propeller consisted of four blades composed of double-camber Clark Y sections. The diameter was 13.5 feet. Characteristics of the blade design as supplied by the manufacturer are given in figure 2. The symbols used in this figure and throughout the report are listed and defined in Appendix A. Specially built blade heating shoes, constructed at the Ames Laboratory, were installed for propeller heating tests, which were made in conjunction with the performance tests. The shoes consisted of several wrappings of cloth tape in which the heater elements were

embedded. Two-inch-wide strips of metal were cemented over the wrappings along the leading edges of the blades in order to protect the shoes from abrasion. An enlarged spinner, built for the purpose of housing instrumentation related to the heating studies, was mounted on the test propeller. Figure 3 shows the test propeller complete with heating shoes and spinner. White marking lines were painted on the blades for ease in noting ice locations.

A thrustmeter and a torquemeter were installed in the right engine for measuring thrust and torque absorbed by the test propeller. Both the thrustmeter and the torquemeter utilized pistons which were hydraulically restrained so that the pressure required to maintain the pistons in a floating condition gave a measure of thrust or torque being absorbed by the propeller. Pressure gages connected to the hydraulic lines provided means for observing and recording the values of thrust and torque. A calibration of the thrustmeter had been made at the engine factory where the thrustmeter was installed. The calibration was made on a thrust dynamometer rig and gave results to an accuracy of ±1 percent through a wide range of propeller thrusts encompassing the normal operating range. The torquemeter was the standard torquemeter supplied with the engine. No special calibration of the torquemeter was made for the purpose of these tests. Since it was not feasible to calibrate the torquemeter or to recalibrate the thrustmeter periodically during the tests, it was decided that occasional checks of the repeatability of the thrustmeter and the torquemeter would serve as a satisfactory indication of their reliability. Consequently, periodic measurements were made of the efficiency of the test propeller in clear air. This provided a check of the repeatability of both the thrustmeter and the torquemeter. The tests gave results of propeller efficiency which repeated within ±2 percent. Thus, although no check of the absolute values of thrust and torque was made, it is believed the measurements of propeller efficiency change are accurate to within ±4 percent of propeller efficiency.

Equipment was developed to enable photographing the test propeller blades while rotating so that pictures could be taken during flight in icing conditions without resort to feathering. The equipment consisted of two cameras synchronized to high-speed flash lamps and to the propeller. One camera was mounted to photograph the camber face and one to photograph the thrust face of the propeller blades. Figure 4 shows one of the cameras installed. Each camera contained two shutters, one leaf type and one rotary-disk type. The purpose of the shutters was to provide a means for eliminating as much of the background light as possible while the flash lamp illuminated the propeller. The disk shutter was mounted on a 1/4-horsepower electric motor which revolved continuously during the photographing procedure. The shutters were arranged such that the leaf shutter opened and allowed the aperture in the disk to pass once before closing again. During the time that the disk aperture was in front of the camera lens, the flash lamp was discharged. The duration of exposure was governed by the flash lamp, which gave an effective exposure time of about 1/10,000 second. Two flash lamps were used, one mounted beside

each camera, as shown in figure 5. The camera shutters, flash lamps, and propeller were synchronized so that pictures could be taken of any one selected blade with either or both cameras. Complete pictures of the propeller, consisting of both sides of all four blades, could be obtained in about 1/2 minute.

A resistance-type pickup was used to indicate the propeller blade angle. Calibrations showed the blade-angle indicator to be accurate within $\pm 0.2^{\circ}$.

A yaw and pitch recorder was used to record the airplane flight attitude. The yaw and pitch recorder utilized a hemispherical differential-pressure-type head, as illustrated in figure 6. An electrical heater was installed inside the head to prevent the formation of ice which might alter the calibration. The accuracy of this instrument was $\pm 1/2^{\circ}$.

The meteorological instruments used to measure the liquid-water content, drop size, and free-air temperature of the icing clouds are described in detail in references 4, 6, and 7. Briefly, the instruments consisted of the following: Rotating cylinders were used to obtain short-interval averages of water content and drop size. Continuous records of water content were secured by means of a rotating-disk icing-rate meter. Free-air temperature was measured with a shielded thermometer consisting of a thermocouple connected to a millivoltmeter.

TEST PROCEDURE

Flight tests were made in clear air to obtain the datum performance of the test propeller, and in natural icing conditions to obtain changes in performance incurred through the formation of ice. The regions of operation in natural icing conditions covered most of the northwestern, and part of the middlewestern, Great Plains, and eastern areas of the United States. Locations of the various icing encounters are listed in table I of reference 4.

During flight in icing conditions the test procedure was to collect a layer of ice on the propeller blades, and at the same time measure the liquid-water content, drop size, and free-air temperature of the icing clouds. Heat was applied to the wings, tail, windshield, and left propeller to keep those components free of ice. The test propeller was maintained in automatic pitch (constant speed) throughout the ice-build-up period. At the end of the period of ice build-up, the airplane generally was climbed above the cloud layer.

Photographs were taken of the propeller blades while measurements were made of airspeed, altitude, and attitude of the airplane; and blade angle, rotational speed, thrust, and torque of the test propeller. The purpose of making the measurements above the cloud layer was to obtain

stable air conditions, which were more conducive to steady readings than the turbulent conditions often existing in icing clouds. During each set of measurements the propeller blades were locked at one blade angle, and all flight conditions were maintained as constant as possible for a time sufficiently long to allow all instruments to indicate stabilized values. Due to the viscosity of the hydraulic oil, the pressure gages indicating thrust and torque took the longest time of any of the instruments to reach equilibrium, especially during flight at low temperatures. When time and other circumstances permitted, readings were taken over a range of advance ratio; then the blade angle was changed to a new position, locked, and another set of measurements obtained. In this manner, an effort was made to obtain data through a range of propeller operating conditions, but frequently the ice accretions would not remain on the blades for the lengthy period required for such measurements. Performance data were secured at three blade angles, 21°, 26°, and 31°, approximately, which covered the normal operating range of cruise and climb conditions for the test airplane.

RESULTS

A tabulation of the meteorological, flight, and propeller operating conditions under which propeller ice accretions were obtained is presented in table I. Also included is a summary of the losses in propeller efficiency obtained from each icing encounter. This column gives the loss in peak efficiency for cases where sufficient measurements were made to define the efficiency curve. The value was taken as the difference between the two curve peaks for the iced and the clean propeller. Where only point values of efficiency were obtained, the loss at the particular operating condition is given. All tabulations of conditions given in table I, with the exception of propeller blade angle, are those which prevailed during the time of accumulation of ice on the propeller. The values of blade angle are those maintained during the recording of performance data, after leaving the icing conditions.

As will be noted in table I, small variations from the desired blade-angle settings of 21°, 26°, and 31° occurred due to inability to set the pitch exactly. In all cases, measurements of propeller efficiency were made at only one or two blade angles for any one particular ice formation.

All values of liquid-water content, except for encounters 6, 8, and 10, were measured with the rotating-disk icing-rate meter described in reference 4. The value of water content given for encounter 6 is the average of three measurements taken with the rotating cylinders during the period of ice build-up on the propeller. The value for encounter 8 is a single measurement obtained with the rotating cylinders during the ice build-up period; whereas that for encounter 10 is the average of four points obtained with the cylinders during ice build-up.

As indicated in table I, the test propeller was unheated except during two encounters. Cyclic heating was applied to the forward 10 percent of the blades during the ice build-up period of encounters 10 and 11. As a consequence of insufficient heat and inadequate chordwise coverage, "runback" formations collected aft of the heated areas, along with primary ice accumulations, but no measurable efficiency loss resulted.

The various ice formations were grouped into different classes, depending on the thickness and radial extent of the formation. The classification is based on a study of the photographs taken of the formations and is outlined in table II. Such a classification was established on the assumption that ice formations of equal thickness and extent would cause about the same performance change. No account was taken of the shape of formation since the photographs were not of such a character as to reveal this feature. Grouping by the size of formation alone, however, proved to be justified, inasmuch as formations in the same class were found to cause approximately equal performance losses. Notation of the class of ice formation is made in table I and on all the propeller efficiency curves.

To establish the datum performance of the propeller with clean blades (no ice formations), clear-air data were secured at the three blade angles. The thrust- and power-coefficient curves are shown in figure 7, and the resulting efficiency curves are given in figure 8. Comparisons of the thrust- and power-coefficient curves for the propeller with the blades clean and with the blades iced under the conditions of table I are presented in figures 9(a) to 9(e). Point values of thrust and power coefficient for the iced propeller are listed in table III for cases where insufficient measurements were made to define curves.

Curves of efficiency as a function of advance ratio for the propeller with ice accumulations are compared with efficiency curves for the clean propeller in figures 10 to 16. These curves were drawn employing values of thrust and power coefficients from table III and from the curves of figure 9 by using the formula

$$\eta = \frac{C_T}{C_P} J \qquad (1)$$

where

η propeller efficiency

C_T thrust coefficient

C_P power coefficient

J advance ratio

Figure 10 presents the variation of efficiency loss for one type of formation at two blade angles, and figure 11 shows the efficiency-loss variation for another class of formation at approximately the same blade angles. A comparison of efficiency losses for two classes of formation for the same blade angle is given in figure 12, while figure 13 compares losses for five formations at a higher blade angle, and figure 14 compares losses for two formations at a still higher blade angle. Figure 15 gives the efficiency loss for a low-temperature condition in which the ice extended nearly to the blade tips. Figure 16 presents a plot of efficiency data for formations which accumulated during two encounters with propeller-blade heating. Heat was applied cyclically to the forward 10 percent of the blade chord and, as was mentioned previously, primary ice formations, together with small amounts of runback, gathered back of the heated regions.

It should be noted that, in figures 11, 13, and 16, singular values of efficiency are shown for the propeller in the iced condition, which are slightly higher than those for the clean blade. In all cases, this error is less than ±4-percent efficiency, which has been noted as the maximum experimental error of the efficiency measurements.

Records of yaw and pitch of the airplane showed that variations of 2° in yaw and 1° in pitch from the clear-air conditions under which the datum performance curves were obtained occurred during the measurements of efficiency with the iced propeller. Wind-tunnel tests of the effects of yaw and pitch variations on propeller efficiency (references 8 and 9) showed that, for a propeller operating in front of a wing, changes in efficiency of only 1 percent resulted from yaw variations up to 5°, or from pitch variations up to 1°. Therefore, it is concluded that efficiency variations resulting from deviations in yaw and pitch from the clear-air datum conditions did not exceed 1 percent.

Photographs of the clean propeller blades with heating shoes installed are shown in figure 17. These show the leading-edge metallic abrasion strips installed on the blades and the white-line markings painted on the shoes to provide a means for identifying the particular blade photographed and the extent of ice formations. It will be noted that, in some of the pictures of the thrust face of the blades, the leading-edge abrasion strips unfortunately give the appearance of ice formations and, therefore, should not be confused with the actual formations. Pictures of the ice accretions for which efficiency data were obtained are presented in figures 18 to 31. All the pictures shown in figures 17 to 30 were taken with the photographic equipment previously described and with the propeller rotating. Figure 31 was obtained with a conventional camera and with the propeller feathered. In all cases in which pictures were taken with the special equipment, attempts were made to secure photographs of both sides of all four blades, but in many instances the equipment failed to function properly and only parts of the photographs were usable.

DISCUSSION

In order to generalize the test results that have been presented, with the view in mind of making possible a reasonably accurate evaluation of propeller efficiency losses likely to be experienced under various icing and operating conditions, the discussion that follows deals with (a) a consideration of those factors that influence propeller efficiency and their relative importance under icing conditions, (b) the changes that ice formations can make in these factors with consideration of the changes in efficiency that may be expected to result, and (c) the influence of operating conditions on propeller efficiency losses in icing conditions.

Factors Influencing Propeller Efficiency

The factors which affect the efficiency of a propeller may be seen from the following formula, which is based on blade-element theory:

$$\eta_e = \frac{\tan \varphi}{\tan (\varphi+\gamma)} \tag{2}$$

where

η_e efficiency of blade element

φ angle of advance of blade element $\left(\tan^{-1} \frac{V}{\pi n D x} \right)$

γ angle, the tangent of which is the blade-element drag-lift ratio $\left(\tan^{-1} \frac{D_o}{L} \right)$

An examination of equation (2) shows that, for any given operating condition (φ = constant), the efficiency is dependent on the blade-element drag-lift ratio. The primary effect of ice accretions on the aerodynamic characteristics of a propeller is to increase the blade-element drag-lift ratio.

Effect of radial distribution of ice accretions.- The change in radial distribution of thrust and torque for a propeller with a full-span ice formation is shown qualitatively in figure 32. The effects of a uniform increase in the blade-element drag-lift ratio are illustrated in

this figure. It is evident that the radial location of ice accumulations has a significant bearing on the over-all efficiency loss since the radial loading of thrust and torque is not uniform and the major portion of the loading is developed by the outer regions of the blades. An indication of the importance of radial location of ice accretions can be obtained from data of the present tests. A study of table I shows that the largest loss (10 percent, encounter 1) was created by a small formation which extended approximately 75 percent of the blade radius; whereas a much larger, but shorter, formation extending about 55 percent of the distance along the blade caused only 4-percent loss at the same blade angle (encounter 3). Thus it is evident that, when formations are limited to small radial extent, large accretions with correspondingly large changes in aerodynamic characteristics are necessary to cause large efficiency losses. An important factor influencing the radial extent to which ice will form on a propeller blade is the kinetic heating of the air passing over the blade. This effect of kinetic heating is discussed in Appendix B.

Effect of changes in blade-element drag-lift ratio on propeller efficiency.- In order to obtain a quantitative indication of the effect of changes in the drag-lift ratio (represented in the symbol γ in equation (2)) on propeller efficiency, calculations were made for two hypothetical propellers for which the value of the over-all drag-lift ratio was adjusted to produce efficiency losses of 5, 10, 15, and 20 percent. The blade-angle distribution shown in figure 2 was taken for both propellers. The two propellers consisted of conventional sections. The changes in drag-lift ratio for the entire blade span necessary to induce the assumed efficiency losses of 5, 10, 15, and 20 percent are shown in figure 33 as a function of advance ratio for the two propellers operating at various blade angles. The envelope values of increment in drag-lift ratio as a function of advance ratio are shown in figure 33 for each of the assumed efficiency losses. It will be noted that the envelope values tend to decrease somewhat with increasing advance ratio. Up to advance ratios of about 2, the decreases in the envelope values are not great and the changes in drag-lift ratio required to produce the various efficiency losses are relatively constant. A plot of increase in drag-lift ratio for decrease in efficiency was made for both propellers by taking the average of the values of the envelope curves between advance ratios of 1 and 2. These data are presented in figure 34. Propellers composed of NACA 16-series sections should exhibit about the same relation of change in drag-lift ratio to change in efficiency as shown in figure 34.

The data of figure 34 apply to cases of advance ratio up to about 2. For advance ratios much above this value, the data of figure 34 would no longer hold, due to the slope of the envelope curves shown in figure 33. Since the normal operating range of advance ratio for typical present-day transports is up to about 2, the remainder of this discussion will be limited to cases of advance ratio of 2 or less.

Effect of Ice Accretions on Airfoil-Section Characteristics and Attendant Efficiency Losses

The following discussion will be divided into two parts covering (1) blade-element drag-lift ratio in the incompressible-flow regime, and (2) blade-element drag-lift ratio in the compressible-flow regime.

Blade-element drag-lift ratio in incompressible flow.- Three investigations have been conducted which contain information bearing on this subject. In reference 10, the effects of a mild simulated ice formation on the lift and drag of an NACA 0012 airfoil were studied. In this investigation, it was shown that the major change in section characteristics arose from an increase in drag and only a relatively small change came from decrease in lift. Although the accretion did not appear to be severe, the maximum increase in drag-lift ratio was about 100 percent, corresponding to a propeller efficiency loss of 8 percent. (See fig. 34.)

A second study, reported in reference 2, consisted of tests of a severe simulated ice formation on a propeller with blades composed of Clark Y sections. The accretion extended about to the blade tips and was very irregular, even more so for the outer portion of the blades than any formation observed during the flight investigations in natural icing conditions conducted by the Ames Laboratory. The formation is believed to be at least as severe, insofar as deleterious effects on performance are concerned, as any which would occur under natural conditions. In reference 2, the basic data from the tests were reduced to mean lift- and drag-coefficient curves. These curves show the change in mean section lift and drag coefficient for the whole propeller and, from the standpoint of computing maximum propeller efficiency losses, are believed to represent the best data of this type available. The curves show a maximum increase in drag-lift ratio of about 200 percent at a normal operating lift coefficient (0.6), due to the presence of the simulated ice. Approximately 14-percent loss in peak efficiency was measured.

The third investigation consisted of the determination of the effect of protuberances on the aerodynamic properties of an NACA 0012 airfoil (reference 11). The results of these tests, when applied to the case of a propeller, indicate that only very improbable locations of ice formations of the shape tested could cause increases in drag-lift ratio greater than about 150 percent.

The results of these three tests indicate that, for propellers operating at relatively low speeds with no effects of compressibility, the maximum increase in blade-element drag-lift ratio possible in icing conditions is about 200 percent. This means, taking figure 34 and the measured loss of reference 2 as a basis, the maximum efficiency loss to be expected at low speeds is about 15 percent.

The largest measurements of efficiency loss of reference 3 are not in agreement with the conclusion of a maximum loss of 15 percent. A discussion of these measurements is given in Appendix C.

Blade-element drag-lift ratio in compressible flow.- The only known high-speed data pertaining to the influence on section properties of alterations to an airfoil in the leading-edge region are given in reference 12. In this study, the effects of skin wrinkles on the aerodynamic characteristics of two NACA airfoils were investigated up to a free-stream Mach number of 0.73. A low-drag and a conventional section were studied. The results showed that only small changes in lift resulted within the speed range tested. However, reductions of the order of 0.05 in drag-divergence Mach number were measured with both airfoils for the most adverse cases. In addition, the normal drag increases associated with surface irregularities prevailed over the entire speed range. From this information, it appears that alterations in the leading-edge contour of a propeller blade, of the nature that could be expected from accumulations of ice, could reduce the blade-element drag-divergence Mach number, thereby reducing the speed range for efficient operation for propellers composed either of low-drag (16-series) or conventional sections.

An illustration of the variation of drag coefficient with Mach number such as might be expected from ice accumulations, using the skin-wrinkle data as a basis, is given in figure 35; this curve is compared with a similar curve for a clean blade. It is apparent from these data that reductions in propeller performance, in addition to the performance losses arising from low-speed drag increases, are possible for propellers with a portion of the blades operating in the speed range of drag divergence. The amount of additional efficiency loss resulting from this cause will be a function of the length of blade affected, which is dependent on the magnitude of reduction of drag-divergence Mach number and the propeller advance ratio. Obviously, the greater the reduction in drag-divergence Mach number, the larger will be the length of blade affected.

In order to obtain an indication of the possible magnitude of these increased losses, comparative calculations were made of the effects of a severe ice formation on the performance of a propeller operating at high speed assuming both a decrease and no change in drag-divergence Mach number. Operating conditions were chosen to be representative of a typical four-engine transport airplane. The advance ratio was about 2, and it was established that the blade tips were operating just at the drag-divergence Mach number for clean blades. A decrease of 0.05 in the drag-divergence Mach number below that for the clean-blade case was selected for the iced condition. The results of the calculations showed that the additional decrease in efficiency due to adverse compressibility effects would be less than 1 percent.

Since the tests of reference 12 on the effects of skin wrinkles were taken as the basis for the assumed decreases in drag-divergence Mach number in the calculations, the above results may not be

representative of the conditions prevailing for actual ice accretions. It is conceivable that larger reductions in drag-divergence Mach number may arise from the presence of ice than measured for the skin wrinkles, but, considering the above results, it is not likely that efficiency losses resulting from such causes would be greater than 5 percent. Therefore, it appears that for propellers operating under the most adverse conditions at advance ratios up to 2, with the most severe full-span ice accretions possible, efficiency losses would not exceed 20 percent.

Normally expected efficiency losses.- In the previous sections, it was concluded that the maximum efficiency loss to be expected at low speeds is about 15 percent and, for propellers operating in the critical speed range, the maximum loss would not exceed 20 percent. For the majority of cases of propeller icing, the losses would be less than these values since they are representative of extreme conditions in which the entire length of blade is adversely affected; whereas, in a large number of instances, ice forms on only part of the blade and usually in a much less detrimental configuration. This is in general agreement with the measured values given in table I, which displays relatively low losses, with a maximum value of 10 percent. Also, a review of the measurements made during the flights of reference 3 showed that, for about 90 percent of the icing encounters, efficiency losses were less than 10 percent. Thus it appears that, in the vast majority of instances of propeller icing, efficiency losses can be expected to be less than 10 percent.

Mention was made previously that large efficiency losses have been reported, based on decreases in airplane performance. In some cases these reported losses have been as high as 30 percent. Such large values are in conflict with both calculated and measured losses, and it is believed that accumulations of ice on other components of the airplanes caused serious increases in drag with corresponding decreases in airspeed, which were falsely attributed to propeller icing. Measurements reported in reference 3 showed that increases in airplane parasite drag of as much as 80 percent are possible when all components, with the exception of the propellers, have accumulated ice.

Influence of Operating Conditions on Propeller Efficiency Losses in Icing Conditions

When a propeller accumulates ice, the resulting changes in propeller performance are reflected in corresponding changes in airplane performance. Depending on how the pilot reacts to the changes, various operating conditions can be established which may have an increased detrimental effect on the propeller performance. This aspect of propeller icing can best be explained by reference to a plot of efficiency as a function of advance ratio (fig. 36). In this figure, curve A represents the envelope-efficiency curve of a clean propeller; whereas curve B represents the

equivalent curve for a case where ice accretions would cause an efficiency loss of a fixed amount. The fact that the two curves would be approximately parallel is substantiated by the data of reference 1. If an airplane operating at point C on curve A encounters icing and the pilot does not adjust his controls, the airspeed will decrease and the airplane will operate at some point such as D, assuming the propeller has a constant revolution-per-minute pitch control. Upon noting this loss of airspeed, the pilot may take two courses of action. He may try to return to a point near the peak of the envelope, such as point E, by adjusting engine speed and power. If the airframe has accumulated ice, resulting in higher airplane drag, this would probably call for a reduction in propeller speed and an increase in engine power. The pilot may try to shed some of the ice on the propeller by increasing propeller speed. The combined action of centrifugal force and kinetic heating (see Appendix B) resulting from an increase in propeller rotational speed is often effective in reducing the extent of the ice accumulation. If he is unsuccessful in this respect, the propeller will continue to operate on curve B at some point such as F. He has thus lost additional efficiency with respect to the possibility of operating at E, shown as $\Delta\eta$ in figure 36, due to the curvature of the envelope curves. On the other hand, if some of the ice is removed, he would operate at some point G, which approaches curve A as a limit. Then, by resuming the initial engine operating conditions, it may be possible to operate at or near the original point C. It should be noted that the foregoing discussion applies to an unprotected or an inadequately protected propeller. If the entire airplane is properly protected, there will be no need for corrective action by the pilot since the propeller will continue to operate near point C.

Thus it appears that in operation of unprotected or inadequately protected propellers in icing conditions, periodic attempts should be made to throw off the accretions by increasing propeller speed. If the ice cannot be removed, it is desirable to operate at or near the peak of the efficiency-envelope curve for the iced propeller. This peak is probably located at about the same value of advance ratio as the peak for clean blades.

CONCLUSIONS

As the result of measurements of propeller performance loss due to ice formation, made during flight in natural icing conditions and supplemented by an analysis of the factors contributing to performance loss (in which all values apply for propeller advance ratios up to about 2), the following conclusions are reached:

1. During the vast majority of icing encounters with unprotected propellers on present-day transports, propeller efficiency losses can be expected to be less than 10 percent.

2. The maximum loss to be anticipated for propellers free of adverse compressibility effects is about 15 percent; whereas, for propellers operating above the critical speed, the maximum loss to be expected is about 20 percent.

3. Reported propeller efficiency losses larger than about 15 or 20 percent, based on reductions in airplane performance, probably are actually due to icing of other components.

4. The magnitude of efficiency loss resulting from an icing encounter can be influenced by the decisions of the pilot in adjusting the engine and propeller controls.

Ames Aeronautical Laboratory,
National Advisory Committee for Aeronautics,
Moffett Field, Calif., June 15, 1950.

APPENDIX A

SYMBOLS

b chord of blade element, feet

c_p specific heat of air at constant pressure, Btu per pound

C_D blade-element drag coefficient

C_L blade-element lift coefficient

C_P power coefficient $\left(\frac{P}{\rho n^3 D^5}\right)$

C_Q torque coefficient $\left(\frac{Q}{\rho n^2 D^5}\right)$

C_T thrust coefficient $\left(\frac{T}{\rho n^2 D^4}\right)$

D propeller diameter, feet

D_o drag of blade element, pounds

g acceleration of gravity, equal to 32.2 feet per second, second

h blade section maximum thickness, feet

j mechanical equivalent of heat, equal to 778 foot-pounds per Btu

J propeller advance ratio $\left(\frac{V}{nD}\right)$

L lift of blade element, pounds

M free-stream Mach number

n propeller rotational speed, revolutions per second

P input power to propeller, foot-pounds per second

Q torque of propeller, foot-pounds

r radius to blade element, feet

R propeller tip radius, feet

t temperature, $^{\circ}F$

T thrust of propeller, pounds

U speed of free stream with respect to propeller-blade section, feet per second

V airplane true airspeed, feet per second

x fraction of tip radius $\left(\frac{r}{R}\right)$

β blade angle, degrees

β_o blade angle at 0.75 radius station, degrees

γ angle between lift force and resultant force $\left(\tan^{-1}\frac{D_o}{L}\right)$, degrees

η propeller efficiency $\left(\frac{C_T}{C_P}\right) J$

η_e efficiency of blade element $\left[\frac{\tan\varphi}{\tan(\varphi+\gamma)}\right]$

ρ mass density of air, slugs per cubic foot

φ angle of advance of propeller-blade element at radius x $\left(\tan^{-1}\frac{V}{\pi nDx}\right)$, degrees

APPENDIX B

CONSIDERATIONS OF THE RELATION OF KINETIC HEATING TO PROPELLER ICING

Kinetic-Temperature Rise Experienced by a Propeller During Flight in Icing Conditions

In clear air the temperature rise at the stagnation point of a blade section is given by

$$\Delta t = \frac{U^2}{2gjc_p} \tag{3}$$

This equation, which is derived from a balance of the thermal and mechanical energies involved, defines the air-temperature rise, and, provided there is no thermal conduction in the propeller blade, the surface temperature also will experience the same increase. If, as is true in the practical case, there is conduction in the blade, the surface temperature rise will be less than that given by equation (3) by an amount dependent on the equivalent conductivity of the blade, its shape, and other factors.

In a cloud composed of water drops, the kinetic-temperature rise of the blade surface is reduced due to cooling by evaporation of the drops impinging on the surface. Equations for computing the kinetic-temperature increase with evaporation prevalent are presented in reference 13. One difficulty involved in the solution of the equations of reference 13 is that they must be solved by trial, a laborious procedure. The stagnation-temperature rise in a cloud may be obtained with considerably less effort by using a pseudo-adiabatic diagram, such as shown in figure 37. The resulting value will be the same as that obtained using the method of reference 13. The procedure for computing this temperature rise is outlined in figure 37 as follows:

Establish point A at the pressure altitude and ambient-air temperature for which the calculation is to be made. Calculate Δt_{dry} using equation (3), add this value to the air temperature, and follow down a dry adiabatic line to the temperature line obtained from the resulting sum (point B). This establishes the pressure in terms of altitude at the stagnation point. Point C is then determined by the intersection of the stagnation-pressure line and the line drawn through point A parallel to the pseudo-adiabatic lines, and this point is the wet stagnation temperature. It will be noted that the wet kinetic-temperature rise is considerably less than that obtained in dry air.

There are two limitations to the above method for computing stagnation-temperature rise in wet air. First, no account is taken of the heat removed from the stagnation region by water not evaporated which flows aft during flight in clouds of high water content. This factor likewise is not considered in the analysis of reference 13. The second limitation is that heat conduction in the blade is neglected. There is no simple way of including this factor in the calculations. A fairly complete analysis and discussion of this aspect of kinetic heating is included in reference 13. In reference 13, comparisons are made between the effects of kinetic heating on a perfectly conducting blade and a completely nonconducting blade in a cloud. Only conduction in a chordwise direction is considered. It is shown that the effect of conduction is to reduce the stagnation temperature from that for a nonconducting blade.

In order to obtain a comparison of kinetic-temperature rise calculated by the above methods with temperature rises prevailing during actual flight in icing conditions, values obtained during the present tests were plotted in figure 38, together with curves computed using equation (3) and a pseudo-adiabatic diagram. The atmospheric conditions assumed for the curve computed using the pseudo-adiabatic diagram are 12,000 feet pressure altitude and 5° F free-air temperature, which are the average of the conditions for the flight values of kinetic-temperature rise. The values obtained during the tests were computed using propeller photographs from icing encounters in which the radial extent of the ice formations apparently was limited by kinetic heating and in which there was no obvious breakoff. By assuming that the end of the formation was at freezing temperature and noting the radial extent from the photographs, it was possible to plot the kinetic-temperature rise above ambient as a function of the section velocity at the end of the formation. For further comparison, experimental data from reference 14, which were acquired in a manner similar to that employed for the above points, also were plotted in this figure.

In the case of the values obtained during the present investigation, it was noted that the points displayed considerable scatter. A study of the data revealed that the points fell into three groups, depending on the atmospheric conditions prevailing at the time the photographs were taken which established the radial extent of the ice formations. The grouping is given in the following table and the data points of figure 38 were correspondingly divided:

Group	Atmospheric condition existing at time of photograph
1	Continuous icing
2	Icing clouds of very low liquid-water content or broken clouds with patches of clear air between
3	Clear air or snow

Group 1 covers the points for the condition in which sufficient liquid water would be present to insure continuous evaporation at the blade leading edge. The points encompassed by group 3 should exhibit close to the full kinetic-temperature rise for clear air in the absence of evaporative cooling from water on the surface. In group 2, periodic exposure of the blade to water clouds, then to clear air, or exposure to very small amounts of water, would cause a smaller degree of evaporation than created under the conditions of group 1. Thus, the points of group 2 would be expected to fall between the points of groups 1 and 3. Such actually proved to be the case. In figure 38, the points falling in group 1 established a fairly well-defined curve, those in group 3 were distributed around the curve determined by equation (3), and the points in group 2 lay in between the two curves. With one exception, the data points from reference 14 followed the same general pattern, covering the same range as the other points. The nonconforming point obtained at a blade-section velocity of 500 miles per hour is believed to be in error.

It will be noted that the curve for continuous icing (group 1) is below that established by the pseudo-adiabatic diagram. This could be due to a combination of two causes. First, some of the kinetic heat developed may have been removed by water flowing back from the leading-edge region. Second, thermal conduction in the blade would tend to lower the experimental values. Neither of these factors is considered in the procedure for determining the calculated curve. If conduction were the predominant cause of the lower experimental values, this effect also would be prevalent for the clear-air points (group 3), but such is not the case. The material used in the construction of the test heating shoes appears to have provided fairly good insulation. It is concluded, therefore, that removal of heat from the leading-edge region by water flowing aft can have considerable effect in reducing the kinetic-temperature rise of a propeller blade in icing conditions.

Beneficial Effect of Kinetic Heating in Preventing Premature Compressibility Effects

With the outer portion of a propeller operating at high velocity, it is possible that the deleterious action of ice accretions in reducing the blade-section drag-divergence Mach number would be prevented through the beneficial effects of kinetic heating. Thus, if ice is prevented from forming on the blades in the critical regions, no adverse results from this cause can occur. The extent to which the beneficial effects will be manifested is a function of the propeller speed and the free-air temperature. A plot of the air temperature down to which protection from kinetic heating will be obtained as a function of the blade-section Mach number is given in figure 39. Values of kinetic-temperature rise from the continuous-icing curve (group 1) of figure 38 were used in the construction of figure 39.

The data of figure 39 may be used to determine the ambient temperature above which adverse compressibility effects due to the presence of ice will be prevented by kinetic heating. If a drag-divergence Mach number of 0.75 is assumed (typical of the outer sections of present-day propellers), kinetic heating will prevent compressibility effects resulting from ice accretions down to an ambient temperature of about 2° F.

Length of Blade Heating Shoes as Influenced by Kinetic Heating

In most cases at the present time, propeller ice protection is obtained through the use of rubber heating shoes cemented to the external surface along the blade leading edges. The shoes are subject to erosion by the abrasive action of foreign matter in the air. This is especially true for the outer regions of the blade where velocities are high. The problem is so critical from a maintenance standpoint that most airline operators have resorted to using relatively short heating shoes to keep abrasion at a practical minimum. A typical extent of shoe currently in use on a 13-foot-diameter propeller is to the 60-percent-radius station. For such a propeller operating at 1000 rpm and 300 miles-per-hour true airspeed, complete protection could be anticipated down to free-air temperatures of about 15° F, due to the combined action of the heating shoes and kinetic heating. Below this temperature ice could form on the blades in the region limited on the inner end by the blade shoes and on the outer end by kinetic heating. At very low temperatures, of course, the ice would extend from the outer end of the blade shoes clear to the tips. Under these circumstances, it can be shown, using blade-element theory, that, with an ice formation over the unprotected portion of the blade of sufficient severity to cause an over-all efficiency loss of 15 percent for a full-span accretion, a loss in efficiency of about 10 percent could result. Thus it is seen that partial-span blade shoes can reduce considerably, but by no means entirely, propeller efficiency losses resulting from the accretion of ice. In a good many instances, air temperatures will be sufficiently high to prevent any ice formation beyond the blade shoe, and only the negligibly small efficiency losses resulting from periodic formations on the blade shoes through cyclic heating will be incurred.

APPENDIX C

CONSIDERATION OF PREVIOUS MEASUREMENTS OF LARGE PROPELLER EFFICIENCY LOSSES IN ICING CONDITIONS

Three measurements of propeller efficiency loss presented in reference 3 produced values of 15 percent or greater. The air temperatures prevailing at the time of these measurements were relatively high; thus the action of kinetic heating (see Appendix B) would have limited the radial extent of the ice accretions. Under such circumstances, the presence of adverse compressibility effects is extremely unlikely, and the maximum efficiency loss to be expected would be about 15 percent, as concluded in the body of the present report. With only partial-span formations, it would be expected that the measured losses should have been somewhat less than 15 percent. In view of this discrepancy between the measured losses of reference 3 and the maximum loss as concluded in this report, it is of interest to investigate the changes in propeller section properties required to produce the measured losses. Accordingly, calculations were made to establish the magnitude of aerodynamic changes necessary to cause the three losses.

The three highest losses recorded in reference 3 are 15, 17, and 19 percent. The air temperature existing at the time of the measurements was 25° F, 21° F, and 18° F for the losses of 15, 17, and 19 percent, respectively. From this information, the radial extent of the formations prevailing for these temperatures was computed, using the curve of kinetic-temperature rise for continuous icing (group 1) of figure 38. The airplane operating conditions given in reference 3 were used in the computations. Results of this calculation established the outer limit of the ice accretion at 33 percent of the blade radius in the case of the 15-percent loss, at 60-percent radius for the 17-percent loss, and at 69-percent radius for the 19-percent loss.

The changes in section drag-lift ratio which would be required for the iced portions of the blades to cause the measured efficiency losses were then computed, using clean-blade thrust- and torque-distribution curves which were considered representative. For the 15- and 19-percent efficiency-loss cases, these curves were calculated by the method of reference 15; and, for the 17-percent loss case, they were approximated from data of reference 16. Results of the calculations showed that over 2000-percent increase in drag-lift ratio would have been required for the iced part of the blades to cause an efficiency loss of 15 percent under the existing conditions. Similarly, increases in drag-lift ratio of 900 and 800 percent for the iced regions were calculated to have been necessary to create the losses of 17 percent and 19 percent, respectively.

In view of the fact that an increase in drag-lift ratio of about 200 percent was concluded previously in this report to be the maximum

possible in icing conditions, it is difficult to reconcile measurements producing 4 to 10 times this change. Possibly the formations encountered during these particular tests of reference 3 were as deleterious as the measurements indicate, but the validity of these three values is seriously questioned. It is not believed that losses of such a magnitude can be experienced at the relatively high air temperatures of the tests. During the experiments of the present report it was learned that erroneous measurements of efficiency are very likely if considerable care is not exercised in allowing conditions to stabilize before taking readings. This is sometimes very difficult to accomplish, in view of the turbulence often associated with icing conditions, and it is believed that the measurements of the three efficiency losses under discussion are in error. Validity of the results of reference 2, from which the maximum value of 200-percent increase in drag-lift ratio was derived, is not disputed since the tests were conducted in a wind tunnel in which stable conditions generally exist; also, there is no reason to believe the data were subject to systematic error, and a large number of observations were made, which would tend to reduce random errors.

REFERENCES

1. Corson, Blake W., Jr., and Maynard, Julian D.: The Effect of Simulated Icing on Propeller Performance. NACA TN 1084, 1946.

2. Haines, A. B.: 24-Foot Tunnel Comparative Tests on Propellers with Simulated Ice and with De-Icing Overshoes. Rep. No. Aero.1847, R.A.E. (British), Dec. 1946.

3. Preston, G. Merritt, and Blackman, Calvin C.: Effects of Ice Formations on Airplane Performance in Level Cruising Flight. NACA TN 1598, 1948.

4. Lewis, William, and Hoecker, Walter H., Jr.: Observations of Icing Conditions Encountered in Flight During 1948. NACA TN 1904, 1949.

5. Jones, Alun R.: An Investigation of a Thermal Ice-Prevention System for a Twin-Engine Transport Airplane. NACA Rep. 862, 1946.

6. Lewis, William: A Flight Investigation of the Meteorological Conditions Conducive to the Formation of Ice on Airplanes. NACA TN 1393, 1947.

7. Lewis, William, Kline, Dwight B., and Steinmetz, Charles P.: A Further Investigation of the Meteorological Conditions Conducive to Aircraft Icing. NACA TN 1424, 1947.

8. Freeman, Hugh B.: The Effect of Small Angles of Yaw and Pitch on the Characteristics of Airplane Propellers. NACA Rep. 389, 1931.

9. Lesley, E. P., Worley, George F., and Moy, Stanley: Air Propellers in Yaw. NACA Rep. 597, 1937.

10. Gulick, Beverly G.: Effects of a Simulated Ice Formation on the Aerodynamic Characteristics of an Airfoil. NACA ACR, May 1938.

11. Jacobs, Eastman N.: Airfoil Section Characteristics as Affected by Protuberances. NACA Rep. 446, 1932.

12. Robinson, Harold L.: High-Speed Investigation of Skin Wrinkles on Two NACA Airfoils. NACA TN 1121, 1946.

13. Hardy, J. K., and Brown, C. D.: Kinetic Temperature of Propeller Blades in Conditions of Icing. Rep. No. Mech. Eng. 2, R.A.E. (British), May 1947.

14. Brown, C. D., and Orr, J. L.: A Theoretical and Experimental Investigation of the Effects of Kinetic Heating on Ice Formation on Aircraft Propeller Blades. Nat. Res. Council of Canada, Rep. No. MD-30, Dec. 1946.

15. Crigler, John L.: Comparison of Calculated and Experimental Propeller Characteristics for Four-, Six-, and Eight-Blade Single-Rotating Propellers. NACA ACR 4B04, 1944.

16. Reid, Elliot G.: Wake Studies of Eight Model Propellers. NACA TN 1040, 1946.

TABLE I

TABULATION OF PROPELLER EFFICIENCY LOSSES AND METEOROLOGICAL CONDITIONS OF ICING

Encounter number	Flight number	Date (1948)	Time of ice build-up M.S.T.	Average propeller speed during ice build-up (rpm)	Blade angle, β_o at 0.75 R during efficiency measurements	Average pressure altitude during ice build-up (ft)	Average true air-speed during ice build-up (mph)	Free air temperature (°F)	Average liquid-water content (grams/cubic meter[1])	Maximum liquid-water content (grams/cubic meter[1])	Average droplet diameter (microns)	Average icing rate[2] (in./hr)	Propeller efficiency loss (percent)	Ice formation type (table II)	Photographic figure number	Data figure number	Remarks[3]
1	150	Feb. 3	1530	1025	25.8	7,500	-	14	-	-	-	-	10[4]	IIB + IVA	18	13	
2	152	Feb. 6	1513 to 1523	1025	31.8	10,000	158	1	.41	1.0	18	6.1	1-2[4]	IB + $\frac{1}{4}$ IIIB	19	14	IIIB formation on one blade only.
3	152	Feb. 6	1549 to 1620	1025	25.8	7,000	145	17	.41	.85	20	5.6	4[4]	IID	20	10,13	
					31.8								6[4]			10,14	
3a					20.7								0-1[4]	ID	21	12	This formation caused by break-off of ice formation of encounter 3.
4	155	Feb. 9	1512 to 1521	1025	25.8	9,200	155	3	.44	1.18	25	6.3	0[5]	ID + $\frac{1}{2}$ VA	22	11	VA formation on two blades only.
					31.8								8[5]				
5	155	Feb. 9	1541 to 1600	1025	25.8	8,200	152	9	.27	1.08	17	3.8	4[4]	IID + $\frac{1}{4}$ VA	23	10,13	VA formation on one blade only.
6	155	Feb. 9	1722 to 1742	1025	25.8	7,500	144	10	.58	-	15	-	4[4]	IIC + $\frac{1}{4}$ VB	24	13	VB formation on one blade only. Partial VB on another blade.
7	159	Feb.13	1140 to 1240	1025	25.8	2,000	140	26	.10	.39	19	1.3	1-3[5]	IA	25	13	This formation encountered in a freezing rain condition.
8	159	Feb.13	1240 to 1310	1025	25.8	2,500	146	20	.04	-	9	-	0[5]	IIA	26	13	Same as encounter 7.
9	167	Mar. 9	1500 to 1502	1025	21.5	15,200	178	-6	.10	.24	27	1.6	1-4[5]	IIC + VA	27	12	IIC formation accumulated prior to this encounter.
10	171	Mar.13	1315 to 1335	1025	26.5	8,500	170	15	.41	-	20	-	0[5]	See remarks	28,29	16	Cyclic heating on forward 10 percent of blades. Runback and primary accretions formed aft of heated regions.
11	171	Mar.13	1515 to 1540	1025	29.5	12,000	155	3	.28	.73	35	4.1	0[5]	See remarks	30	16	Same as encounter 10.
12	195	Apr.18	1402 to 1435	1175	28.0	22,700	178	-22	.14	.39	14	2.3	5[5]	VB	31	15	

[1] Grams of water per cubic meter of air.
[2] Icing rate on rotating-disk icing-rate meter. (See reference 4.)
[3] Propeller blades unheated during all encounters excepting 10 and 11.
[4] Efficiency loss at peak of efficiency curves.
[5] Point values of efficiency loss at a particular operating condition.

TABLE II

ICE FORMATION CLASSIFICATION SYSTEM USED THROUGHOUT REPORT

Class	Outer limit of ice formation (percent tip radius)	Class	Thickness of ice at leading edge in chordwise direction (in.)
I	26 to 41	A	Less than 1/4
II	42 to 54	B	1/4 to 1/2
III	55 to 68	C	1/2 to 1
IV	69 to 81	D	Over 1
V	82 to 95	–	– – –

NACA

TABLE III

EXPERIMENTAL VALUES OF THRUST AND POWER COEFFICIENT FOR SEVERAL ICING ENCOUNTERS IN WHICH ONLY SINGULAR VALUES OF PROPELLER EFFICIENCY WERE MEASURED

Encounter number	Advance ratio, V/nD	Thrust coefficient, C_T	Power coefficient, C_p	Blade angle, β_o (deg)	Data figure number	Photo figure number
4	1.07	0.066	0.078	25.8	11	22
	1.07	.064	.077	25.8		
	1.16	.104	.159	31.8		
	1.17	.101	.152	31.8		
7	.95	.074	.084	25.8	13	25
	.98	.074	.084			
	1.03	.071	.086			
	1.03	.070	.083			
8	1.07	.073	.088	25.8	13	26
	1.07	.073	.088			
	1.07	.073	.089			
	1.08	.073	.088			
	1.08	.072	.088			
	1.09	.073	.089			
9	.90	.104	.115	21.5	12	27
	.92	.109	.121	21.5		
10	1.13	.096	.126	26.5	16	28, 29
	1.14	.090	.118			
	1.15	.096	.127			
11	1.28	.102	.149	29.5	16	30
	1.29	.102	.149	29.5		
12	.98	.115	.139	28.0	15	31
	1.00	.111	.140			
	1.04	.102	.128			

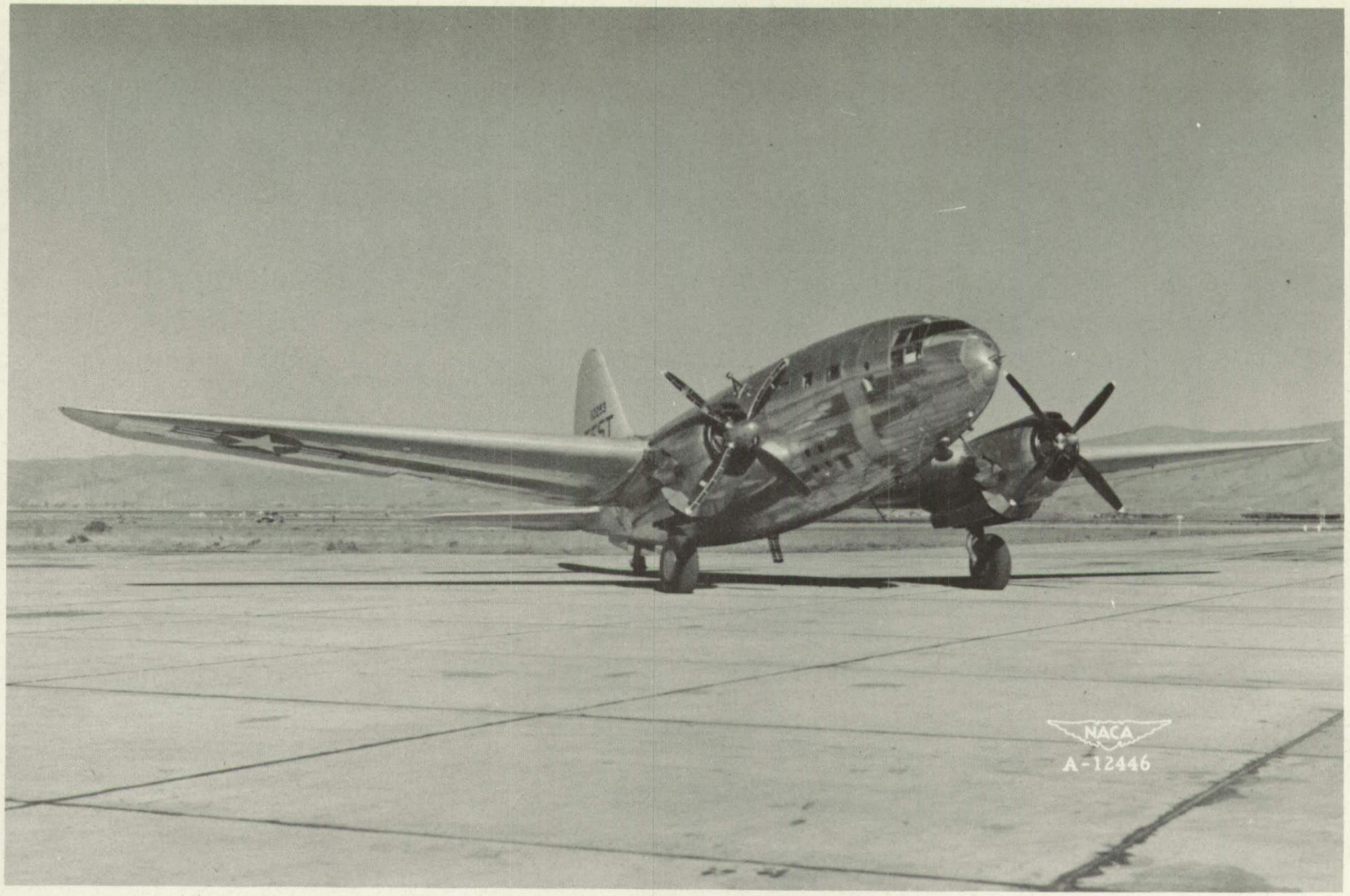

Figure 1.– The test airplane used for the flights in natural icing conditions to investigate propeller–efficiency loss.

Page intentionally left blank

Page intentionally left blank

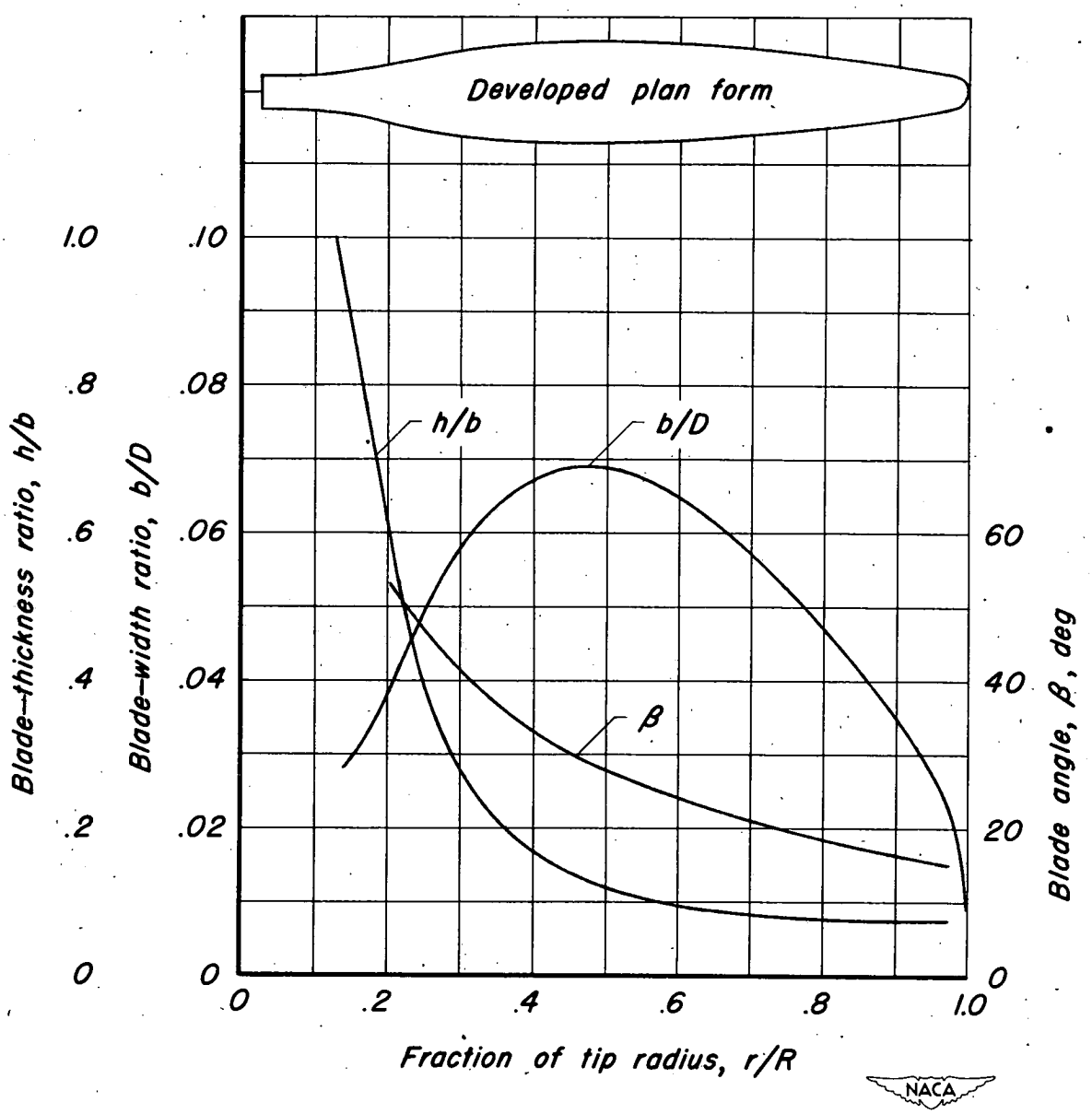

Figure 2.- Characteristics of the test propeller; diameter, 13.5 feet.

Page intentionally left blank

Page intentionally left blank

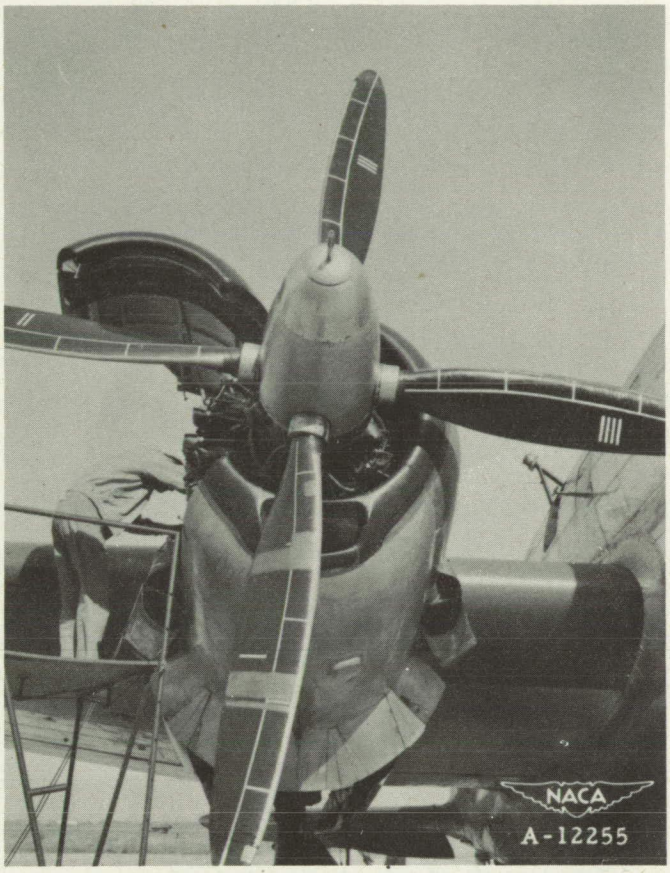

Figure 3.— Test propeller showing the specially constructed blade heating shoes and the spinner.

Page intentionally left blank

Page intentionally left blank

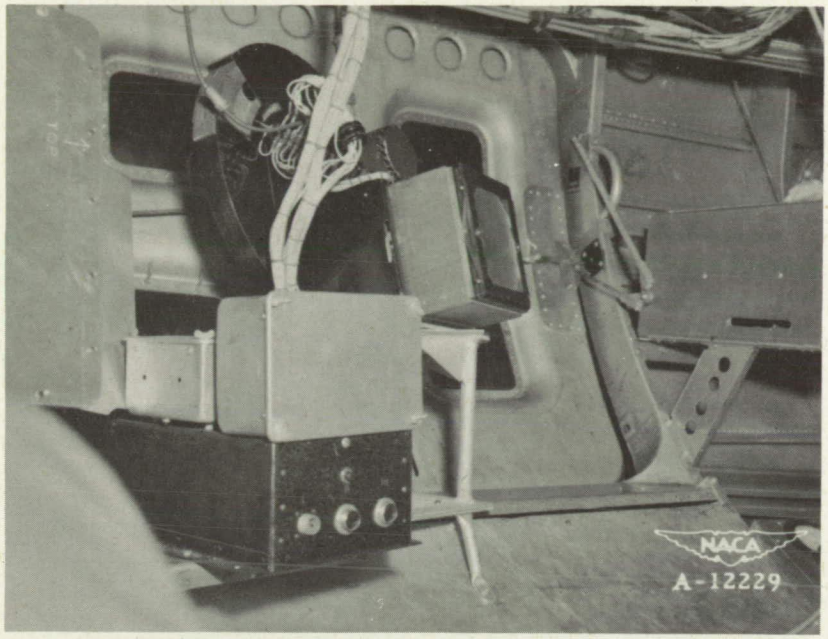

Figure 4.– Camera installation for photographing the thrust face of the test propeller blades.

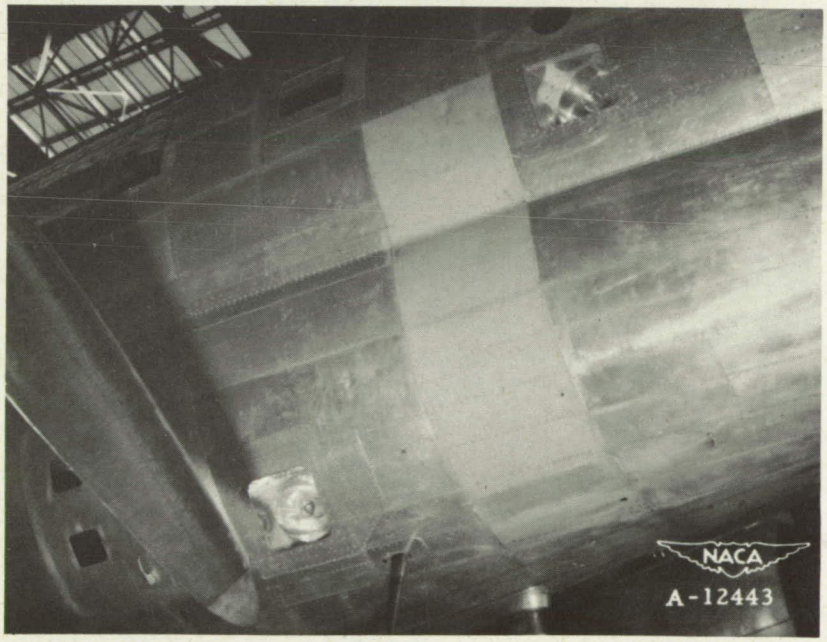

Figure 5.– Propeller camera–flash–lamp installations.

Page intentionally left blank

Page intentionally left blank

Figure 6.- Hemispherical differential-pressure type yaw and pitch head. Airspeed total-pressure heads are mounted on either side of the yaw and pitch head.

Page intentionally left blank

Page intentionally left blank

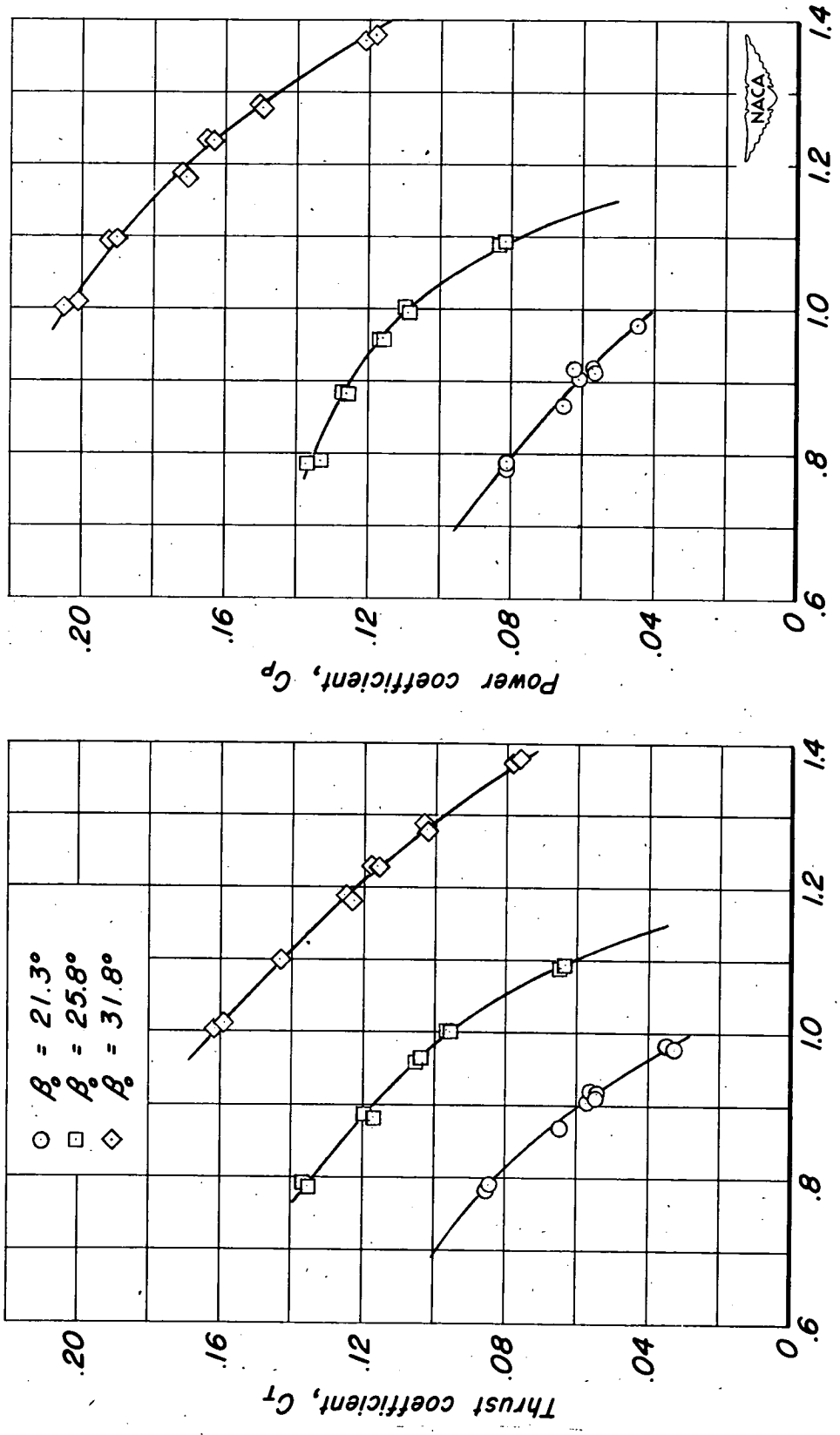

Figure 7.- Thrust and power coefficients for the test propeller with blade heating shoes and with no ice formations.

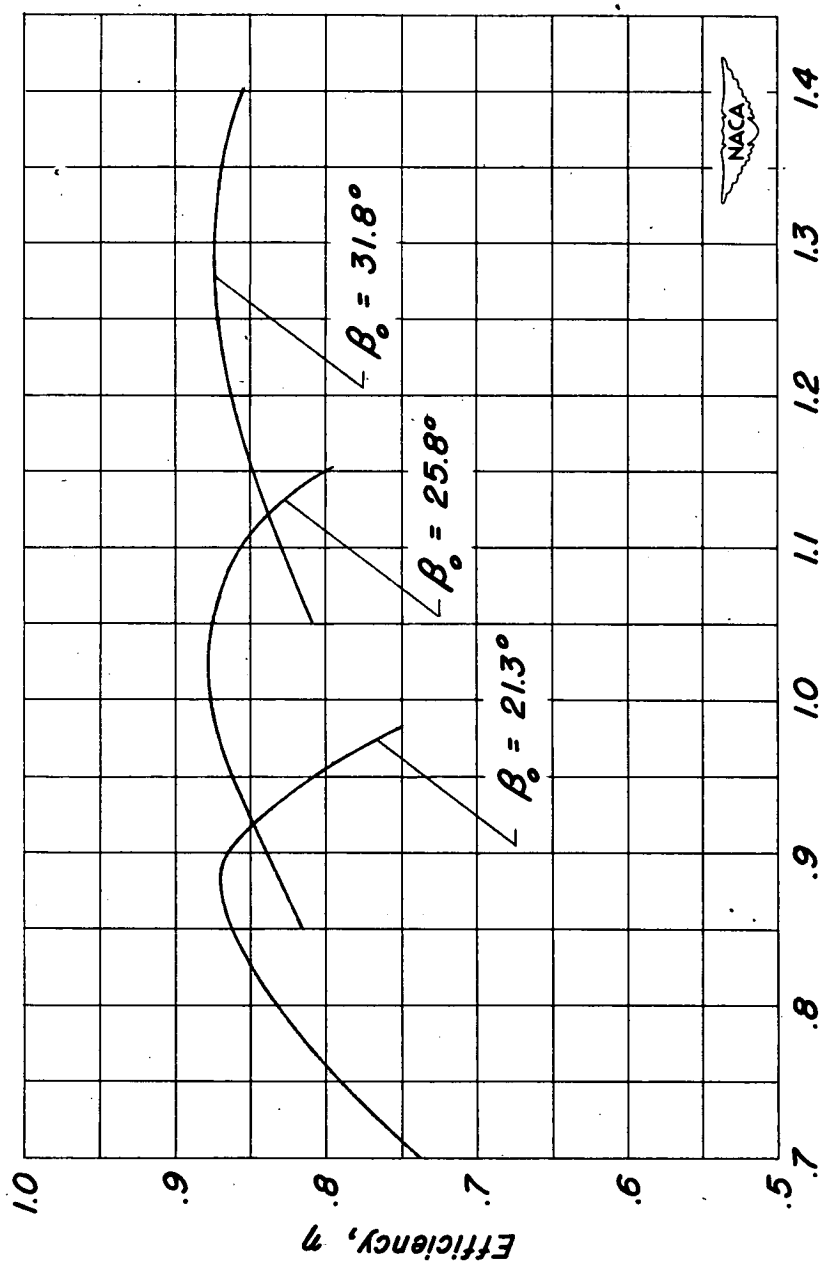

Figure 8.- Efficiency curves for the test propeller with blade heating shoes and with no ice formations.

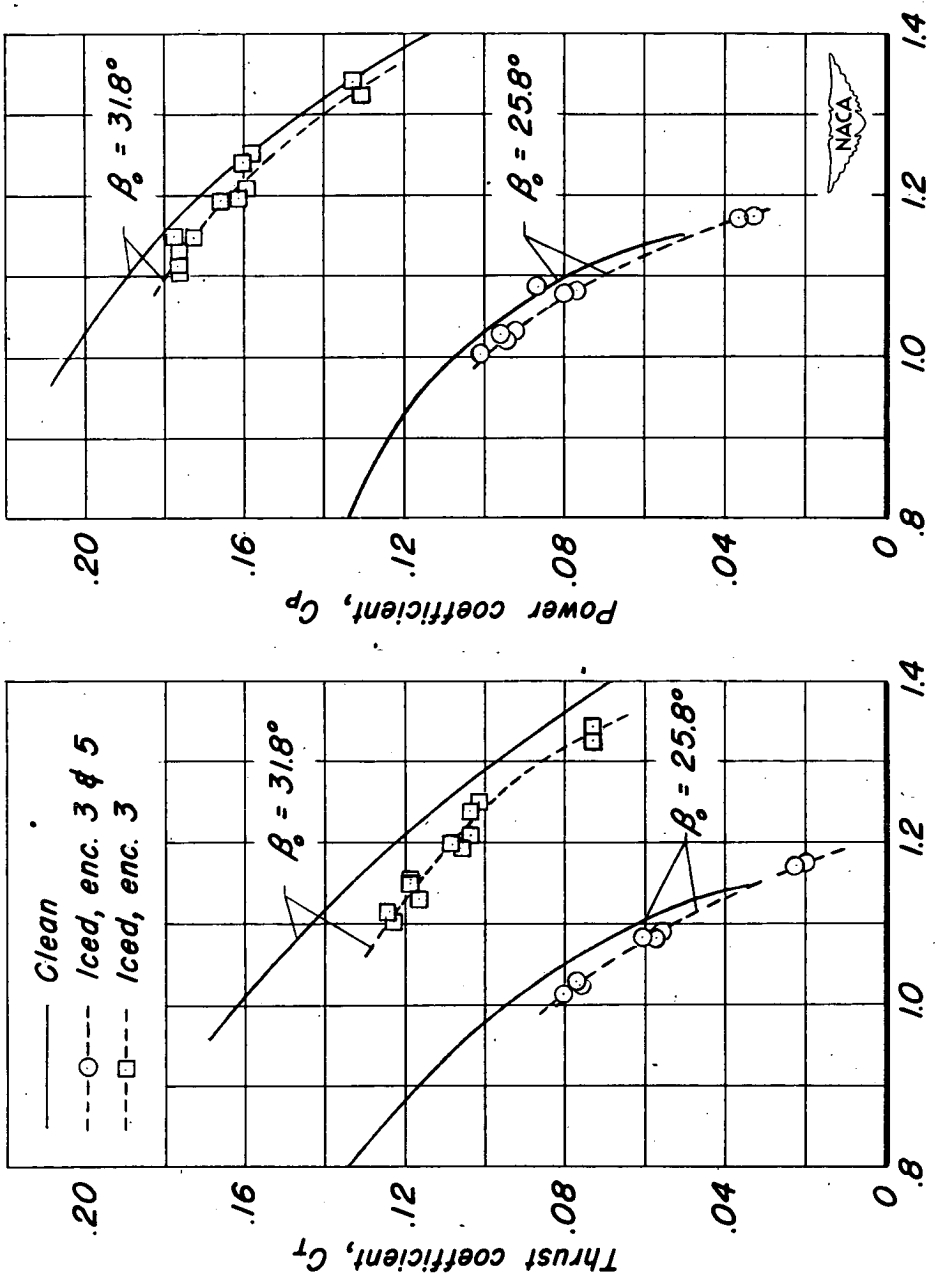

(a) Encounters 3 and 5. β_o = 25.8° and 31.8°.

Figure 9.- The effect of ice formations on the variation of thrust and power coefficients with advance ratio.

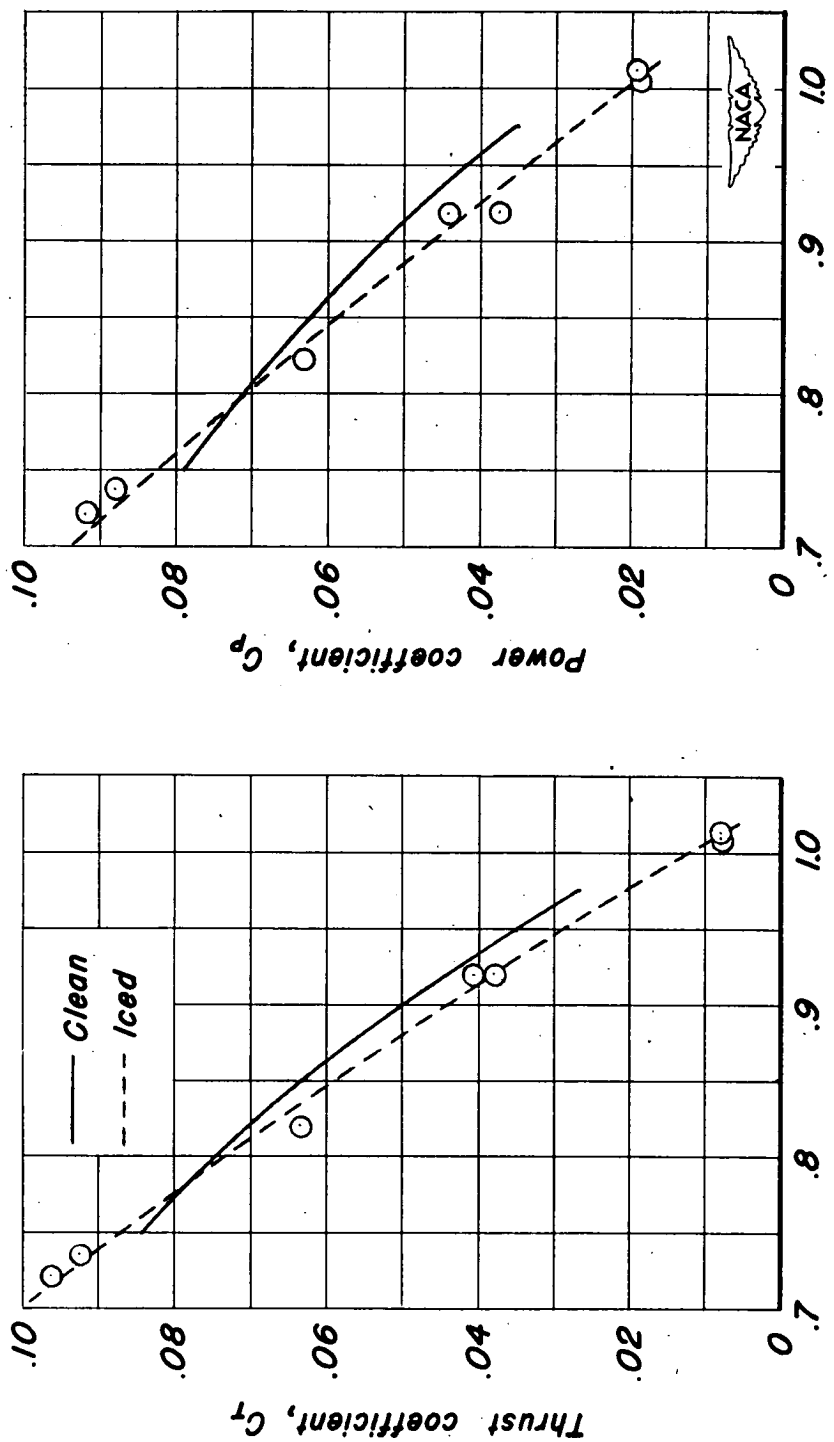

(b) Encounter 3a. $\beta_o = 20.7°$.

Figure 9. – Continued.

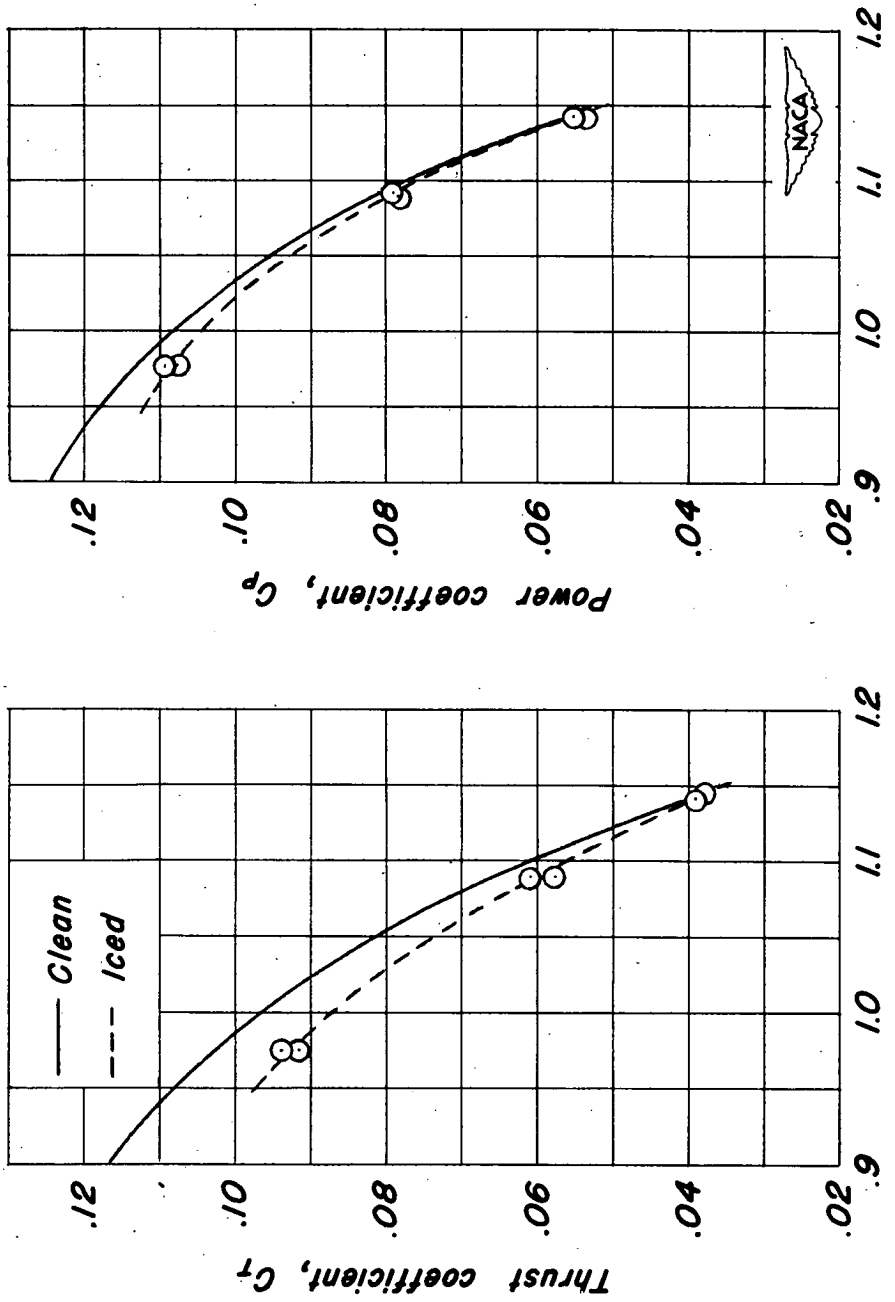

(c) Encounter 6. $\beta_0 = 25.8°$.

Figure 9.- Continued.

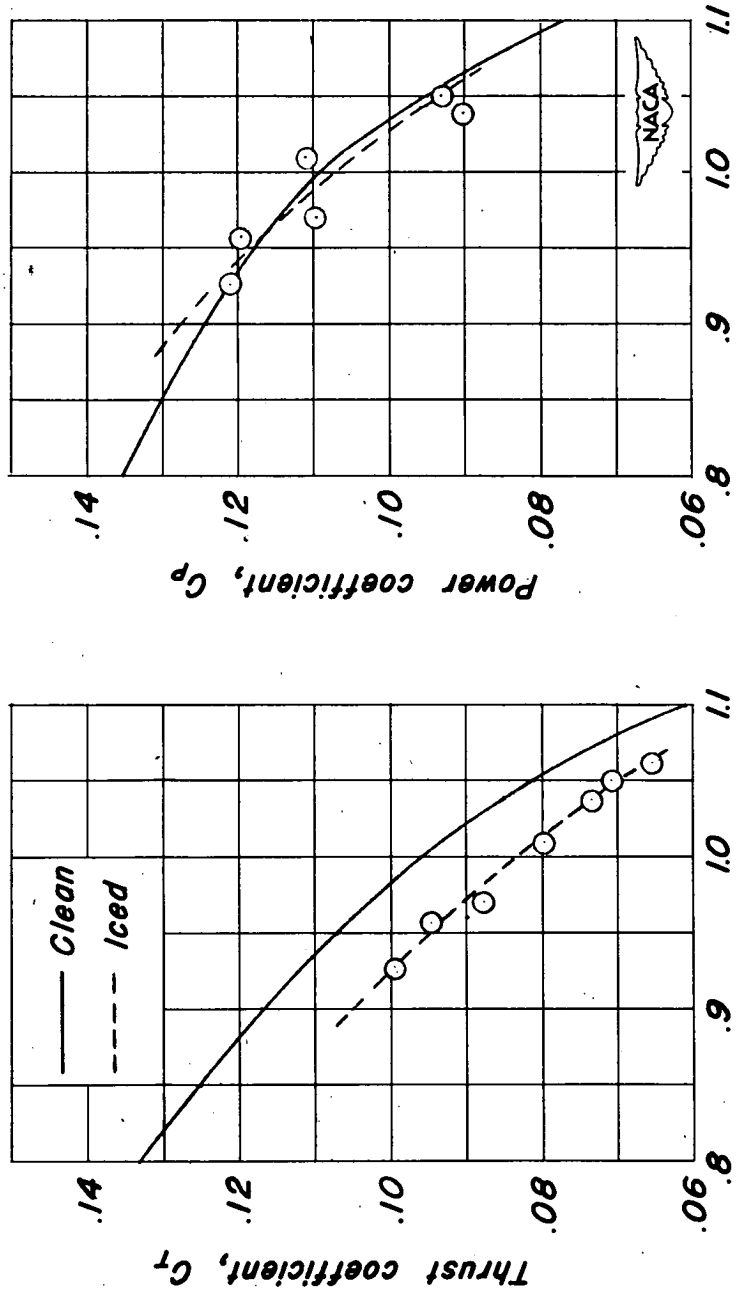

(d) Encounter 1. $\beta_0 = 25.8°$.

Figure 9.- Continued.

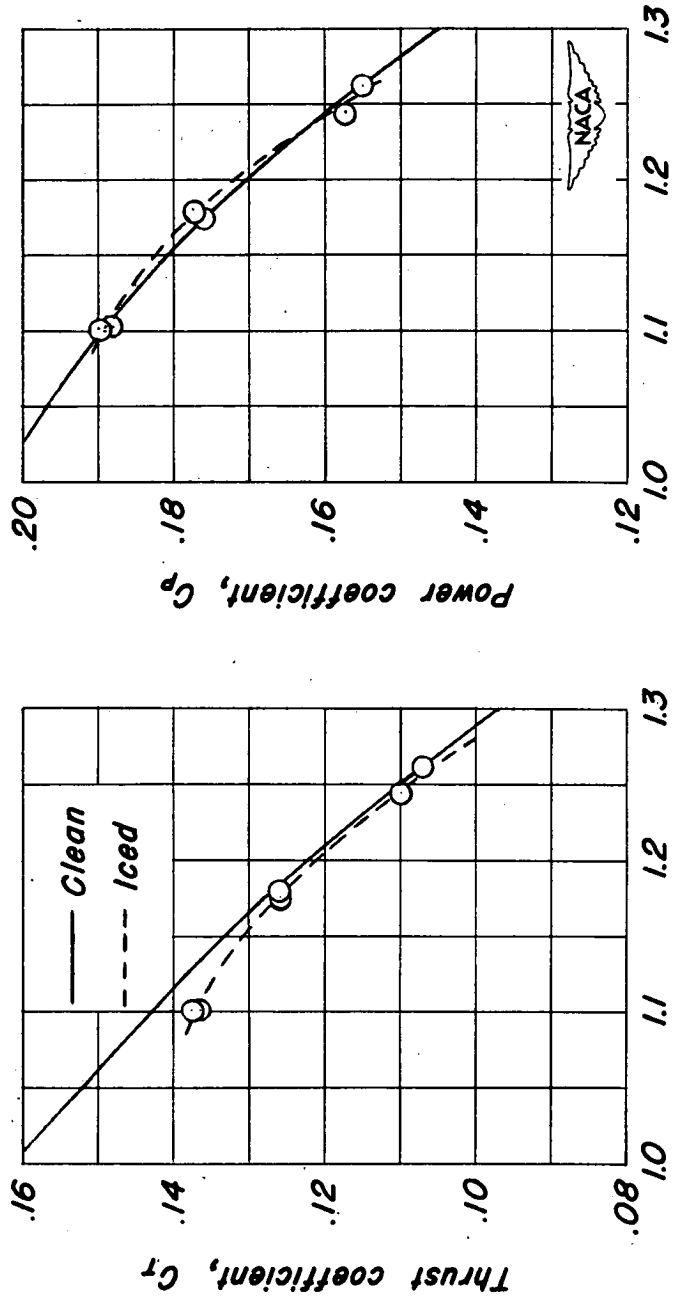

(e) Encounter 2. $\beta_o = 31.8°$.

Figure 9.- Concluded.

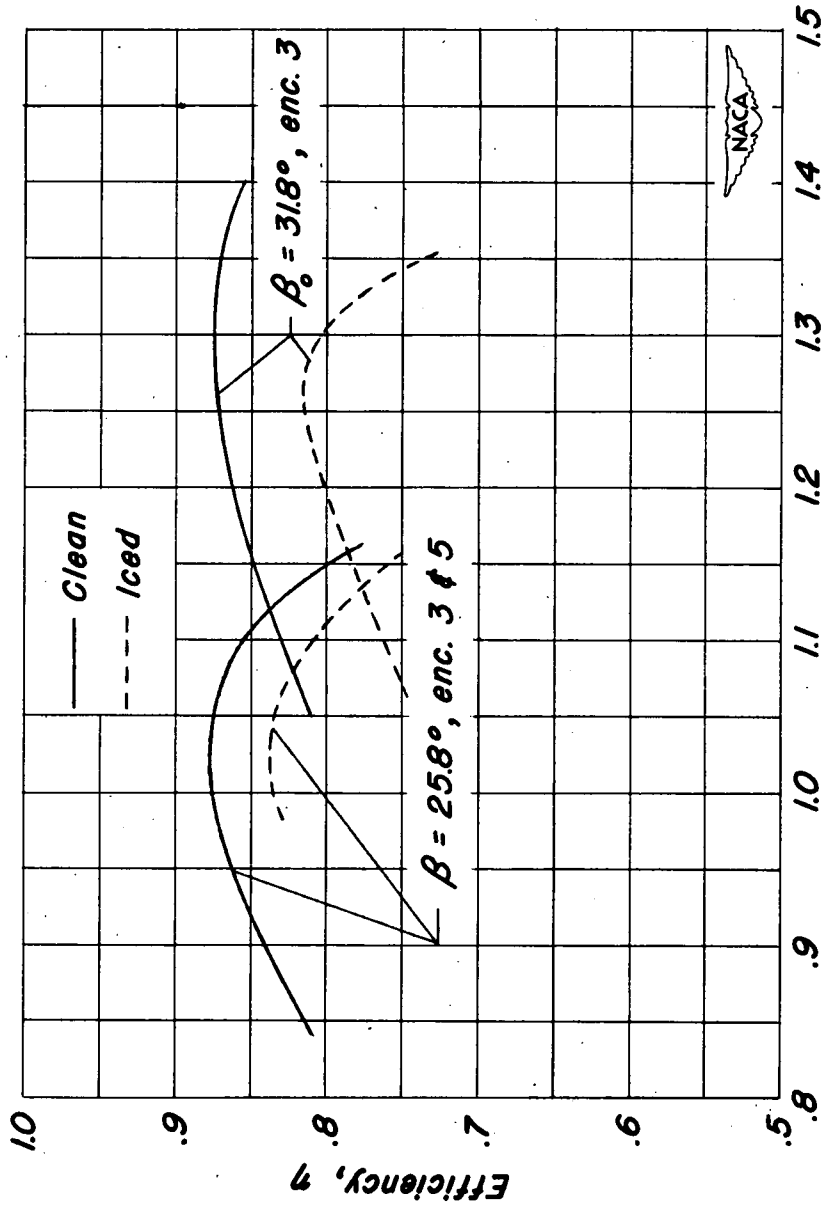

Figure 10.- Comparison of efficiencies for clean and iced propeller at two blade angles for ice formation type II D. Thrust- and power-coefficient data from figure 9(a).

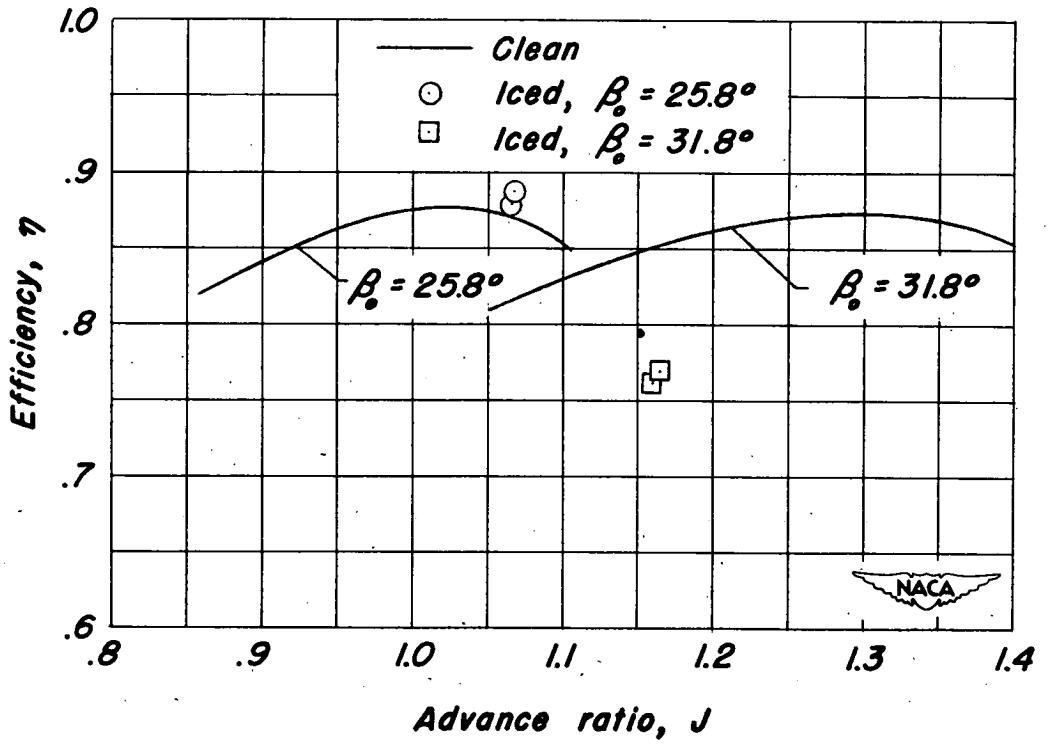

Figure 11.– Comparison of efficiencies for clean and iced propeller at two blade angles for ice formation type ID + 1/2 VA. Encounter 4. Thrust- and power-coefficient data from table III.

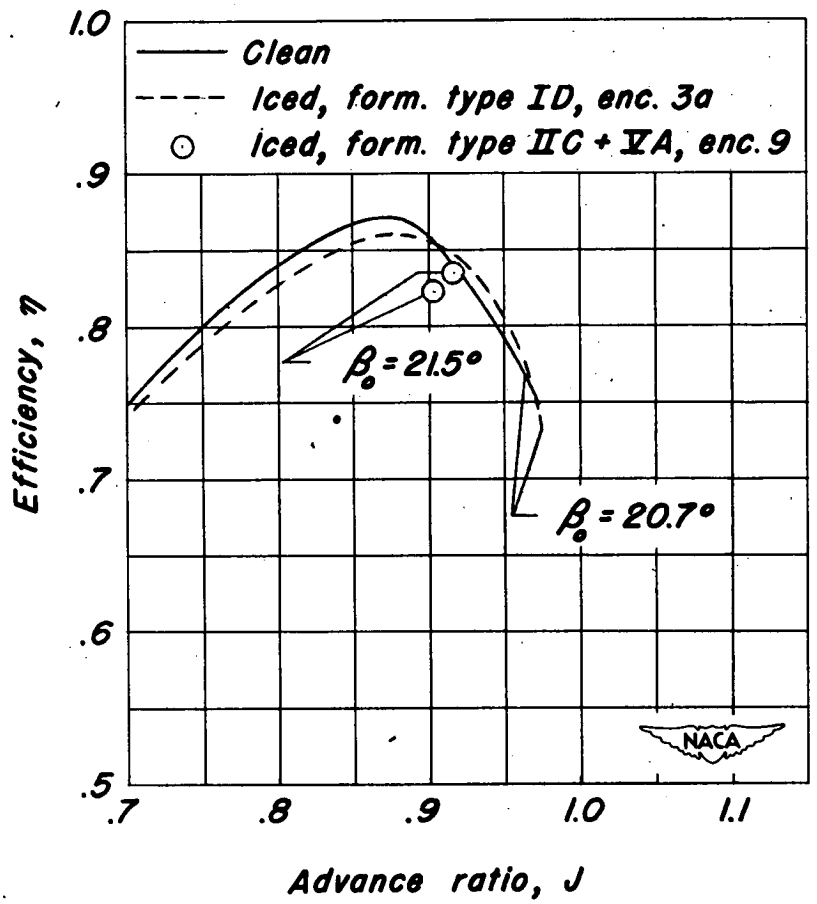

Figure 12.- Comparison of efficiencies for clean and iced propeller for two ice formations. Thrust- and power-coefficient data at β_o = 20.7° from figure 9(b); at β_o = 21.5° from table III.

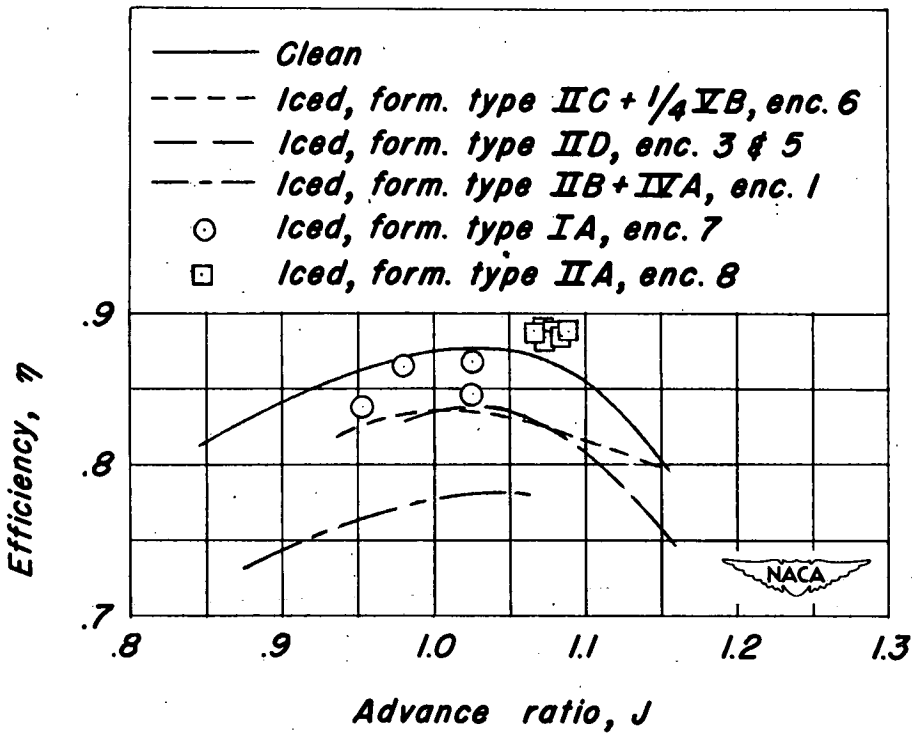

Figure 13.– Comparison of efficiencies for clean and iced propeller for five ice formations at one blade angle. $\beta_o = 25.8°$. Thrust- and power-coefficient data from figures 9(a), 9(c), and 9(d), and table III.

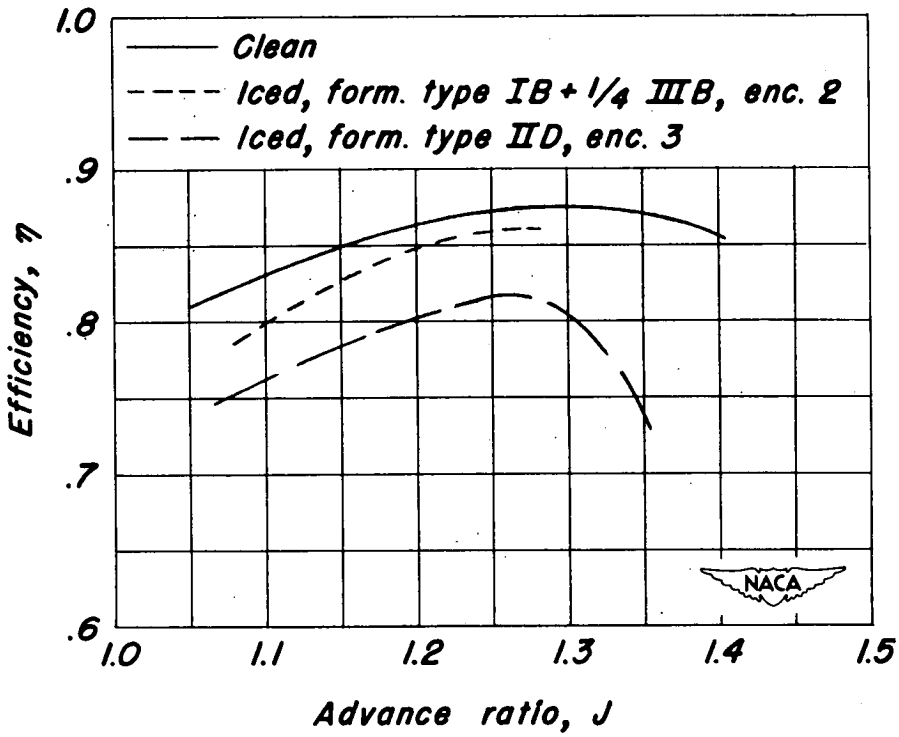

Figure 14.– Comparison of efficiencies for clean and iced propeller for two ice formations at one blade angle. $\beta = 31.8°$. Thrust- and power-coefficient data from figures 9(a) and 9(e).

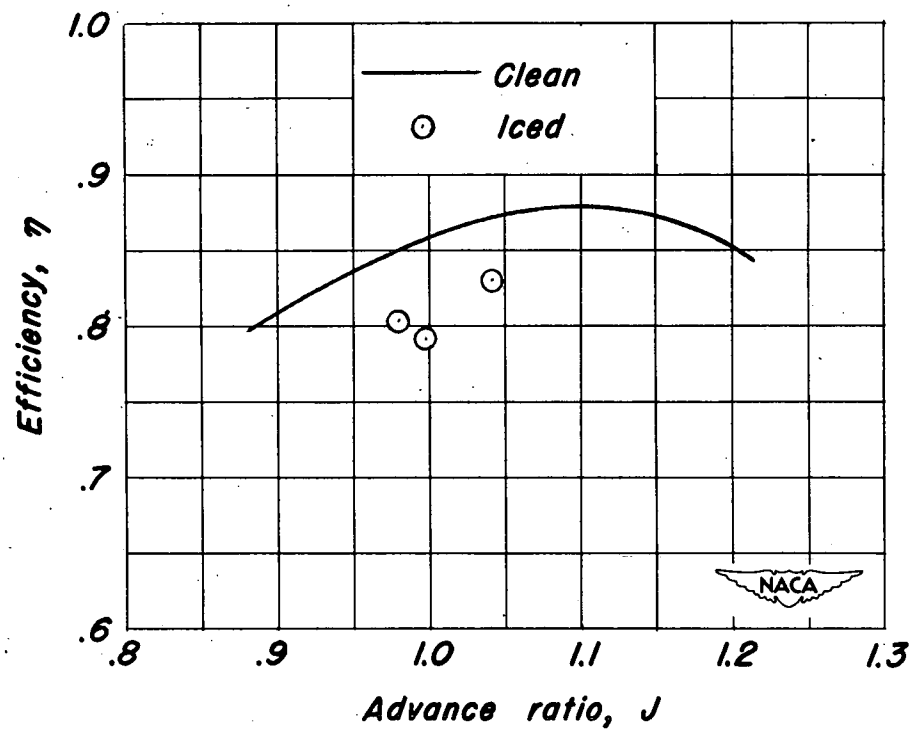

Figure 15.- Comparison of efficiencies for clean and iced propeller for ice formation type V B. $\beta_o = 28.0°$. Encounter 12. Thrust- and power-coefficient data from table III.

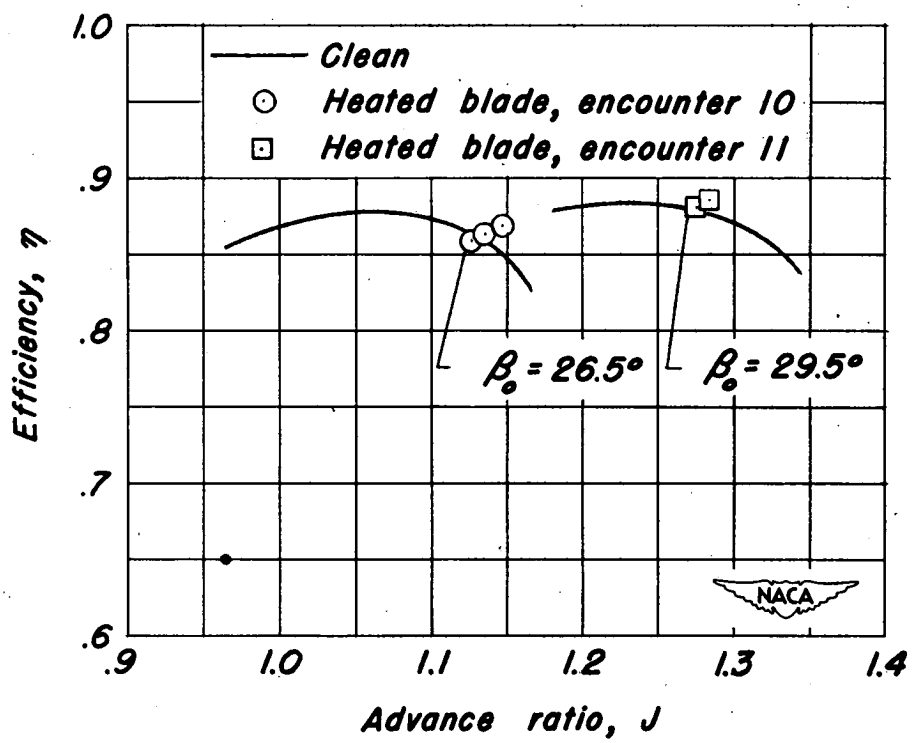

Figure 16.- Comparison of propeller efficiencies for blades clean and with small ice formations resulting from inadequate cyclic heating. Thrust- and power-coefficient data from table III.

Page intentionally left blank

Pages 54 — 88 (every other page left blank)

Page intentionally left blank

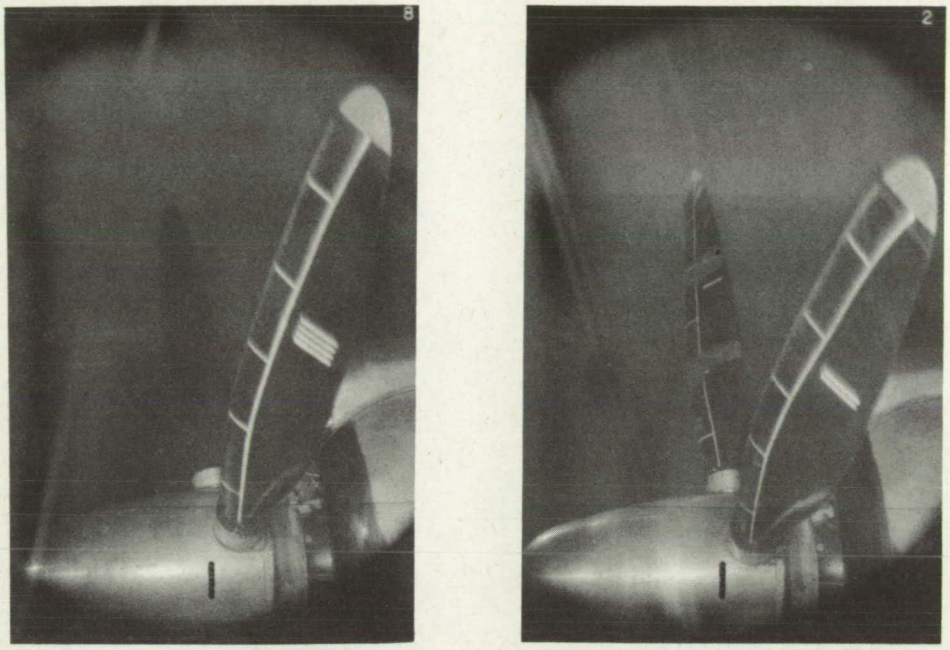

(a) Camber face of blade.

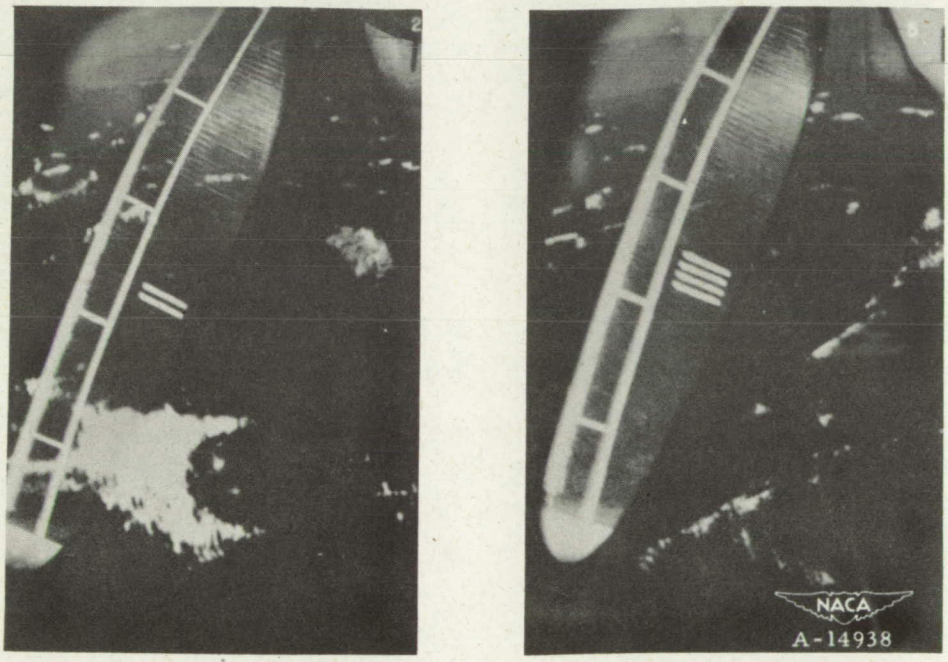

(b) Thrust face of blade.

Figure 17.- Photographs of clean propeller blades.

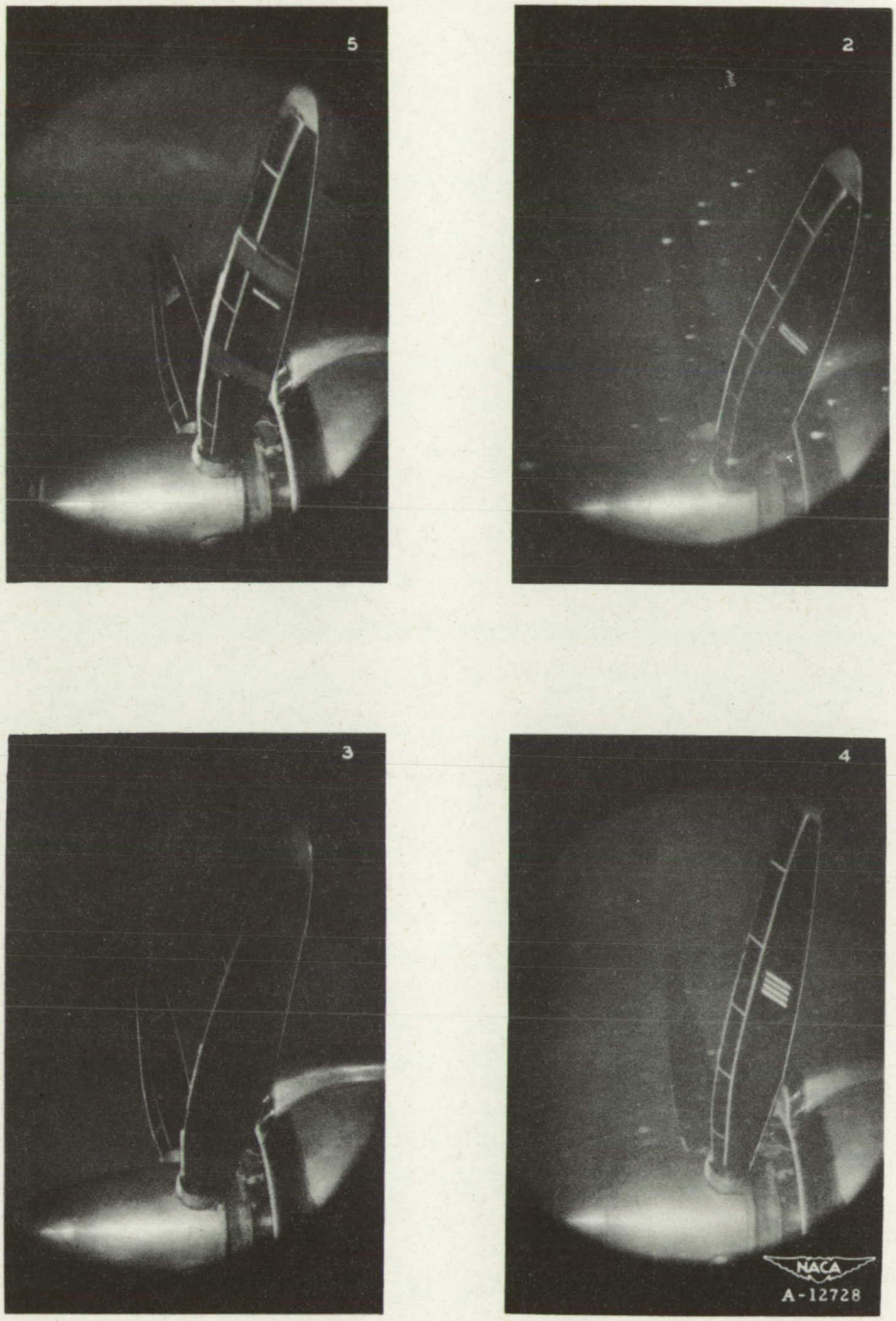

Figure 18.– Ice formation of encounter 1. Camber face. Peak efficiency loss, 10 percent.

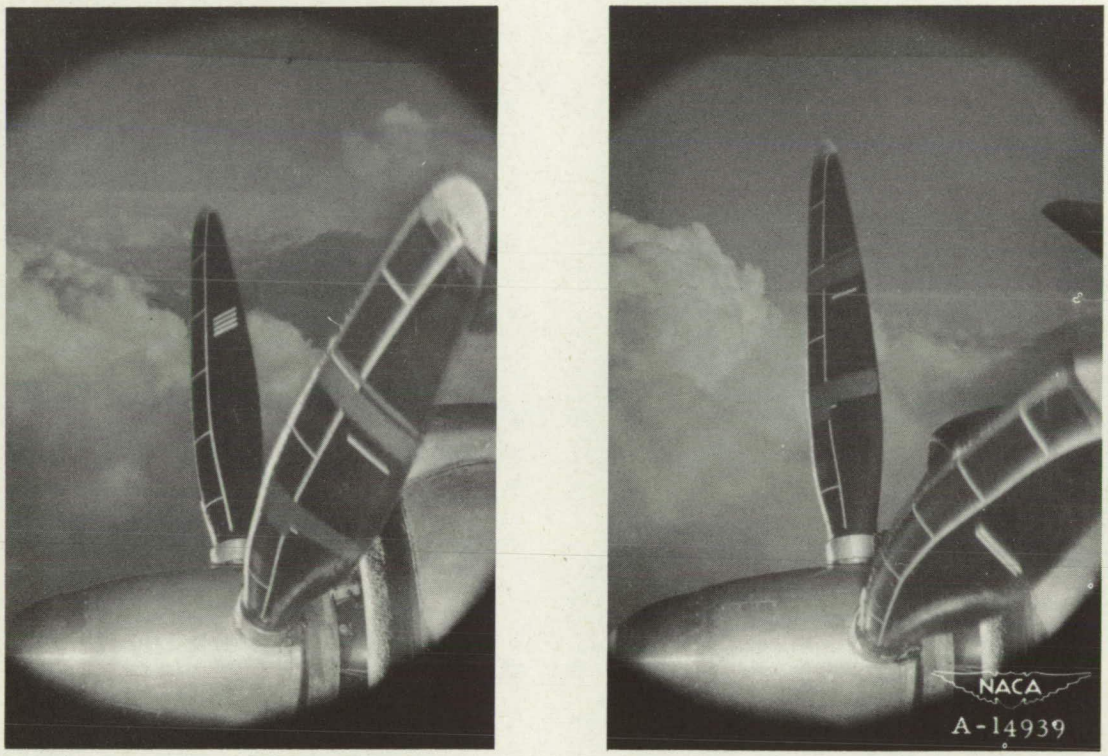

Figure 19.– Ice formation of encounter 2. Camber face. Peak efficiency loss, 1 to 2 percent.

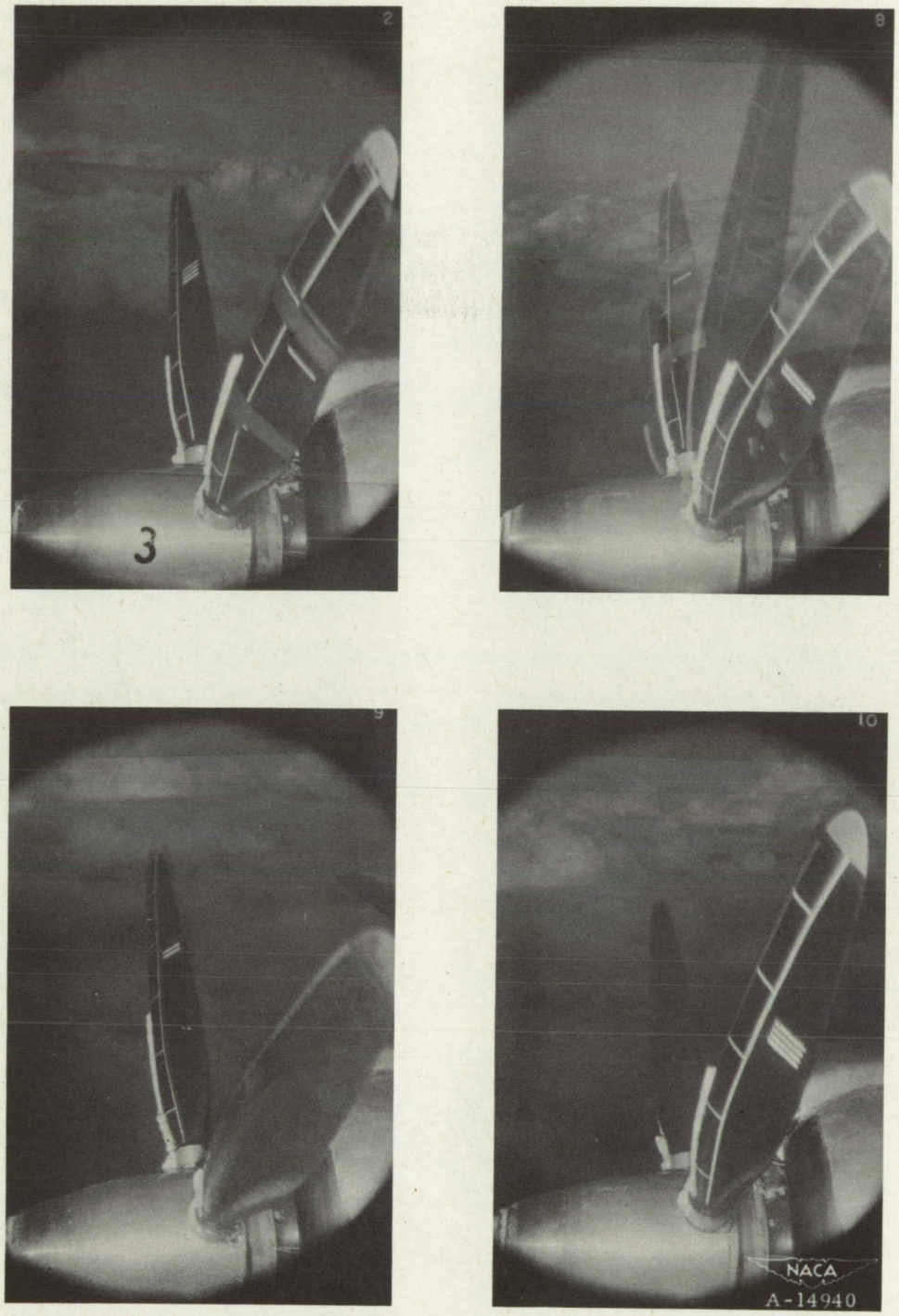

Figure 20.– Ice formation of encounter 3. Camber face. Peak efficiency loss, 4 percent at $\beta_o = 25.8^\circ$; 6 percent at $\beta_o = 31.8^\circ$.

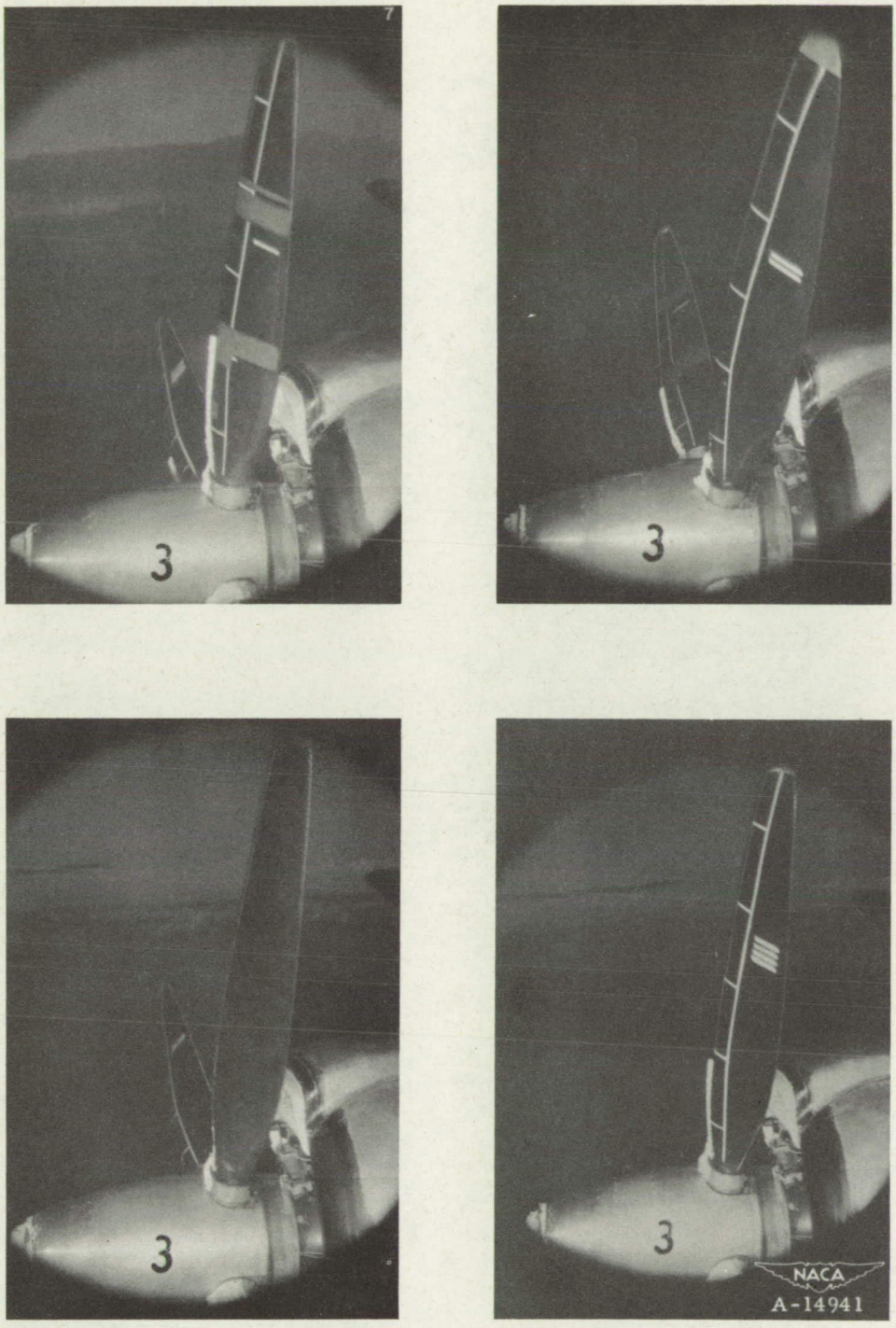

Figure 21.– Ice formation of encounter 3a. Camber face. Peak efficiency loss, 0 to 1 percent.

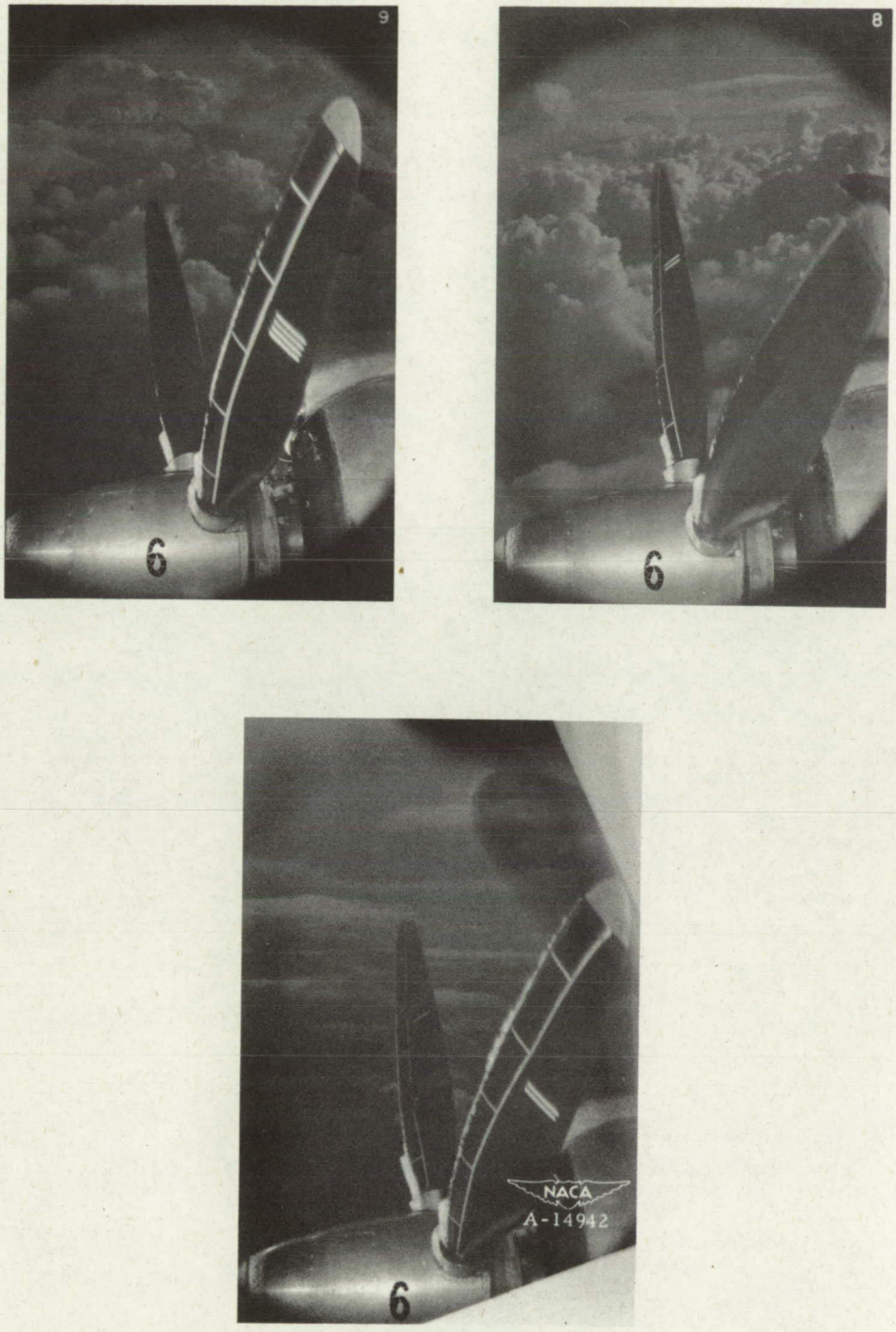

(a) Camber face.

Figure 22.– Ice formation of encounter 4. Efficiency loss, 0 percent at $\beta_o = 25.8^o$; 8 percent at $\beta_o = 31.8^o$.

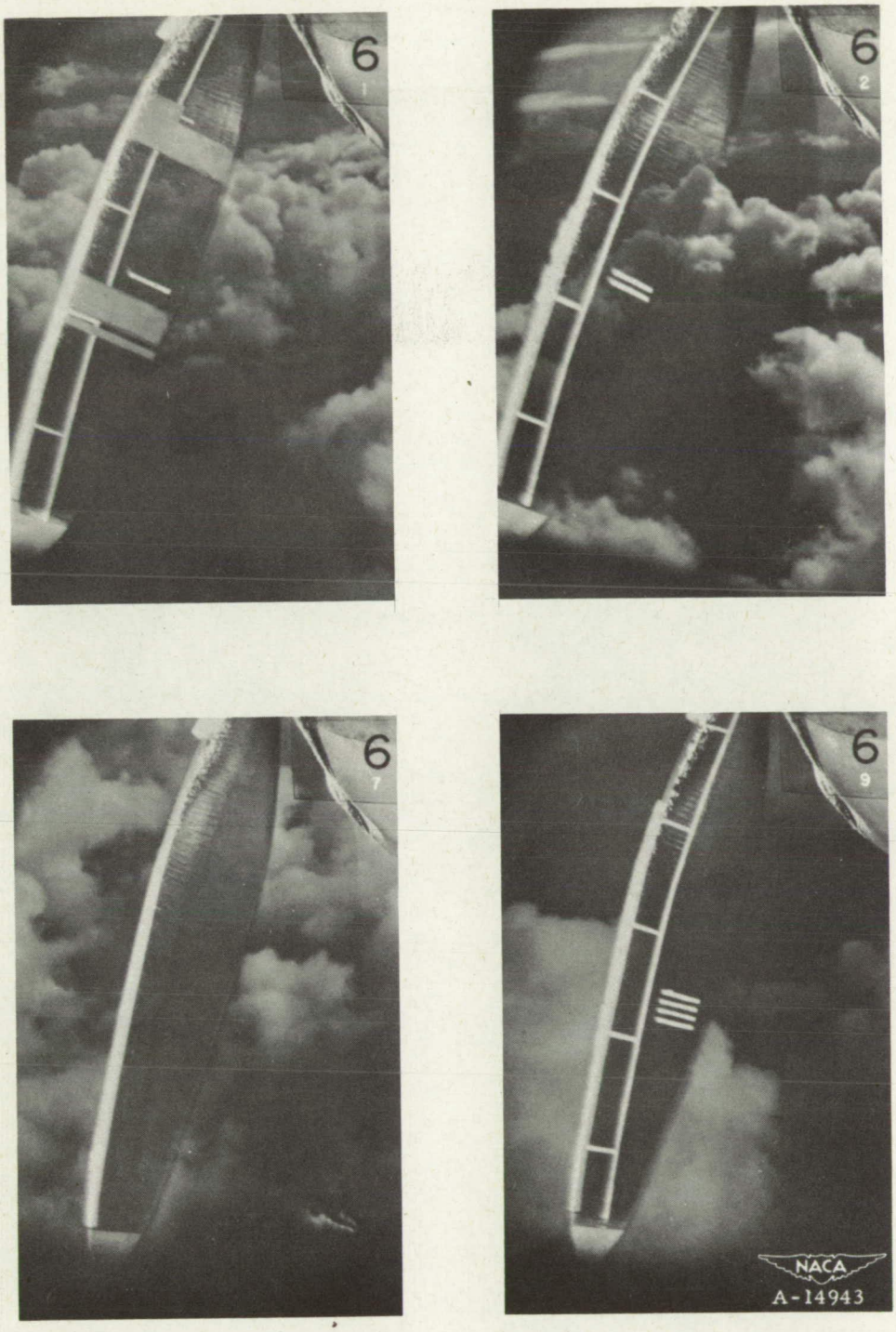

(b) Thrust face.

Figure 22.– Concluded.

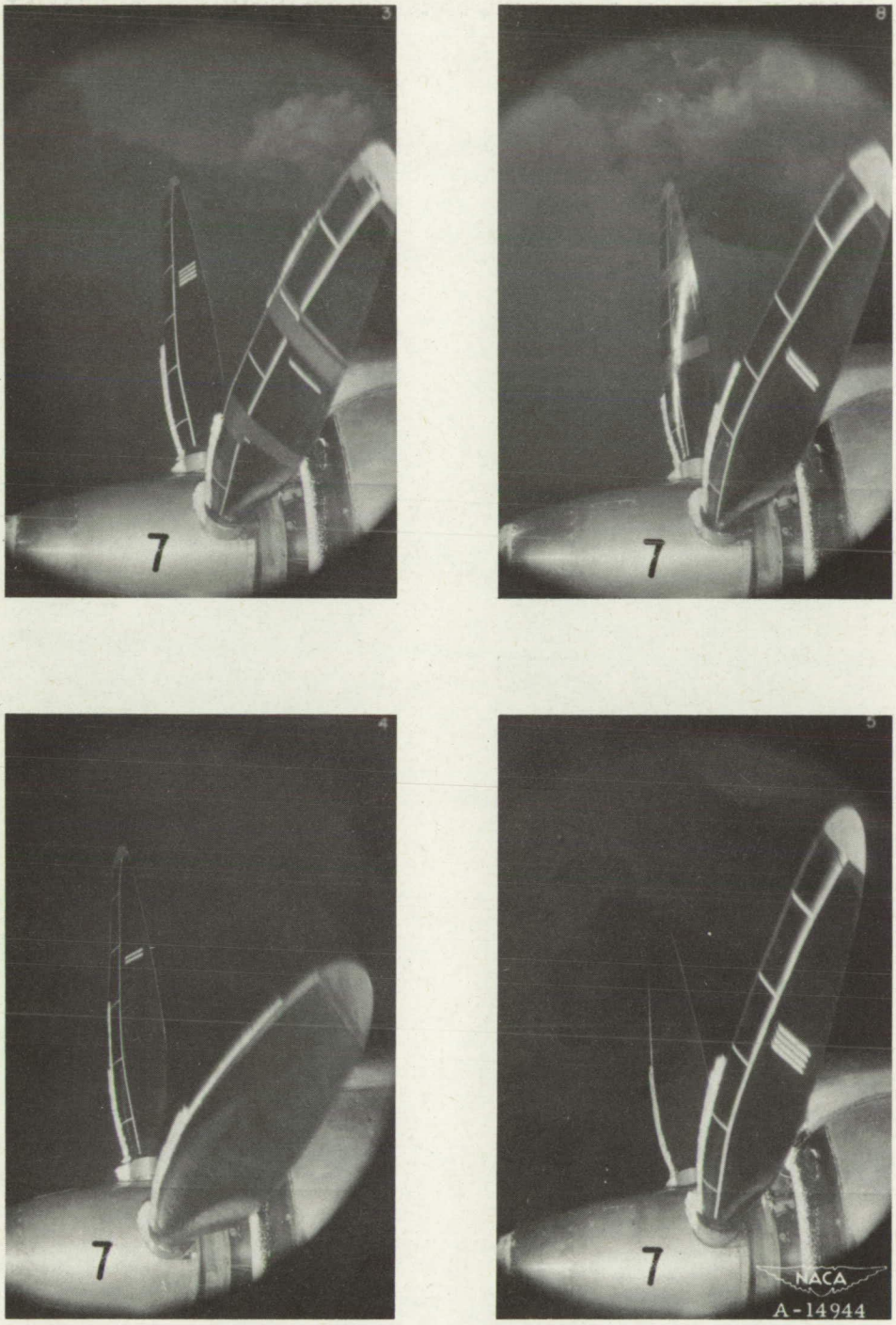

(a) Camber face.

Figure 23.– Ice formation of encounter 5. Peak efficiency loss, 4 percent.

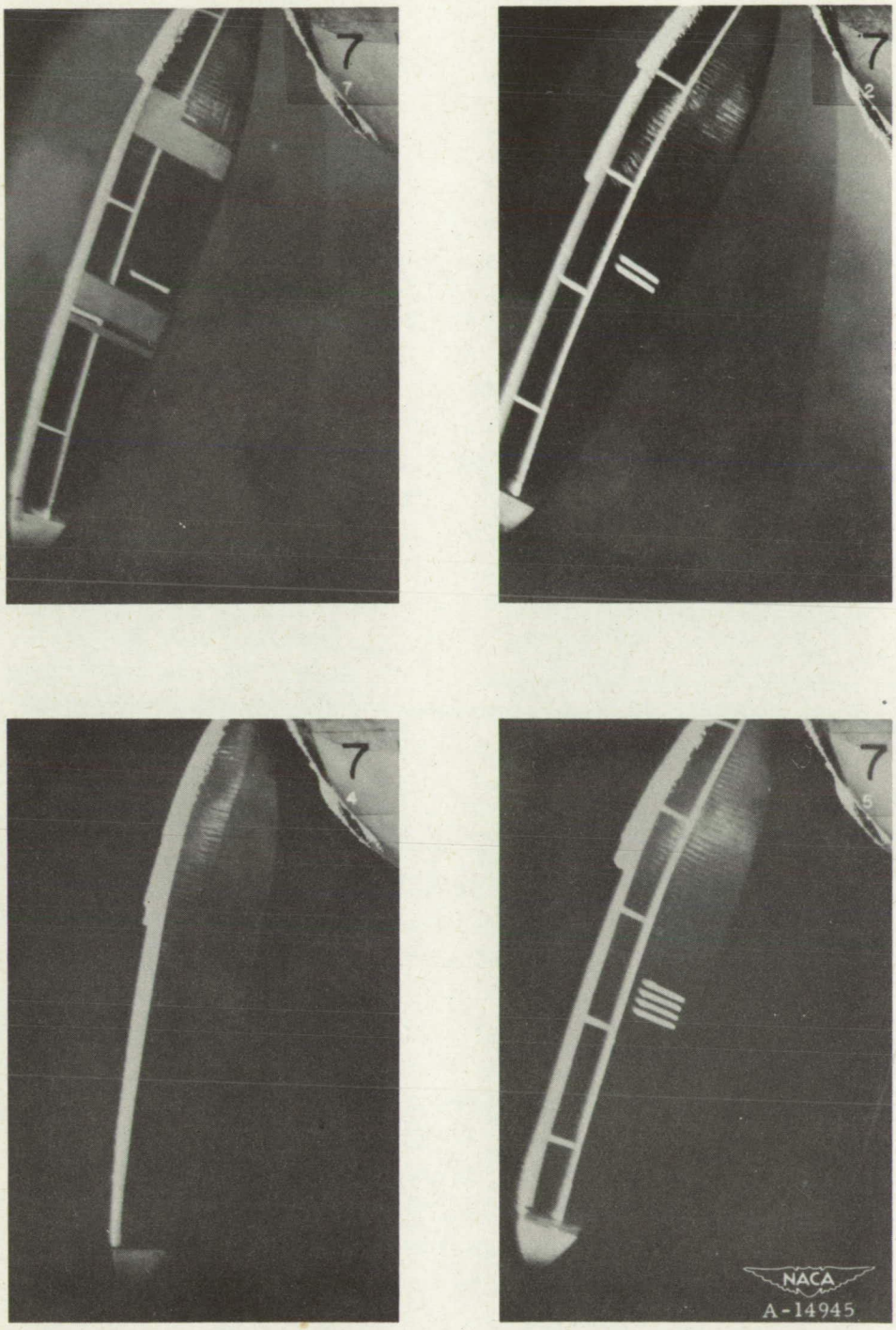

(b) Thrust face.

Figure 23.- Concluded.

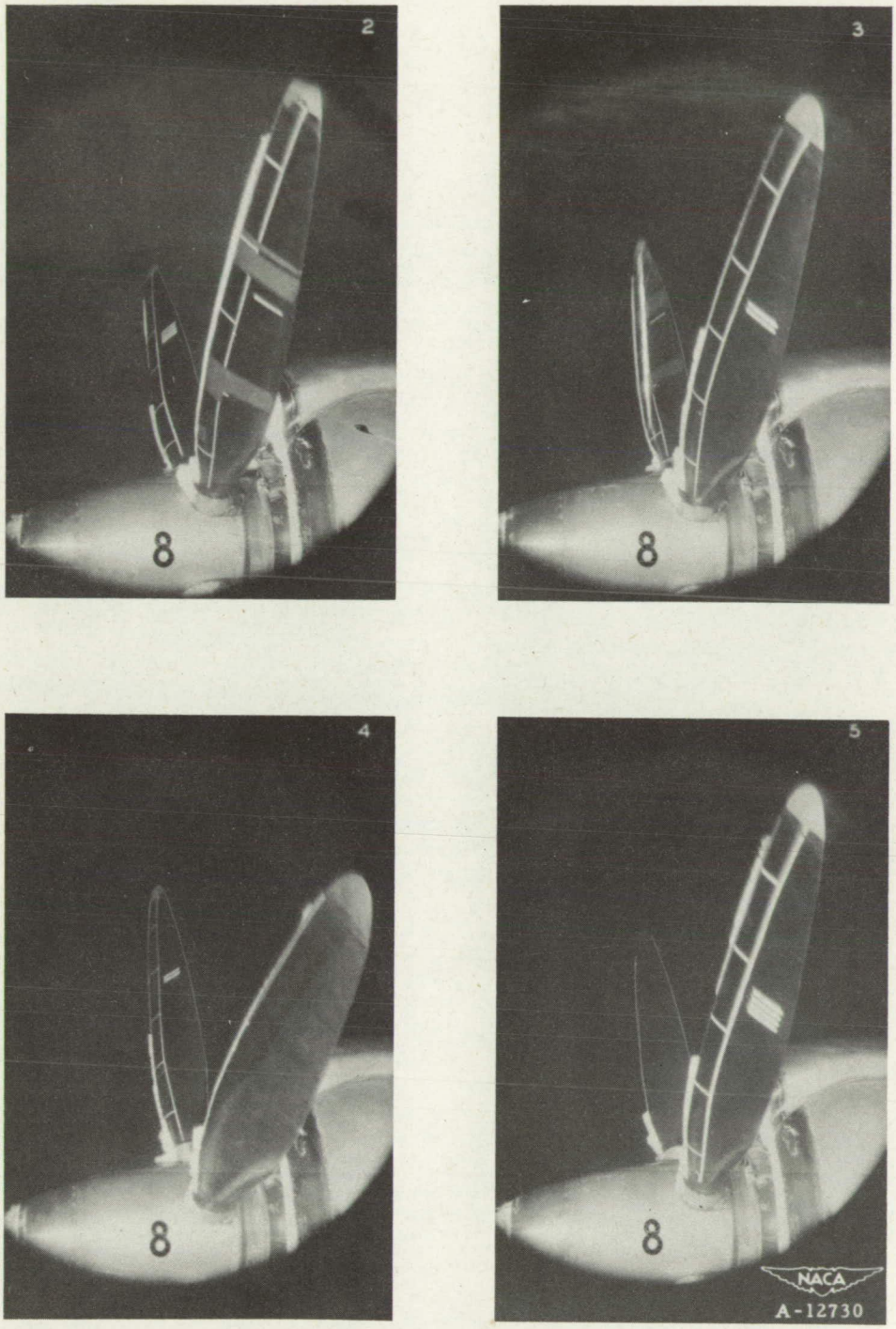

(a) Camber face.

Figure 24.– Ice formation of encounter 6. Peak efficiency loss, 4 percent.

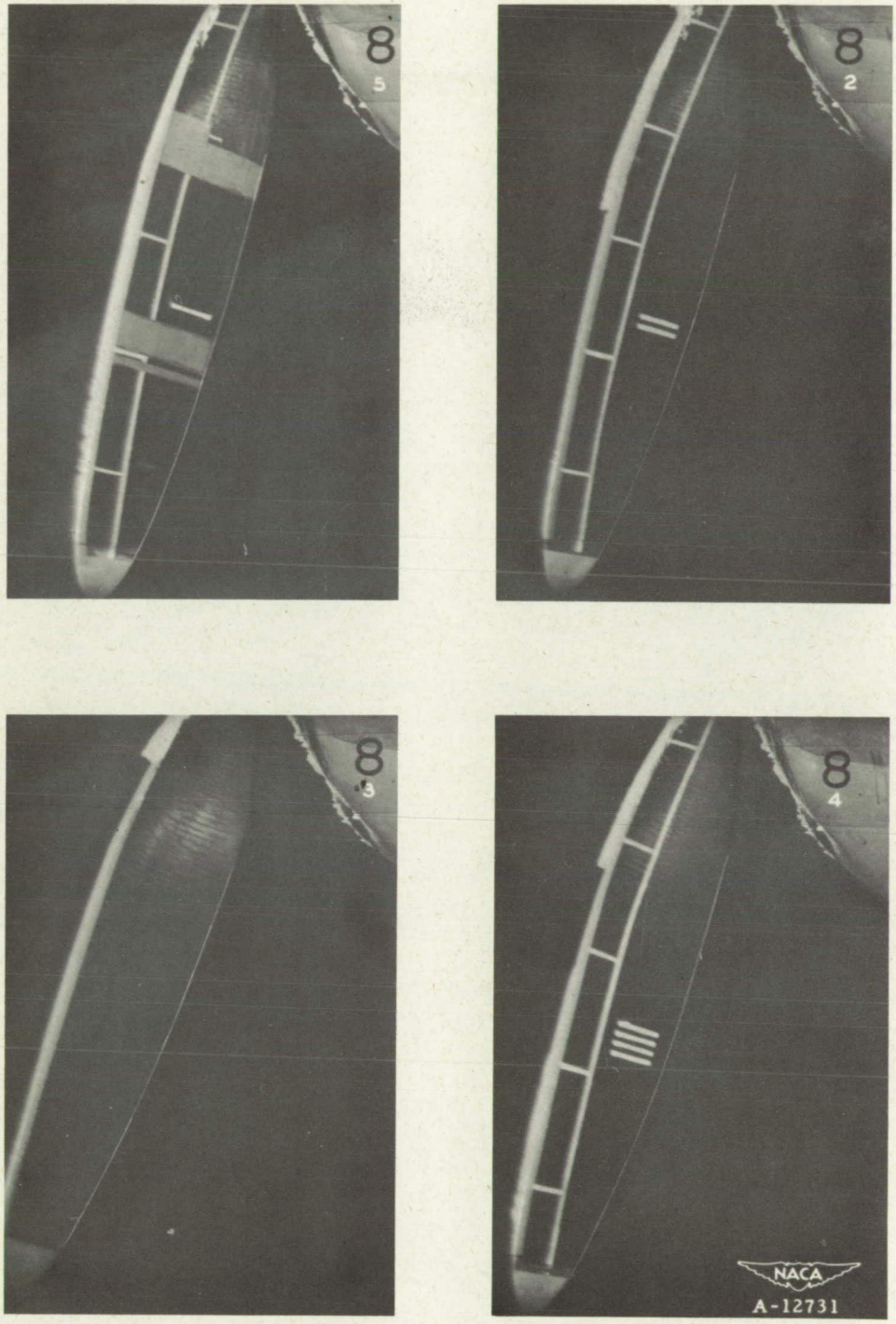

(b) Thrust face.

Figure 24.- Concluded.

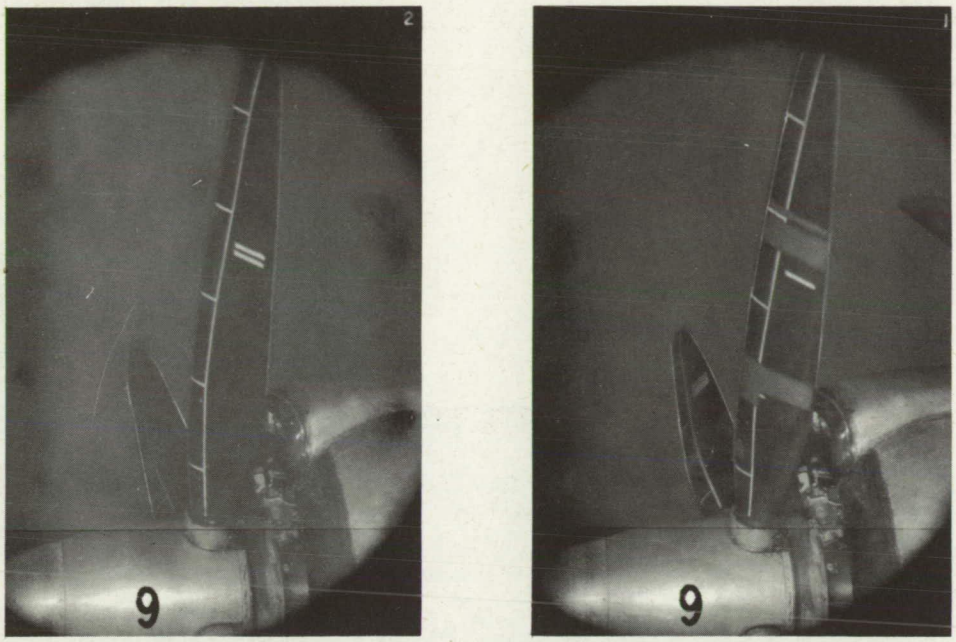

(a) Camber face.

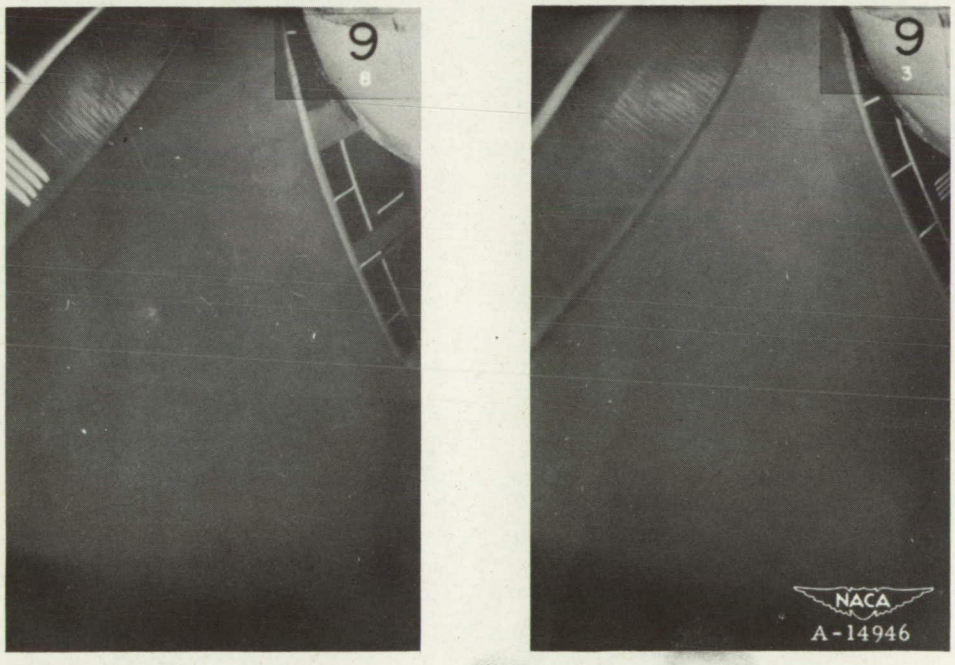

(b) Thrust face.

Figure 25.- Ice formation of encounter 7. Efficiency loss, 1 to 3 percent.

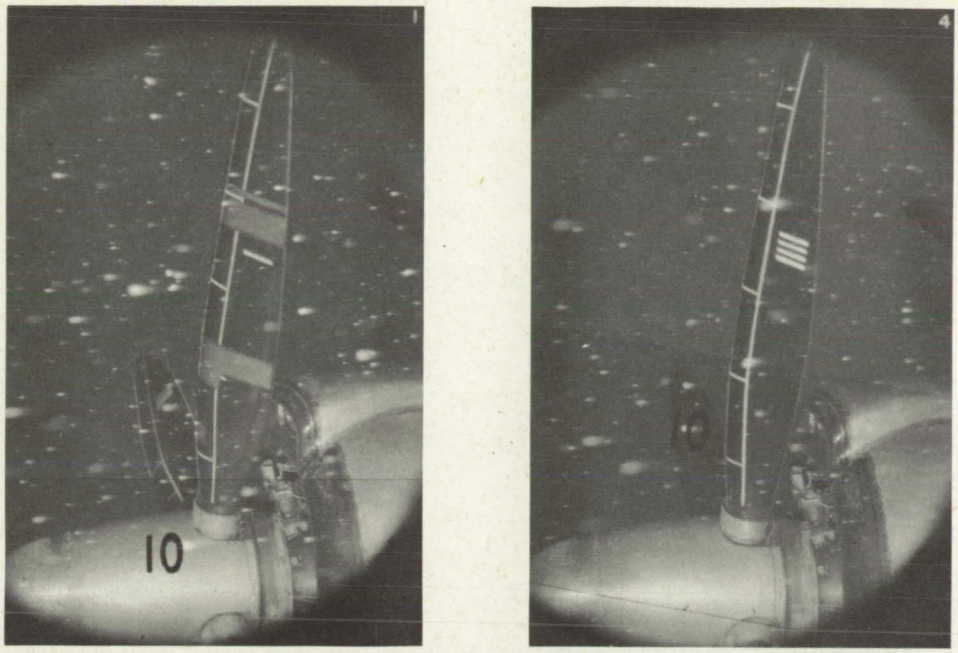

(a) Camber face.

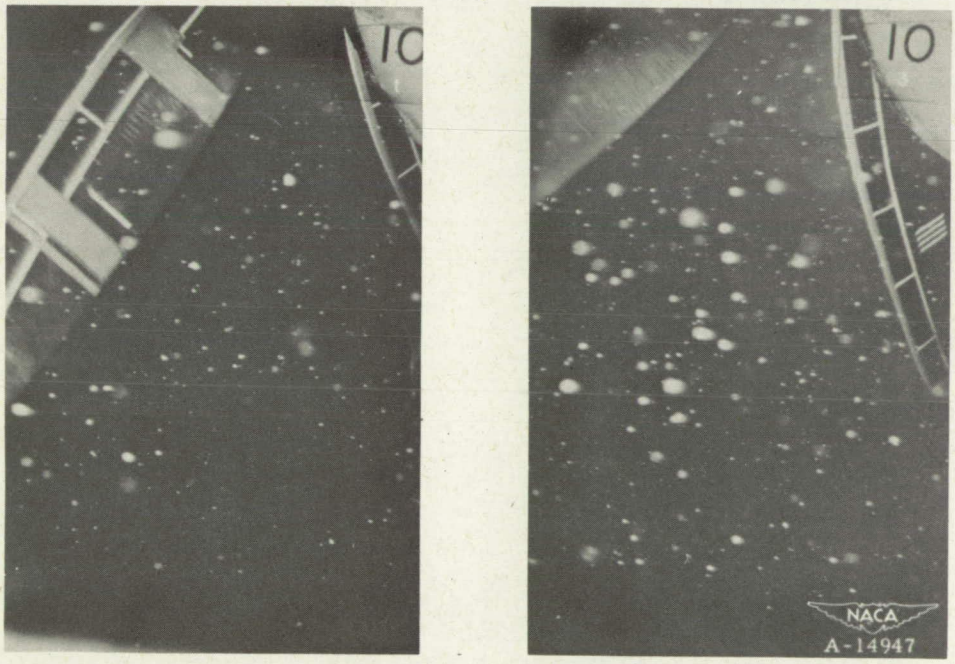

(b) Thrust face.

Figure 26.- Ice formation of encounter 8. Efficiency loss, 0 percent.

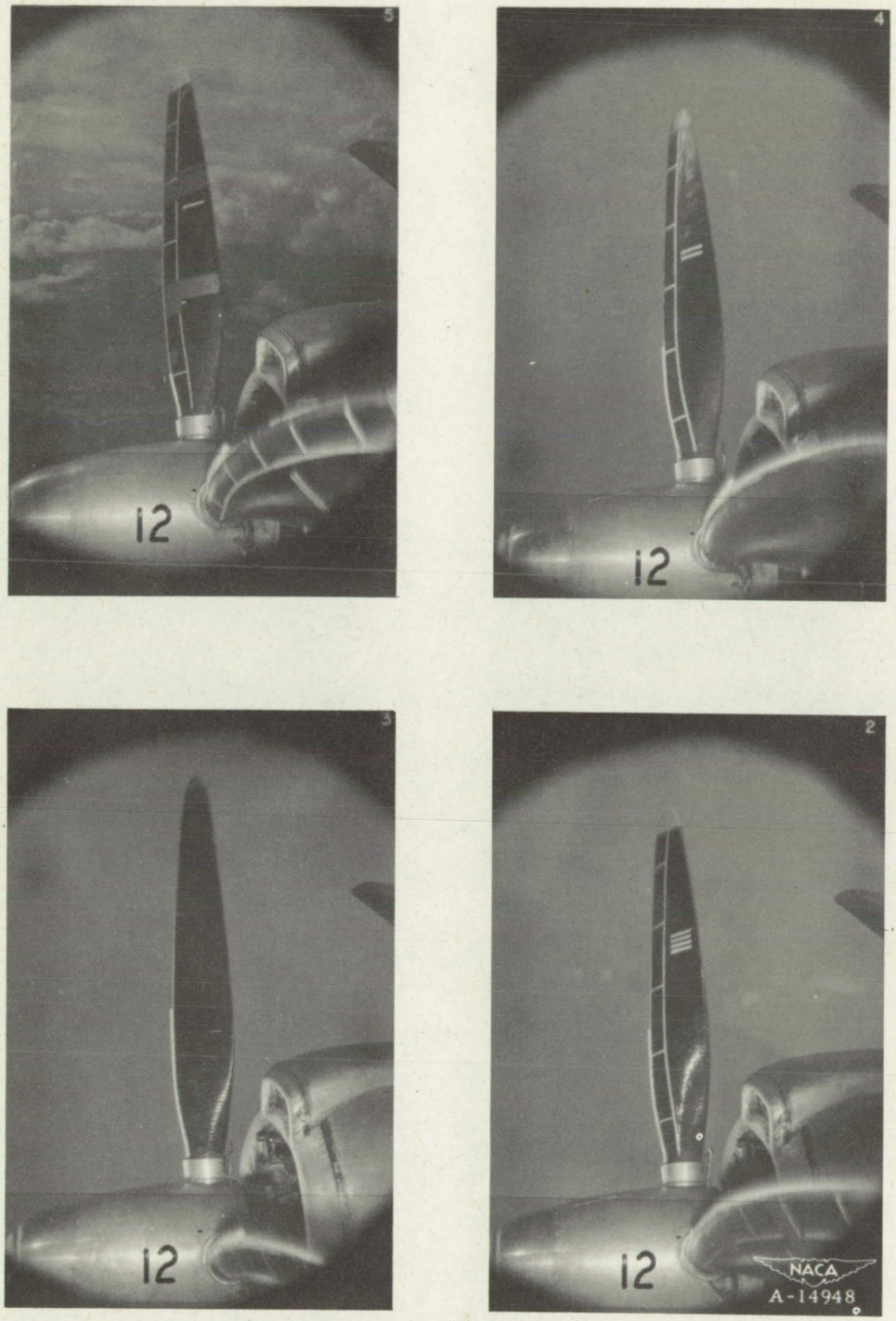

(a) Camber face.

Figure 27.– Ice formation of encounter 9. Efficiency loss, 1 to 4 percent.

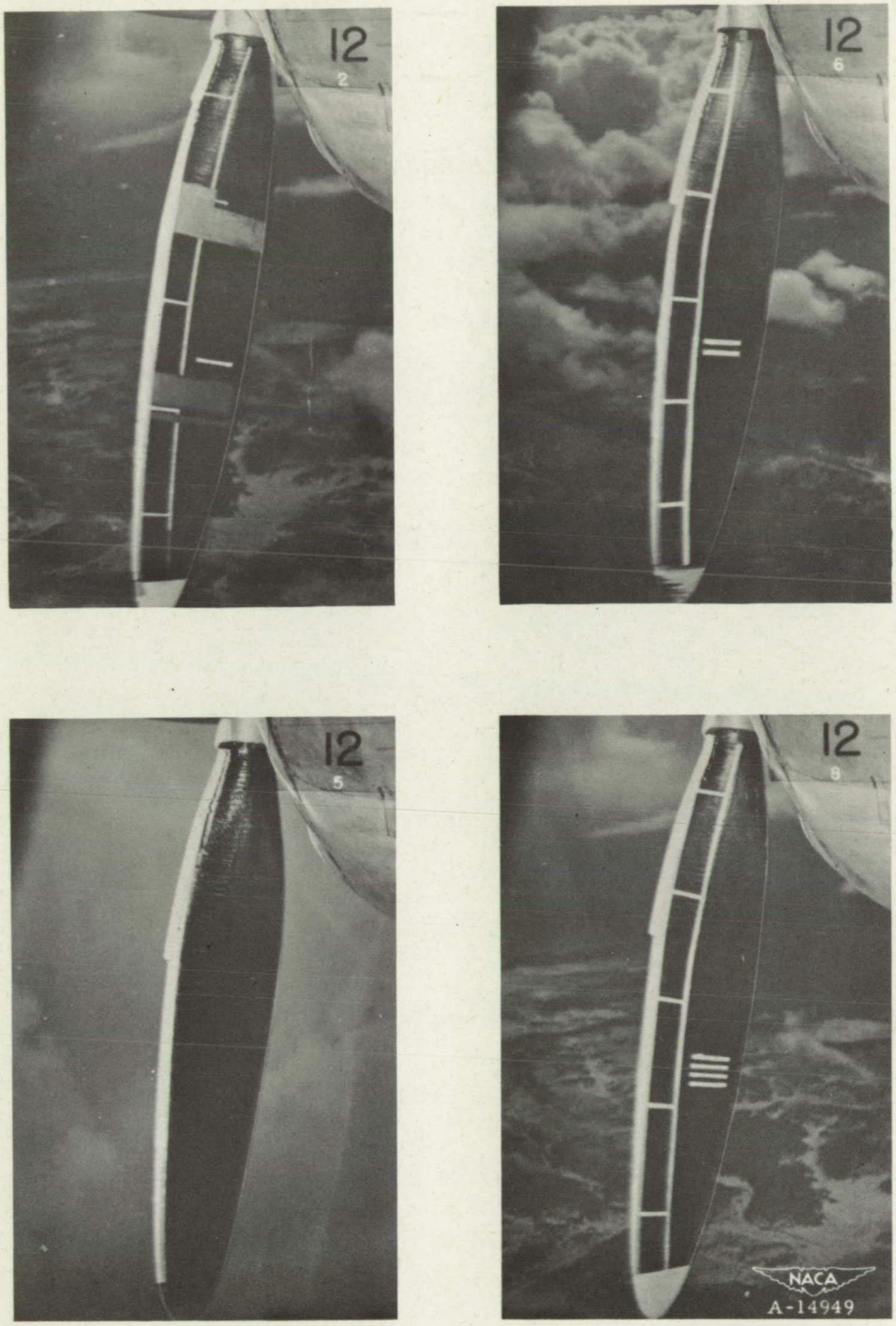

(b) Thrust face.

Figure 27.- Concluded.

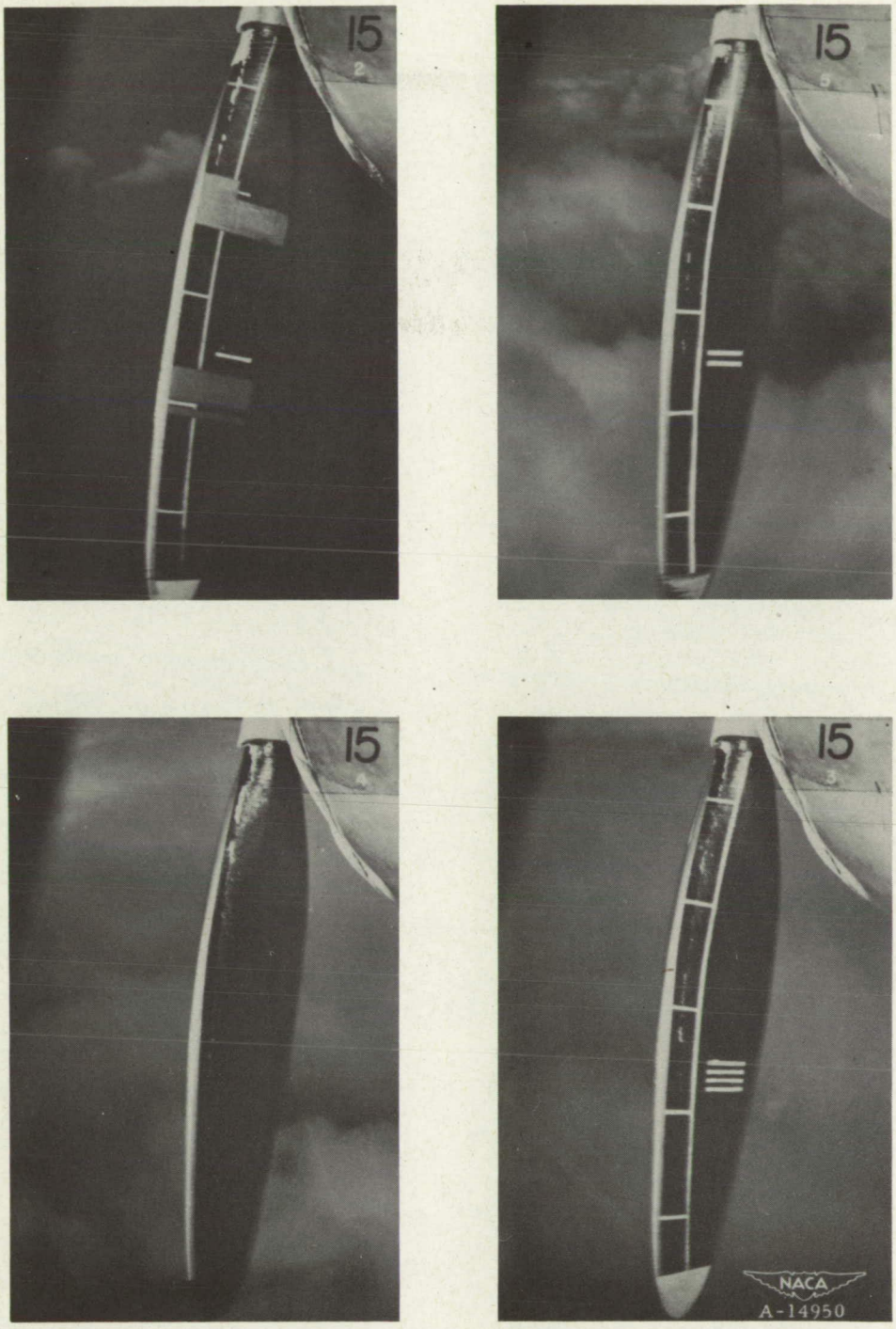

Figure 28.– Ice formation of encounter 10. Thrust face. Efficiency loss, 0 percent.

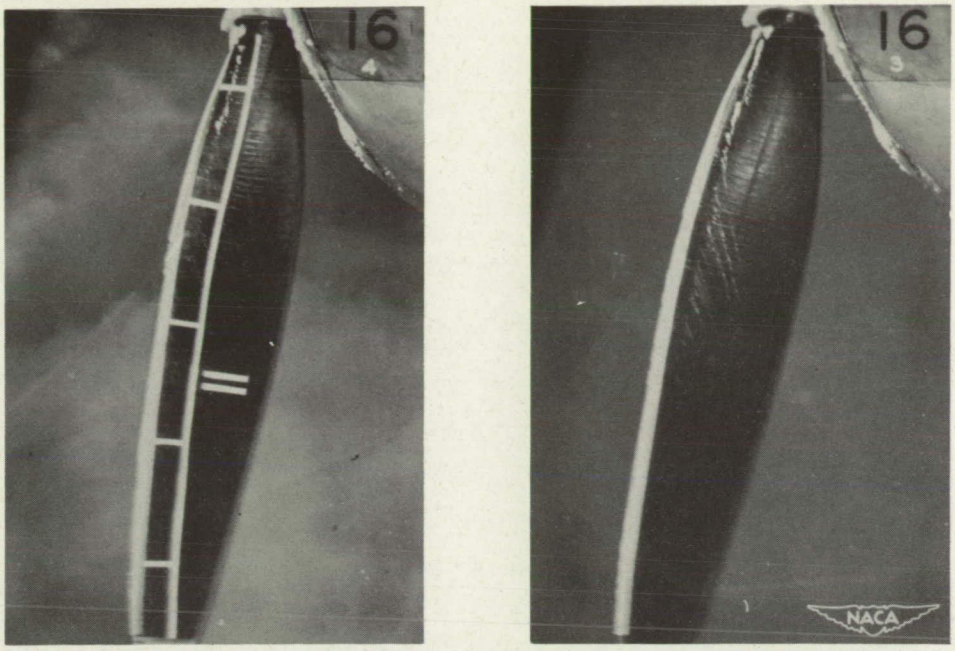

Figure 29.– Ice formation of encounter 10. Thrust face. Efficiency loss, 0 percent.

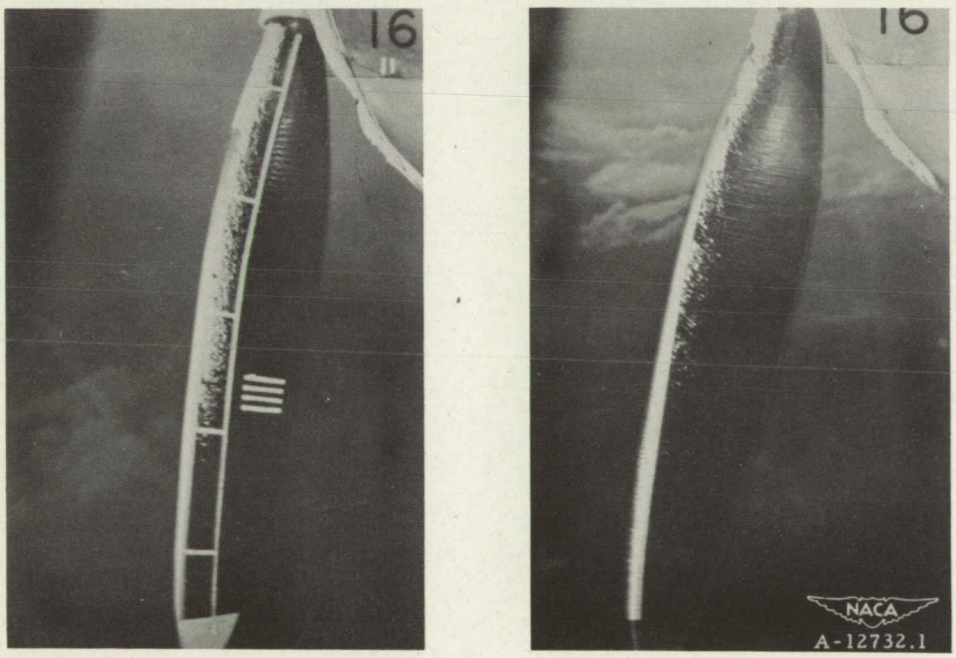

Figure 30.– Ice formation of encounter 11. Thrust face. Efficiency loss, 0 percent.

Figure 31.– Ice formation of encounter 12. Camber face. Efficiency loss, 5 percent.

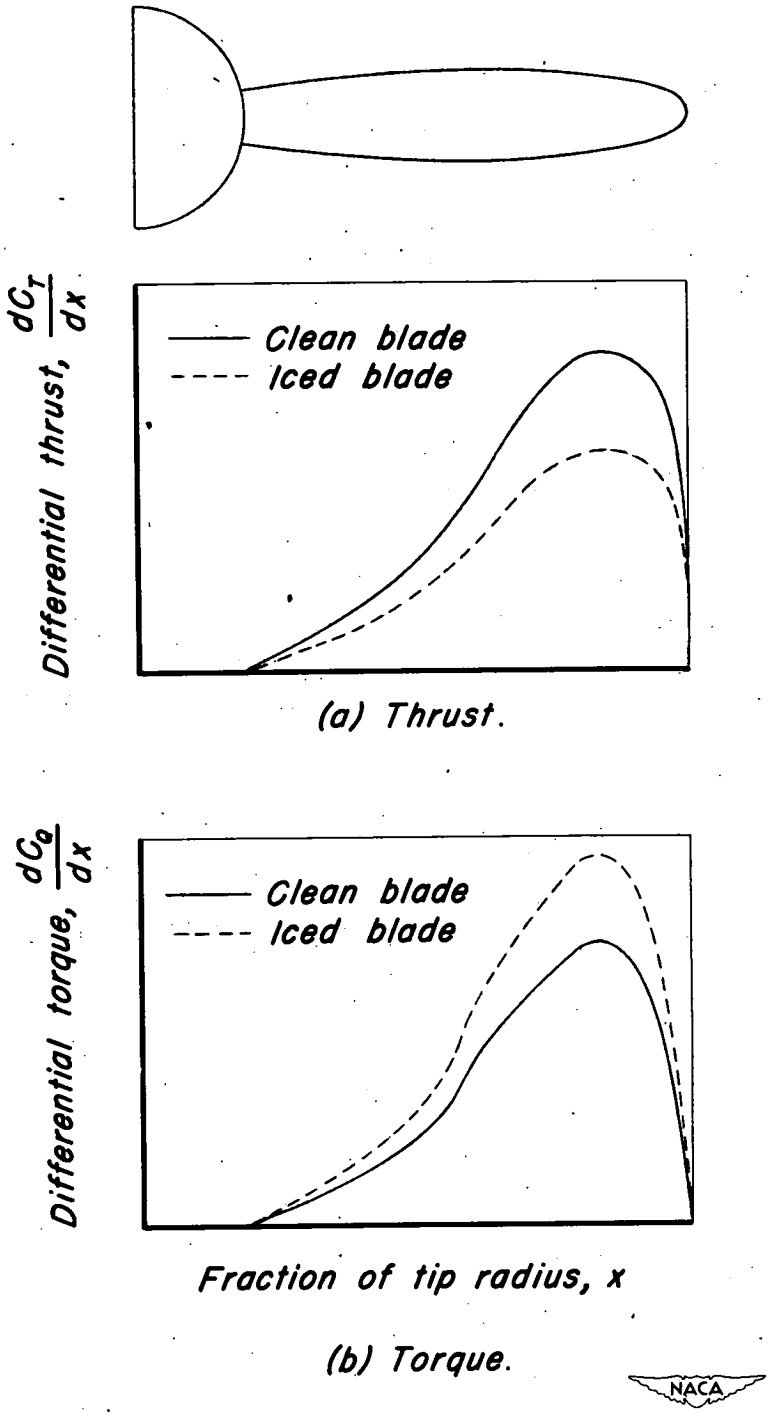

Figure 32.- Qualitative indication of changes in spanwise distribution of thrust and torque for a propeller with a full-span ice formation.

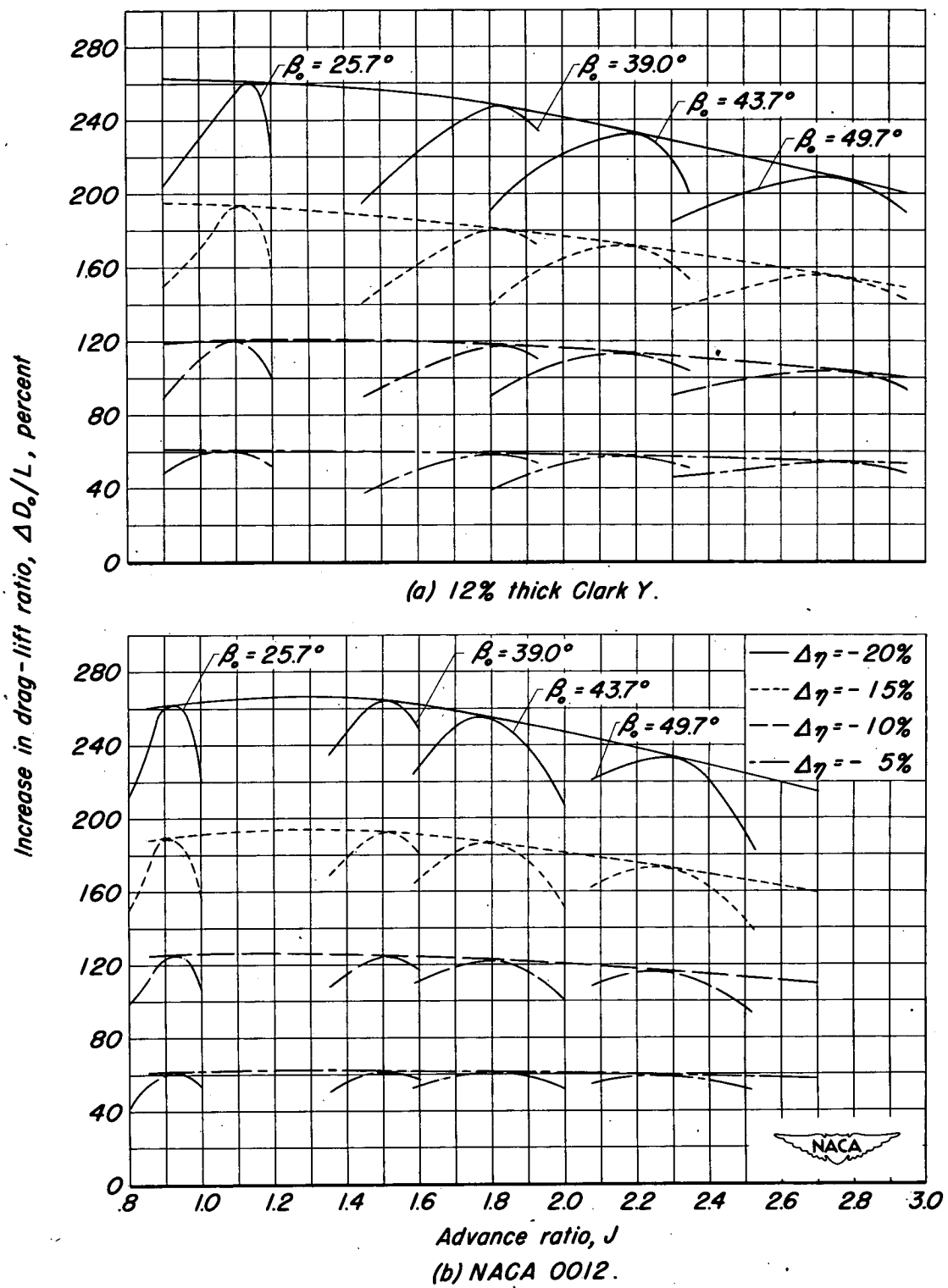

Figure 33.– Calculated curves of change in section drag-lift ratio for entire blade span required to produce various efficiency losses for two propellers composed of different airfoil sections.

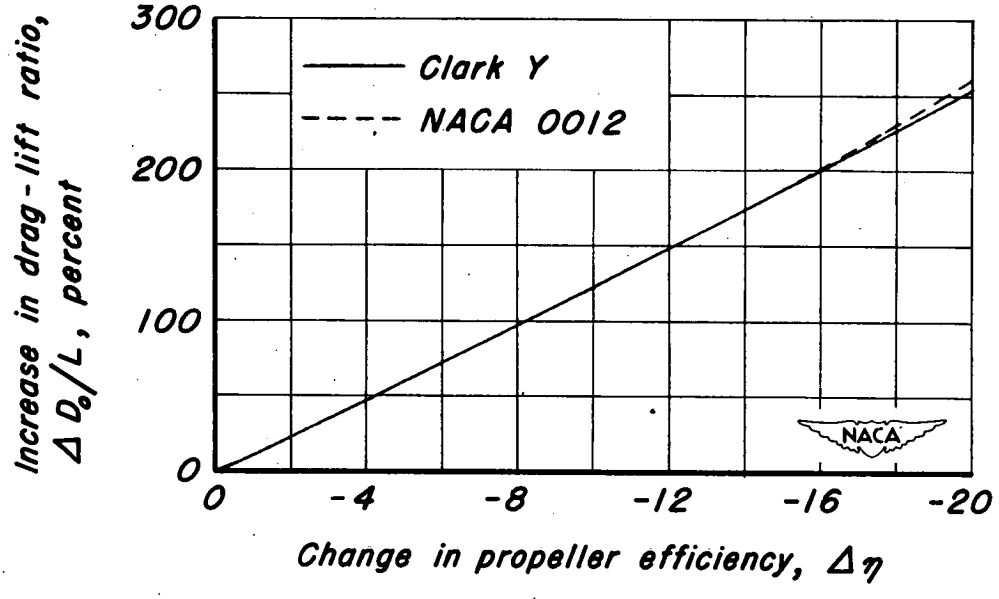

Figure 34.- The calculated variation of the maximum decrease in propeller efficiency with increase in over-all blade-element drag-lift ratio. Data not applicable for advance ratios greater than 2.

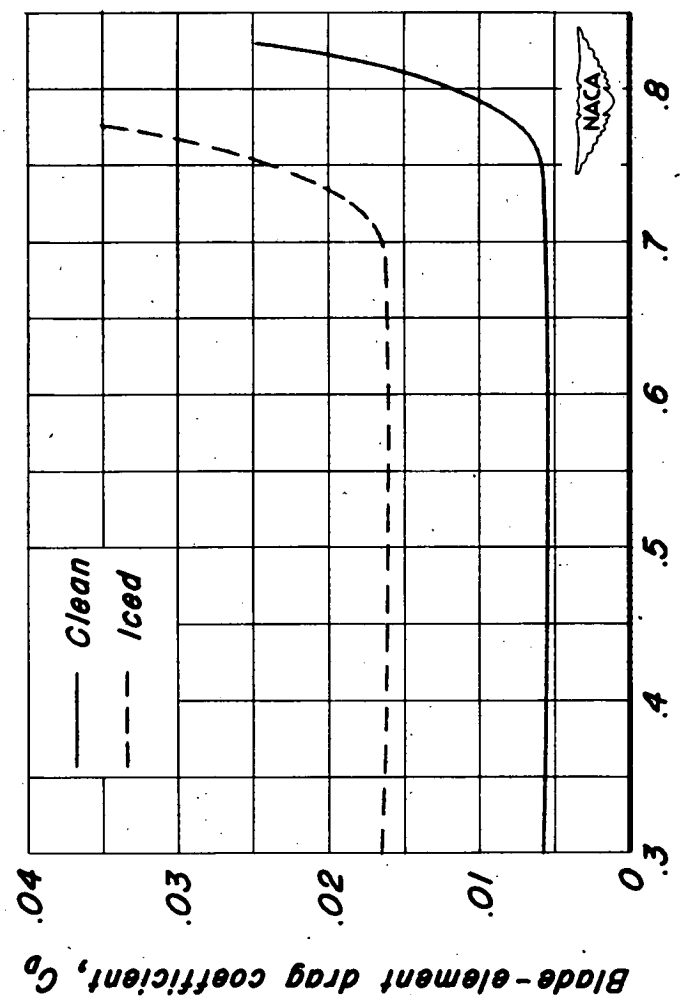

Figure 35.- Variation of blade-element drag coefficient with Mach number, as estimated from data of reference 12.

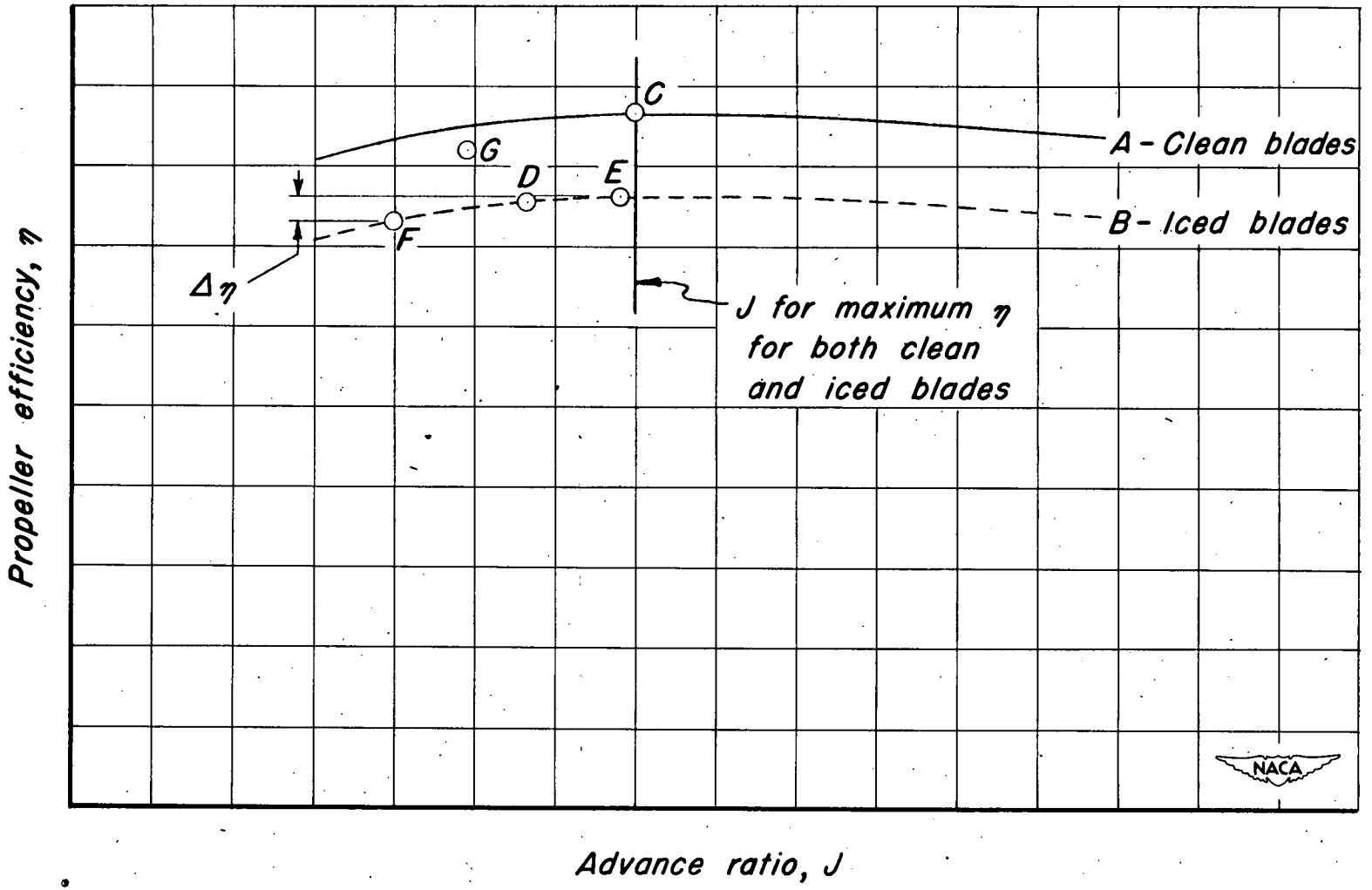

Figure 36. – Comparison of various propeller operating possibilities in conditions of icing.

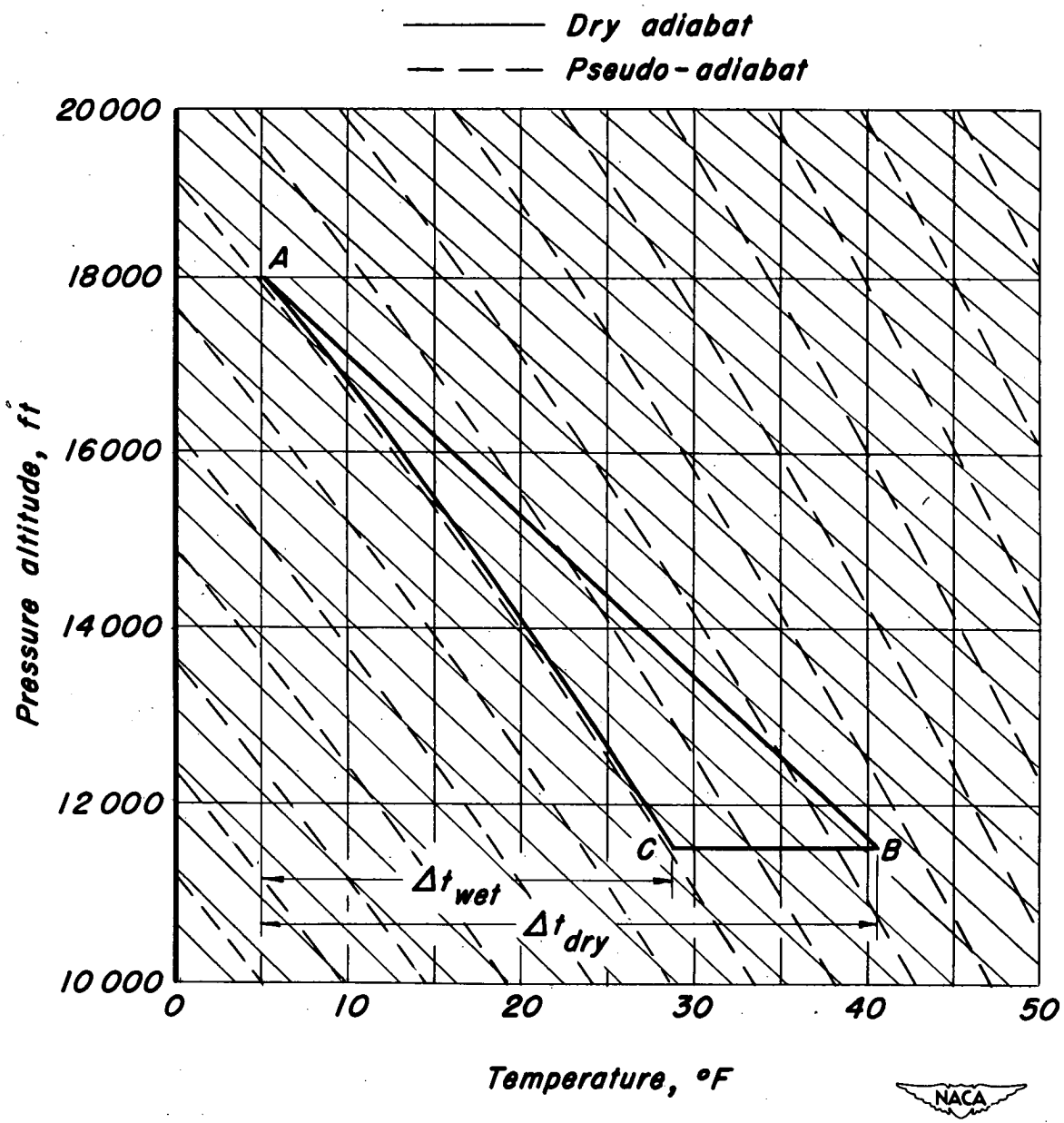

Figure 37.- Pseudo-adiabatic diagram showing procedure for computing kinetic-temperature rise at stagnation point in a cloud (wet air).

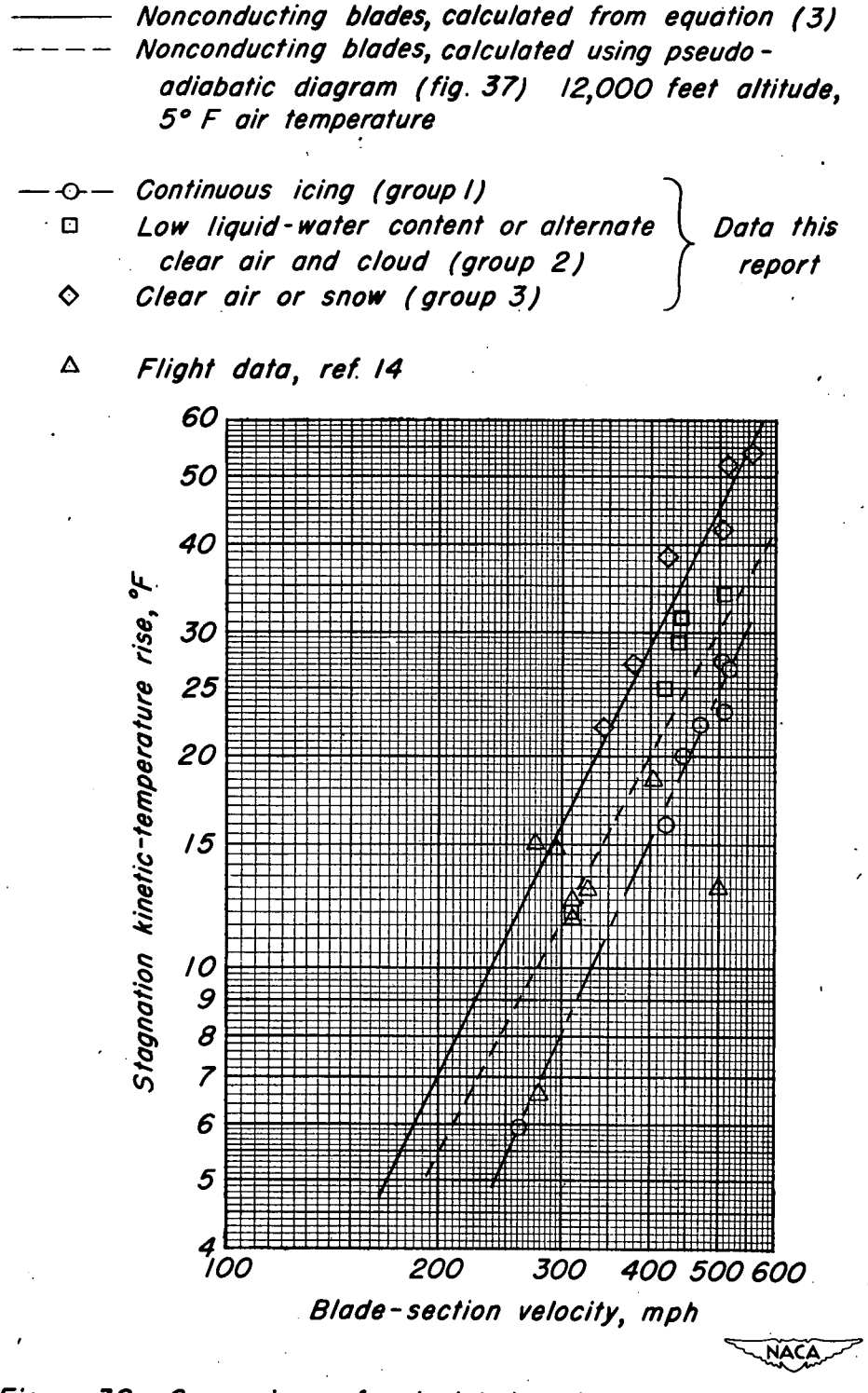

Figure 38.- Comparison of calculated and measured values of kinetic-temperature rise at stagnation line of a propeller blade as a function of blade-section velocity.

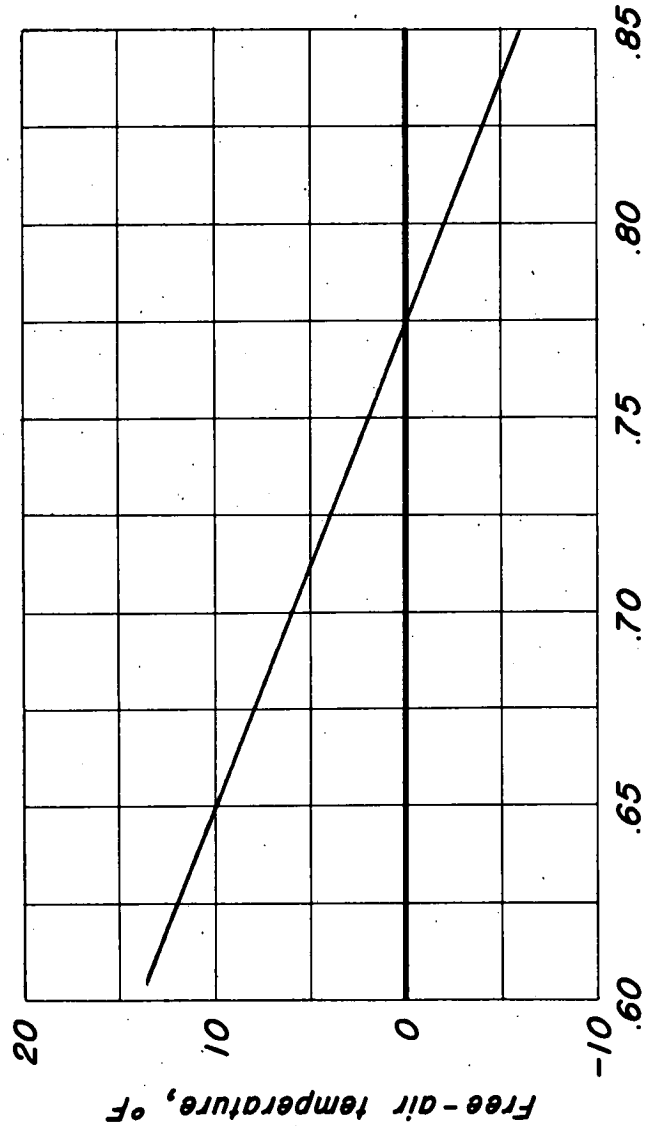

Figure 39.- Variation with blade-section Mach number of free-air temperature down to which ice formation will be prevented by kinetic heating.

$$\begin{vmatrix} \beta_{11}-\lambda & \beta_{12} & \beta_{13} & \cdots & \beta_{1n} \\ \beta_{21} & \beta_{22}-\lambda & \beta_{23} & \cdots & \beta_{2n} \\ \beta_{31} & \beta_{32} & \beta_{33}-\lambda & \cdots & \beta_{3n} \\ \cdots & \cdots & \cdots & \cdots & \cdots \\ \beta_{n1} & \beta_{n2} & \beta_{n3} & \cdots & \beta_{nn}-\lambda \end{vmatrix} = 0 \tag{11}$$

or

$$\left|\lambda I - \left[\beta_{ij}\right]\right| = 0 \tag{11a}$$

where

$$\lambda \equiv \frac{B_0}{m_0 \delta^4} \frac{1}{\omega^2}$$

The dynamical matrix is $\left[\beta_{ij}\right]$.

Coupled bending-torsion vibration. - The torsional and bending deflections due to coupled bending-torsion vibrations of a cantilever beam are given by (see appendix B):

$$\left.\begin{aligned} \theta_i &= \omega^2 \frac{m_0}{B_0} \delta^4 \sum_{j=1}^{n} \left(\Gamma \alpha_{ij} \theta_j + \epsilon \Gamma \gamma_{ij} \frac{y_j}{r_0} \right) \\ \frac{y_i}{r_0} &= \omega^2 \frac{m_0}{B_0} \delta^4 \sum_{j=1}^{n} \left(\delta_{ij} \theta_j + \beta_{ij} \frac{y_j}{r_0} \right) \end{aligned}\right\} \tag{12}$$

where

$$\epsilon \equiv \frac{r_0^2}{r_{g0}^2}$$

$$\Gamma \equiv \frac{1}{\delta^2} \frac{I_0}{C_0} \frac{B_0}{m_0}$$

r_0 absolute magnitude of projection of distance from elastic axis to center of gravity or perpendicular to bending direction for root section

r_{g0} radius of gyration about elastic axis at root section

Equations (2) and (8) define α_{ij} and β_{ij}. The quantities γ_{ij} and δ_{ij} are given by

$$\left.\begin{aligned}\gamma_{ij} &\equiv \sum_{k=1}^{i} \frac{1}{C_k}\left[S_k N'_{jk} - (k-1) S_k M'_{jk} + \sum_{r=k+1}^{n} S_r M'_{jr}\right] \\ \delta_{ij} &\equiv \sum_{k=1}^{i} \frac{1}{B_k}\left(S_k(iP_{jk}-Q_{jk}) + \sum_{r=k+1}^{n} S_r\left\{(i-k+\tfrac{1}{2})N_{jr} - \left[\frac{k^3-(k-1)^3}{3} - \frac{(2k-1)i}{2}\right]M_{jr}\right\}\right)\end{aligned}\right\} \quad (13)$$

where

$$P_{jk} \equiv \int_{k-1}^{k}\left[\frac{z^2}{2} - (k-1)z + \frac{1}{2}(k-1)^2\right] f_j(z)dz$$

$$Q_{jk} \equiv \int_{k-1}^{k}\left[\frac{z^3}{6} - \frac{1}{2}(k-1)^2 z + \frac{1}{3}(k-1)^3\right] f_j(z)dz$$

S_k is the ratio of average static mass unbalance of k^{th} interval to static mass unbalance at the root section.

The Station Numbers P_{jk} and Q_{jk} are listed in tables I to VIII with the other Station Numbers. The determinantal equation becomes

$$\begin{vmatrix} \Gamma\alpha_{11}-\lambda & \Gamma\alpha_{12} & \cdots & \Gamma\alpha_{1n} & \epsilon\Gamma\gamma_{11} & \epsilon\Gamma\gamma_{12} & \cdots & \epsilon\Gamma\gamma_{1n} \\ \Gamma\alpha_{21} & \Gamma\alpha_{22}-\lambda & \cdots & \Gamma\alpha_{2n} & \epsilon\Gamma\gamma_{21} & \epsilon\Gamma\gamma_{22} & \cdots & \epsilon\Gamma\gamma_{2n} \\ \cdots & \cdots & \cdots & \cdots & \cdots & \cdots & \cdots & \cdots \\ \Gamma\alpha_{n1} & \Gamma\alpha_{n2} & \cdots & \Gamma\alpha_{nn}-\lambda & \epsilon\Gamma\gamma_{n1} & \epsilon\Gamma\gamma_{n2} & \cdots & \epsilon\Gamma\gamma_{nn} \\ \delta_{11} & \delta_{12} & \cdots & \delta_{1n} & \beta_{11}-\lambda & \beta_{12} & \cdots & \beta_{1n} \\ \delta_{21} & \delta_{22} & \cdots & \delta_{2n} & \beta_{21} & \beta_{22}-\lambda & \cdots & \beta_{2n} \\ \cdots & \cdots & \cdots & \cdots & \cdots & \cdots & \cdots & \cdots \\ \delta_{n1} & \delta_{n2} & \cdots & \delta_{nn} & \beta_{n1} & \beta_{n2} & \cdots & \beta_{nn}-\lambda \end{vmatrix} = 0 \tag{14}$$

or

$$\left|\lambda I - \left[\eta_{ij}\right]\right| = 0 \tag{14a}$$

where $\left[\eta_{ij}\right]$ is the dynamical matrix and I is the identity matrix.

The first n roots of equation (14) will give the first n coupled frequencies.

APPLICATIONS AND RESULTS

In applying the previously discussed method, it is necessary to determine for a given beam the elements α_{ij}, β_{ij}, γ_{ij}, and δ_{ij} of the dynamical matrices. These quantities will depend on the physical properties of the beam and on the number of stations chosen. If the physical properties of the beam are known, the quantities α_{ij}, β_{ij}, γ_{ij}, and δ_{ij} can be directly calculated from equations (2), (8), and (13). The numbers M_{jk}, N_{jk}, P_{jk}, Q_{jk}, M'_{jk}, N'_{jk}, P'_{jk}, and Q'_{jk} appearing in these equations depend on the number of stations n that are used and can be read directly from tables I to VIII for any given number of stations up to eight. Once these quantities have been calculated, equations (6), (11), or (14) can be solved for the frequencies by any method desired. The

matrix-iteration method used herein is simple and rapid and requires no particular computing skill. As will be indicated, however, the accuracy of equations (6), (11), and (14) is such that relatively few stations need be used, in which case it may be convenient to expand the determinants and to solve the resultant low-order algebraic equation.

In order to illustrate the accuracy, this method was applied to torsional vibrations, bending vibrations, and coupled vibrations of a uniform cantilever beam. The exact theoretical values for torsional vibrations and bending vibrations of uniform cantilevers are well known. The exact theoretical values for the coupled bending-torsion vibration of a uniform beam were calculated (appendix D). A comparison was then made between the values obtained by the method presented and the exact theoretical values. The number of stations used was 1, 2, and 3 ($n = 1$, $n = 2$, and $n = 3$). The comparisons are summarized in table IX.

Torsional vibration. - For the case of a uniform beam, $C_k = I_k = 1$ and equation (2) becomes

$$\alpha_{ij} = \sum_{k=1}^{i} \left[N_{jk} - (k-1) M_{jk} + \sum_{r=k+1}^{n} M_{jr} \right] \tag{15}$$

The values of N_{jk} and M_{jk} are given in tables I to VIII. The table to be used depends on the choice of the number of stations.

Let $n = 1$

$$\therefore \alpha_{11} = N_{11}$$

From table I, $N_{11} = 5/12$

$$\therefore \alpha_{11} = 5/12$$

and

$$\theta_1 = \frac{5}{12} l^2 \frac{I_0}{C_0} \omega^2 \theta_1$$

or

$$\omega^2 = \frac{12}{5}\frac{C_0}{I_0 l^2} = 2.400\frac{C_0}{I_0 l^2}$$

$$\omega = 1.549\sqrt{\frac{C_0}{I_0 l^2}}$$

The exact theoretical value for the first torsional frequency is

$$\omega = 1.571\sqrt{\frac{C_0}{I_0 l^2}}$$

The error is -1.4 percent when only one station is used.

The mode shape obtained by the method of Station Functions agrees well with the theoretical mode shape, as is shown in figure 2(a).

Let $n = 2$, then by equation (15) and table II

$$\alpha_{11} = N_{11} + M_{12} = \frac{8}{15} + \frac{5}{12} = \frac{57}{60}$$

$$\alpha_{12} = N_{21} + M_{22} = -\frac{31}{240} + \frac{29}{48} = \frac{57}{120}$$

$$\alpha_{21} = N_{11} + N_{12} = \frac{8}{15} + \frac{8}{15} = \frac{16}{15}$$

$$\alpha_{22} = N_{21} + N_{22} = -\frac{31}{240} + \frac{239}{240} = \frac{13}{15}$$

The determinantal equation then becomes

$$\begin{vmatrix} \frac{57}{60} - \lambda & \frac{57}{120} \\ \frac{16}{15} & \frac{13}{15} - \lambda \end{vmatrix} = 0$$

which gives

$$\lambda_1 = 1.6214$$

$$\lambda_2 = 0.1953$$

Therefore

$$\omega_1 = 1.571\sqrt{\frac{C_0}{I_0 l^2}}$$

$$\omega_2 = 4.526\sqrt{\frac{C_0}{I_0 l^2}}$$

The exact theoretical values are

$$\omega_1 = 1.571\sqrt{\frac{C_0}{I_0 l^2}}$$

$$\omega_2 = 4.712\sqrt{\frac{C_0}{I_0 l^2}}$$

The percentage error of the first two modes, for only two stations, is found to be 0 and -4 percent.

The mode shapes are shown in figures 2(b) and 2(c). Agreement of the first mode with the exact theoretical shape is excellent; the second mode agrees fairly well.

Let $n = 3$, then by equation (15) and table III

$$\alpha_{11} = N_{11} + M_{12} + M_{13} = 0.945833$$

$$\alpha_{12} = N_{21} + M_{22} + M_{23} = 0.958333$$

$$\alpha_{13} = N_{31} + M_{32} + M_{33} = 0.520834$$

$$\alpha_{21} = N_{11} + N_{12} + 2M_{13} = 1.033333$$

$$\alpha_{22} = N_{21} + N_{22} + 2M_{23} = 1.883333$$

$$\alpha_{23} = N_{31} + N_{32} + 2M_{33} = 1.011113$$

$$\alpha_{31} = N_{11} + N_{12} + N_{13} = 1.012500$$

$$\alpha_{32} = N_{21} + N_{22} + N_{23} = 2.025000$$

$$\alpha_{33} = N_{31} + N_{32} + N_{33} = 1.387501$$

The determinantal equation is

$$\begin{vmatrix} 0.945833-\lambda & 0.958333 & 0.520834 \\ 1.033333 & 1.883333-\lambda & 1.011113 \\ 1.012500 & 2.025000 & 1.387501-\lambda \end{vmatrix} = 0$$

The solutions are

$$\lambda_1 = 3.6474$$

$$\lambda_2 = 0.4093$$

$$\lambda_3 = 0.1599$$

Therefore

$$\omega_1 = 1.571\sqrt{\frac{C_0}{I_0 l^2}}$$

$$\omega_2 = 4.689\sqrt{\frac{C_0}{I_0 l^2}}$$

$$\omega_3 = 7.502\sqrt{\frac{C_0}{I_0 l^2}}$$

The exact theoretical values are

$$\omega_1 = 1.571\sqrt{\frac{c_0}{I_0 l^2}}$$

$$\omega_2 = 4.712\sqrt{\frac{c_0}{I_0 l^2}}$$

$$\omega_3 = 7.854\sqrt{\frac{c_0}{I_0 l^2}}$$

The percentage errors of the first three modes, calculated by use of three stations, are found to be 0, -0.5, and -4.5 percent, respectively.

The mode shapes are shown in figures 2(d) to 2(f). The first two modes agree very well with the theoretical shapes; agreement of the third mode is fair.

This procedure can be carried out as shown for any number of stations desired.

Bending vibrations. - For a uniform beam, $B_k = m_k = 1$ and equation (8) becomes

$$\beta_{ij} = \sum_{k=1}^{i} \left\{ iP'_{jk} - Q'_{jk} + \sum_{r=k+1}^{n} \left[\left(i-k+\frac{1}{2}\right) N'_{jr} + \left(\frac{k^3-(k-1)^3}{3} - \frac{(2k-1)}{2} i \right) M'_{jr} \right] \right\} \tag{16}$$

Let $n = 1$

$$\therefore \beta_{11} = P'_{11} - Q'_{11}$$

and from table I

$$\beta_{11} = \frac{71}{630} - \frac{31}{1008} = \frac{59}{720}$$

Therefore, from equation (7)

$$\omega = 3.493\sqrt{\frac{B_0}{m_0 l^4}}$$

The exact theoretical value is

$$\omega = 3.516\sqrt{\frac{B_0}{m_0 l^4}}$$

The percentage error for just one station is found to be -0.65 percent.

The mode shape is shown in figure 3(a) and is seen to agree very well with the theoretically exact shape.

Let n = 2; then by equation (16) and table II

$$\beta_{11} = P'_{11} - Q'_{11} + \frac{1}{2}N'_{12} - \frac{1}{6}M'_{12} = 0.422745$$

$$\beta_{12} = P'_{21} - Q'_{21} + \frac{1}{2}N'_{22} - \frac{1}{6}M'_{22} = 0.295925$$

$$\beta_{21} = 2P'_{11} + 2P'_{12} - Q'_{11} - Q'_{12} + \frac{3}{2}N'_{12} - \frac{2}{3}M'_{12} = 1.145167$$

$$\beta_{22} = 2P'_{21} + 2P'_{22} - Q'_{21} - Q'_{22} + \frac{3}{2}N'_{22} - \frac{2}{3}M'_{22} = 0.905530$$

The characteristic equation is

$$\begin{vmatrix} 0.422745-\lambda & 0.295925 \\ 1.145167 & 0.905530-\lambda \end{vmatrix} = 0$$

The roots are

$$\lambda_1 = 1.2943$$

$$\lambda_2 = 0.0339$$

$$\therefore \omega_1 = 3.516\sqrt{\frac{B_0}{m_0 l^4}}$$

$$\omega_2 = 21.71\sqrt{\frac{B_0}{m_0 l^4}}$$

The exact theoretical values are

$$\omega_1 = 3.516\sqrt{\frac{B_0}{m_0 l^4}}$$

$$\omega_2 = 22.04\sqrt{\frac{B_0}{m_0 l^4}}$$

The percentage error for two stations is therefore found to be 0 for the first mode and -1.5 percent for the second mode. The mode shapes are plotted in figures 3(b) and 3(c). The first mode agrees excellently with the theoretically exact shape; the second mode agrees fairly well.

Let n = 3, then by equation (16) and table III

$$\beta_{11} = P'_{11} - Q'_{11} + \frac{1}{2}N'_{12} + \frac{1}{2}N'_{13} - \frac{1}{6}M'_{12} - \frac{1}{6}M'_{13} = 0.270604$$

$$\beta_{12} = P'_{21} - Q'_{21} + \frac{1}{2}N'_{22} + \frac{1}{2}N'_{23} - \frac{1}{6}M'_{22} - \frac{1}{6}M'_{23} = 1.009943$$

$$\beta_{13} = P'_{31} - Q'_{31} + \frac{1}{2}N'_{32} + \frac{1}{2}N'_{33} - \frac{1}{6}M'_{32} - \frac{1}{6}M'_{33} = 0.487441$$

$$\beta_{21} = 2P'_{11}+2P'_{12}-Q'_{11}-Q'_{12}+\frac{3}{2}N'_{12}+2N'_{13}-\frac{2}{3}M'_{12}-\frac{4}{3}M'_{13} = 0.648170$$

$$\beta_{22} = 2P'_{21}+2P'_{22}-Q'_{21}-Q'_{22}+\frac{3}{2}N'_{22}+2N'_{23}-\frac{2}{3}M'_{22}-\frac{4}{3}M'_{23} = 3.266250$$

$$\beta_{23} = 2P'_{31}+2P'_{32}-Q'_{31}-Q'_{32}+\frac{3}{2}N'_{32}+2N'_{33}-\frac{2}{3}M'_{32}-\frac{4}{3}M'_{33} = 1.689891$$

$$\beta_{31} = 3P'_{11}+3P'_{12}+3P'_{13}-Q'_{11}-Q'_{12}-Q'_{13}+\frac{5}{2}N'_{12}+4N'_{13}-\frac{7}{6}M'_{12}-\frac{10}{3}M'_{13} = 0.985135$$

$$\beta_{32} = 3P'_{21}+3P'_{22}+3P'_{23}-Q'_{21}-Q'_{22}-Q'_{23}+\frac{5}{2}N'_{22}+4N'_{23}-\frac{7}{6}M'_{22}-\frac{10}{3}M'_{23} = 5.822852$$

$$\beta_{33} = 3P'_{31}+3P'_{32}+3P'_{33}-Q'_{31}-Q'_{32}-Q'_{33}+\frac{5}{2}N'_{32}+4N'_{33}-\frac{7}{6}M'_{32}-\frac{10}{3}M'_{33} = 3.204301$$

The characteristic equation is

$$\begin{vmatrix} 0.270604-\lambda & 1.009943 & 0.487441 \\ 0.648170 & 3.266250-\lambda & 1.689891 \\ 0.985135 & 5.822852 & 3.204301-\lambda \end{vmatrix} = 0$$

The roots are

$$\lambda_1 = 6.5521$$

$$\lambda_2 = 0.1667$$

$$\lambda_3 = 0.0223$$

Therefore

$$\omega_1 = 3.516\sqrt{\frac{B_0}{m_0 l^4}}$$

$$\omega_2 = 22.04\sqrt{\frac{B_0}{m_0 l^4}}$$

$$\omega_3 = 60.20\sqrt{\frac{B_0}{m_0 l^4}}$$

The exact values are

$$\omega_1 = 3.516\sqrt{\frac{B_0}{m_0 l^4}}$$

$$\omega_2 = 22.04\sqrt{\frac{B_0}{m_0 l^4}}$$

$$\omega_3 = 61.70\sqrt{\frac{B_0}{m_0 l^4}}$$

The percentage error for three stations is found to be 0, 0, and -2.4 percent, respectively. The modes are plotted in figures 3(d) to 3(f). The first two modes are seen to agree very well with the theoretical mode shape; agreement of the third mode is fair.

Coupled bending-torsion vibrations. - A uniform beam with the following constants was chosen:

$$\gamma = \frac{\omega_t^2}{\omega_b^2} = 38.56$$

$$\epsilon = 0.8$$

$$\Gamma = \frac{n^2}{193.2}$$

$$\epsilon\Gamma = \frac{n^2}{241.5}$$

The values of α_{ij} and β_{ij} are obtained as previously and are the same as given before for $n = 1$, $n = 2$, and $n = 3$. Also, because $S_k = B_k = C_k = m_k = I_k = 1$, equation (13) becomes

$$\gamma_{ij} = \sum_{k=1}^{i} \left[N'_{jk} - (k-1) M'_{jk} + \sum_{r=k+1}^{n} M'_{jr} \right]$$

$$\delta_{ij} = \sum_{k=1}^{i} \left\{ iP_{jk} - Q_{jk} + \sum_{r=k+1}^{n} \left[\left(i-k+\frac{1}{2}\right) N_{jr} + \left(\frac{k^3-(k-1)^3}{3} - \frac{2k-1}{2} i \right) M_{jr} \right] \right\}$$

Let $n = 1$, then the determinant is

$$\begin{vmatrix} \Gamma\alpha_{11}-\lambda & \epsilon\Gamma\gamma_{11} \\ \delta_{11} & \beta_{11}-\lambda \end{vmatrix} = \begin{vmatrix} 0.002156-\lambda & 0.001196 \\ 0.111111 & 0.081944-\lambda \end{vmatrix} = 0$$

The roots are

$$\lambda_1 = 0.0837$$

$$\lambda_2 = 0.0005$$

$$\omega_1 = 3.46\sqrt{\frac{B_0}{m_0 l^4}}$$

$$\omega_2 = 44.7\sqrt{\frac{B_0}{m_0 l^4}}$$

The procedure for calculating the exact theoretical values is derived in appendix D. The exact values are

$$\omega_1 = 3.49\sqrt{\frac{B_0}{m_0 l^4}}$$

$$\omega_2 = 20.6\sqrt{\frac{B_0}{m_0 l^4}}$$

$$\omega_3 = 49.1\sqrt{\frac{B_0}{m_0 l^4}}$$

The percentage error for the first mode, calculated by use of one station, is -0.9 percent.

Let $n = 2$, then the determinant is

$$\begin{vmatrix} \Gamma\alpha_{11}-\lambda & \Gamma\alpha_{12} & \epsilon\Gamma\gamma_{11} & \epsilon\Gamma\gamma_{12} \\ \Gamma\alpha_{21} & \Gamma\alpha_{22}-\lambda & \epsilon\Gamma\gamma_{21} & \epsilon\Gamma\gamma_{22} \\ \delta_{11} & \delta_{12} & \beta_{11}-\lambda & \beta_{12} \\ \delta_{21} & \delta_{22} & \beta_{21} & \beta_{22}-\lambda \end{vmatrix} = 0$$

Substituting the known values and solving for λ gives for the first two roots

$$\lambda_1 = 1.3197$$

$$\lambda_2 = 0.0412$$

and the frequencies become

$$\omega_1 = 3.48\sqrt{\frac{B_0}{m_0 l^4}}$$

$$\omega_2 = 19.7\sqrt{\frac{B_0}{m_0 l^4}}$$

The percentage errors for two stations are:

-0.3 percent for the first mode

-4.4 percent for the second mode

This procedure can be carried out for any number of stations desired. For three stations, the frequencies obtained are

$$\omega_1 = 3.48\sqrt{\frac{B_0}{m_0 l^4}}$$

$$\omega_2 = 20.6\sqrt{\frac{B_0}{m_0 l^4}}$$

$$\omega_3 = 48.2\sqrt{\frac{B_0}{m_0 l^4}}$$

The percentage errors are

-0.3 percent for the first mode

0 percent for the second mode

-1.8 percent for the third mode

The results obtained by the method presented are seen to agree very well with the exact theoretical values.

These results are summarized in table IX, where a comparison is also made with the results obtained for uncoupled bending and torsional vibrations by use of influence coefficients with weighted matrices (reference 12). The values using weighted matrices were taken from table I of reference 12. It can be seen that for a given number of stations, the results obtained by the method presented herein are considerably better than those obtained by using influence coefficients with weighted matrices. In general, it is indicated that for a uniform cantilever beam using n stations along the beams, the first $n - 1$ frequencies and modes are in excellent agreement with exact theoretical values and even the n^{th} mode is given within the accuracy with which the physical properties of the material are known. For a tapered beam, more stations may be required, depending on the amount of taper. The number of stations required to give satisfactory accuracy is listed in table X. A comparison is also made by using weighted influence coefficients; the values are taken from table II of reference 12.

The first vibrational frequency is also given approximately by equation (C2) appendix C) when coupling exists between bending and torsion; it is plotted in figure 4. In order to check these curves, the exact solution was obtained (appendix D) for the ratio $(\omega_t/\omega_b)^2$ equal to 4 and was plotted on the same figure. The values given by equation (C2) are seen to be in excellent agreement with the theoretically exact values.

The effect of the coupling between bending and torsion is to reduce the first natural frequency below that which would exist if there were no coupling. This effect is shown in figure 4, wherein the value of Ω is always less than 1. This decrease in the first natural frequency due to coupling is, however, relatively unimportant in the practical range of $(\omega_t/\omega_b)^2 > 4$ and $\epsilon < 0.75$.

SUMMARY OF RESULTS

A method based on the use of Station Functions is presented for calculating uncoupled and coupled bending-torsion modes and frequencies of arbitrary continuous cantilever beams. The results of calculations made by this method indicated that by the use of Station Functions derived herein, at least $n - 1$ modes and frequencies can be obtained accurately by using just n stations

along the beam if the beam is uniform. For a tapered beam, more stations may be required, depending on the amount of taper. The amount of computational labor is markedly less than for other methods. The use of Station Numbers tabulated herein further reduces the amount of calculation necessary. It is shown that the effect of coupling between bending and torsion is to reduce the first natural frequency to a value below that which it would have if there were no coupling.

Lewis Flight Propulsion Laboratory,
National Advisory Committee for Aeronautics,
Cleveland, Ohio. October 18, 1949.

APPENDIX A

SYMBOLS

The following symbols are used in this report:

a_{ij}	coefficient in equation for Station Function in torsion
B	bending stiffness of beam, function of z
B_0	bending stiffness at root section of beam
B_k	ratio of average bending stiffness of k^{th} interval to bending stiffness of root section
b_{ij}	coefficient in equation for Station Function in bending
C	torsional stiffness of beam, function of z
C_0	torsional stiffness of root section of beam
C_k	ratio of average torsional stiffness of k^{th} interval to torsional stiffness at root section
c_1, c_2, c_3	constants defined in appendix B
$f_j(z)$	Station Function in torsion for j^{th} station (defined in text)
$g_j(z)$	Station Function in bending for j^{th} station (defined in text)
I	mass moment of inertia per unit length of beam about elastic axis, function of z, except where otherwise defined
I_0	mass moment of inertia per unit length of beam about elastic axis at root section

I_k	ratio of average mass moment of inertia per unit length of k^{th} interval to mass moment of inertia per unit length at root section
i,j,k,n	station indices
j,k,r	summation indices
l	length of beam
M_{jk}, N_{jk}, P_{jk}, Q_{jk}, M'_{jk}, N'_{jk}, P'_{jk}, Q'_{jk}	Station Numbers (defined in text); function of indices j, k, and n
m	mass per unit length of beam, function of z
m_0	mass per unit length of beam at root section
m_k	ratio of average mass per unit length of k^{th} interval to mass per unit length at root section
n	number of stations along beam
$q_b(z)$	bending loading function on beam
$q_t(z)$	torsional loading function on beam
r	absolute magnitude of projection of distance from elastic axis to center of gravity on perpendicular to bending direction
r_{g0}	radius of gyration about elastic axis at root section
r_0	absolute magnitude of projection of distance from elastic axis to center of gravity on perpendicular to bending direction for root section
S	static mass unbalance, function of z, mr
S_0	static mass unbalance at root section, m_0r_0

S_k	ratio of average static mass unbalance at k^{th} section to static mass unbalance at root section
x	distance from root of beam, except where otherwise defined
y	bending deflection, function of z
y_i	bending deflection at i^{th} station
z	dimensionless distance along beam, x/δ
α_{ij}, β_{ij}, γ_{ij}, δ_{ij}, η_{ij}	elements of dynamical matrix defined in text
Γ	$\frac{1}{\delta^2}\frac{I_0}{C_0}\frac{B_0}{m_0}$
γ	uncoupled frequency ratio $(\omega_t/\omega_b)^2$
δ	length of interval along beam between two stations
ϵ	coupling coefficient $(r_0/r_{g0})^2$
θ	torsional deflection, function of z
θ_i	torsional deflection at i^{th} station
λ	root of frequency equation or characteristic root of dynamical matrix
Ω	frequency ratio $(\omega/\omega_b)^2$
ω	frequency of vibration
ω_b	frequency of uncoupled fundamental bending mode
ω_t	frequency of uncoupled fundamental torsional mode
$\ddot{}$	second derivative of deflection with respect to time

APPENDIX B

STATION FUNCTIONS AND DETERMINANTAL EQUATIONS

Torsional Vibrations

A schematic diagram of a cantilever beam divided into n intervals of length δ is shown in figure 1. The Station Functions for the torsional vibrations of such a beam must satisfy the following conditions:

at

$$z = 0 \qquad f_i(o) = 0 \tag{B1}$$

$$z = n \qquad f'_i(n) = 0 \tag{B2}$$

$$z = i \qquad f_i(i) = 1 \tag{B3}$$

$$z = j \qquad f_i(j) = 0 \quad j \neq i \tag{B4}$$

where $f'(z)$ denotes the derivative with respect to z.

Equations (B1) and (B2) represent the boundary conditions that must be satisfied by a cantilever beam vibrating in torsion; equations (B3) and (B4) represent the further conditions imposed upon the Station Functions. These conditions will be satisfied by a function of the type

$$f_1(z) = a_{1i}z + a_{2i}z^2 + \ldots + a_{(n+1)i}z^{(n+1)} \tag{B5}$$

where the coefficients a_{ij} must satisfy the following simultaneous equations obtained from conditions (B2), (B3), and (B4):

$$0 = a_{1i} + 2na_{2i} + 3n^2a_{3i} + \ldots + (n+1)n^n a_{(n+1)i} \tag{B2a}$$

$$1 = ia_{1i} + i^2a_{2i} + i^3a_{3i} + \ldots + i^{(n+1)} a_{(n+1)i} \tag{B3a}$$

$$0 = ja_{1i} + j^2a_{2i} + j^3a_{3i} + \ldots + j^{(n+1)} a_{(n+1)i} \qquad j \neq i \tag{B4a}$$

The coefficients a_{ij} can be obtained by solving equations (B2a) to (B4a) and the functions $f_i(z)$ determined for each station. Equation (B5), however, can also be written in the following form:

$$f_i(z) = \frac{\prod_{j \neq i} (z-j)\ z(z-c_1)}{\prod_{j \neq i} (i-j)\ i(i-c_1)} \tag{B5a}$$

where $\prod_{j \neq i}$ represents the product for all values of j except $j = i$. The function in equation (B5a) obviously satisfies conditions (B1), (B3), and (B4), because it has zeros at all points specified by equation (B4), it equals 1 at the point specified by equation (B3), and it equals zero at the point specified by equation (B1). In order to satisfy condition (B2), the constant c_1 is determined by substitution of equation (B5a) into equation (B2).

$$c_1 = n \quad \text{for} \quad 1 \neq n$$

$$c_1 = n\left(1 + \frac{1}{1 + \sum_{j \neq n} \frac{n}{n-j}}\right) \text{for} \quad i = n$$

Equation (B5) can be obtained from equation (B5a) by carrying out the indicated multiplications. The complete deflection function is then given by

$$\begin{aligned} \theta(z) &= f_1(z)\theta_1 + f_2(z)\theta_2 + \ldots + f_n(z)\theta_n \\ &= \sum_{j=1}^{n} f_j(z)\theta_j \end{aligned} \tag{B6}$$

The continuous loading function $q_t(z)$ can now be written as

$$q_t(z) = I\omega^2\theta(z) = I\omega^2 \sum_{j=1}^{n} f_j(z)\theta_j \tag{B7}$$

A continuous loading function, which is a function of the deflections at the reference stations, has thus been obtained.

Bending Vibrations

The Station Functions for the bending vibrations of the beam shown in figure 1 must satisfy the following conditions:

at

$$z = 0 \qquad g_i(0) = 0 \tag{B8}$$

$$z = 0 \qquad g'_i(0) = 0 \tag{B9}$$

$$z = n \qquad g''_i(n) = 0 \tag{B10}$$

$$z = n \qquad g'''_i(n) = 0 \tag{B11}$$

$$z = i \qquad g_i(i) = 1 \tag{B12}$$

$$z = j \qquad g_i(j) = 0 \quad j \neq i \tag{B13}$$

where $g'(z)$, $g''(z)$, and $g'''(z)$ denote the first, second, and third derivative, respectively, of $g(z)$ with respect to z.

Equations (B8) to (B11) represent the boundary conditions that must be satisfied by a cantilever beam vibrating in bending and equations (B12) and (B13) represent the additional conditions imposed upon the Station Functions.

These conditions will be satisfied by functions of the type

$$g_i(z) = b_{2i}z^2 + b_{3i}z^3 + \ldots + b_{(n+3)i}z^{(n+3)} \tag{B14}$$

where the coefficients b_{ij} must satisfy the following equations obtained from conditions (B10) to (B13):

$$0 = 2b_{2i} + 6n\,b_{3i} + \ldots \quad \ldots + (n+3)(n+2)n^{(n+1)}\,b_{(n+3)i} \tag{B10a}$$

$$0 = 6b_{3i} + 24nb_{4i} + \ldots + (n+3)(n+2)(n+1)n^n b_{(n+3)i} \tag{B11a}$$

$$1 = i^2\,b_{2i} + i^3\,b_{3i} + \ldots + i^{(n+3)}\,b_{(n+3)i} \tag{B12a}$$

$$0 = j^2\,b_{2i} + j^3\,b_{3i} + \ldots + j^{(n+3)}\,b_{(n+3)i} \quad j \neq i \tag{B13a}$$

The coefficients can therefore be obtained from equations (B10a) to (B13a) and the functions $g_i(z)$ determined for each station i. Equation (B14) can, however, be written in the following form:

$$g_i(z) = \frac{\prod_{j \neq i} (z-j)\, z^2(z^2+c_2z+c_3)}{\prod_{j \neq i} (i-j)\, i^2(i^2+c_2i+c_3)} \qquad \text{(B14a)}$$

where $\prod_{j \neq i}$ represents the product for all values of j except j = i. The function in equation (B14a) obviously satisfies conditions (B8), (B9), (B12), and (B13), because it has zeros at all points specified by conditions (B8), (B9), and (B13) and equals 1 at the point specified by equation (B12). In order to satisfy conditions (B10) and (B11), the constants c_2 and c_3 are determined by substitution of equation (B14a) into equations (B10) and (B11). The general forms for c_2 and c_3 are, however, complicated and it is easier to obtain the numerical values of these constants for each specific case. Equation (B14) can then be obtained from equation (B14a) by carrying out the indicated multiplications. The complete deflection function is then given by

$$y(z) = \sum_{j=1}^{n} g_j(z)\, y_j \qquad \text{(B15)}$$

The continuous bending loading function $q_b(z)$ can now be written as

$$q_b(z) = m\omega^2 y(z) = m\omega^2 \sum_{j=1}^{n} g_j(z) y_j \qquad \text{(B16)}$$

Coupled Bending-Torsion Vibrations

The Station Functions for the coupled bending torsion vibrations are the same as previously given for the bending vibrations and the torsion vibrations. The loading functions, however, are given as follows (see reference 7):

$$q_t(z) = I\omega^2\theta(z) + S\omega^2\, y(z)$$

$$= \omega^2 \sum_{j=1}^{n} \left[I f_j(z)\theta_j + S g_j(z)\, y_j \right] \qquad \text{(B17)}$$

and

$$q_b(z) = S\omega^2\theta(z) + m\omega^2 y(z)$$

$$= \omega^2 \sum_{j=1}^{n} \left[Sf_j(z)\theta_j + mg_j(z)\, y_j \right] \qquad \text{(B18)}$$

Determinantal Equations and Dynamical Matrices

Once the Station Functions and the corresponding loading functions have been determined, the deflections at the reference stations can be obtained in terms of the loading function. A homogeneous equation in the reference-station deflections for each station is thereby obtained. The determinant of the coefficients of the resultant set of homogeneous equations can be set equal to zero; the determinantal frequency equation is thus derived. The deflections at the reference stations are obtained by the well-known equations for obtaining influence coefficients.

Torsion. - The deflection at the station i due to the continuous loading $q_t(z)$ on the beam is given by

$$\theta_i = \delta^2 \int_0^i q_t(z) \int_0^z \frac{dz_1}{C}\, dz + \delta^2 \int_i^n q_t(z) \int_0^i \frac{dz_1}{C}\, dz \qquad \text{(B19)}$$

If C is assumed to have a constant value for each interval, then these integrals may be written as the sum of integrals over each section. Equation (B19) then becomes

$$\theta_i = \frac{\delta^2}{C_0} \sum_{k=1}^{i} \frac{1}{C_k} \left[\int_{k-1}^{k} z\, q_t(z)\, dz + \int_{k-1}^{k} (1-k)\, q_t(z)\, dz + \int_k^n q_t(z)\, dz \right] \qquad \text{(B20)}$$

By substituting the relation

$$q_t(z) = \omega^2 I \sum_{j=1}^{n} f_j(z)\, \theta_j$$

and by assuming a constant value for I for each interval and changing the summation order

$$\theta_i = \omega^2\delta^2 \frac{I_0}{C_0} \sum_{j=1}^{n} \left\{ \sum_{k=1}^{i} \frac{1}{C_k} \left[I_k \int_{k-1}^{k} z f_j(z)dz - (k-1)\, I_k \int_{k-1}^{k} f_j(z)dz + \sum_{r=k+1}^{n} I_r \int_{r-1}^{r} f_j(z)dz \right] \right\} \theta_j \tag{B21}$$

Let

$$\left.\begin{aligned} \int_{k-1}^{k} z\, f_j(z)\, dz &\equiv N_{jk} \\ \int_{k-1}^{k} f_j(z)\, dz &\equiv M_{jk} \end{aligned}\right\} \tag{B22}$$

Then

$$\theta_i = \omega^2 \frac{I_0}{C_0} \delta^2 \sum_{j=1}^{n} \alpha_{ij}\, \theta_j \tag{B23}$$

where

$$\alpha_{ij} \equiv \sum_{k=1}^{i} \frac{1}{C_k} \left[I_k N_{jk} - (k-1)\, I_k M_{jk} + \sum_{r=k+1}^{n} I_r M_{jr} \right] \tag{B24}$$

If $C_k = I_k = 1$ (constant cross section), then

$$\alpha_{ij} = \sum_{k=1}^{i} \left[N_{jk} - (k-1)\, M_{jk} + \sum_{r=k+1}^{n} M_{jr} \right] \tag{B25}$$

Let

$$\lambda \equiv \frac{C_0}{I_0\omega^2\delta^2} \tag{B26}$$

Then

$$\lambda \theta_i = \sum_{j=1}^{n} \alpha_{ij} \theta_j \tag{B23a}$$

and the characteristic equation is

$$\left| \left[\alpha_{ij} \right] - \lambda I \right| = 0 \tag{B27}$$

where I is the identity matrix.

Bending. - The deflection at the station i due to the continuous loading $q_b(z)$ on the beam will be given by

$$y_i = \delta^4 \int_0^i q_b(z) \int_0^z \frac{(z-z_i)(i-z_1)}{B} dz_1 \, dz + \delta^4 \int_i^n q_b(z) \int_0^i \frac{(z-z_1)(i-z_1)}{B} dz_1 \, dz \tag{B28}$$

If B is assumed to have a constant value for each interval, these integrals may be written as the sum of integrals over each interval. Equation (B28) then becomes

$$y_i = \frac{\delta^4}{B_0} \sum_{k=1}^{i} \frac{1}{B_k} \left\{ i \int_{k-1}^{k} \left[\frac{z^2}{2} - (k-1)z + \frac{1}{2}(k-1)^2 \right] q_b(z) dz - \int_{k-1}^{k} \left[\frac{z^3}{6} - \frac{1}{2}(k-1)^2 z + \frac{1}{3}(k-1)^3 \right] q_b(z) \, dz + i \int_k^n \left[z - \frac{1}{2}(2k-1) \right] q_b(z) \, dz + \int_k^n \left[\frac{1}{2}(2k-1)z - \frac{k^3-(k-1)^3}{3} \right] q_b(z) \, dz \right\} \tag{B29}$$

By substituting the relation

$$q_b(z) = \omega^2 m \sum_{j=1}^{n} g_j(z)\, y_j \tag{B30}$$

and by assuming a constant average value for m in each interval and changing the summation order

$$y_i = \frac{\omega^2 m_0 \delta^4}{B_0} \sum_{j=1}^{n} \beta_{ij}\, y_j \tag{B31}$$

where

$$\beta_{ij} \equiv \sum_{k=1}^{i} \frac{1}{B_k} \left\{ m_k (iP'_{jk} - Q'_{jk}) + \sum_{r=k+1}^{n} m_r \left[(i-k+\tfrac{1}{2})\, N'_{jr} + \left(\frac{k^3-(k-1)^3}{3} - \frac{(2k-1)}{2}\, i \right) M'_{jr} \right] \right\} \tag{B32}$$

$$\left.\begin{aligned} P'_{jk} &\equiv \int_{k-1}^{k} \left[\frac{z^2}{2} - (k-1)\, z + \tfrac{1}{2}(k-1)^2 \right] g_j(z)\, dz \\ Q'_{jk} &\equiv \int_{k-1}^{k} \left[\frac{z^3}{6} - \tfrac{1}{2}(k-1)^2\, z + \tfrac{1}{3}(k-1)^3 \right] g_j(z)\, dz \\ N'_{jk} &\equiv \int_{k-1}^{k} z\, g_j(z)\, dz \\ M'_{jk} &\equiv \int_{k-1}^{k} g_j(z)\, dz \end{aligned}\right\} \tag{B33}$$

For a uniform beam, $m_k = B_k = 1$ and equation (B32) becomes

$$\beta_{ij} = \sum_{k=1}^{i} \left(iP'_{jk} - Q'_{jk} + \sum_{r=k+1}^{n} \left\{ \left(i-k+\frac{1}{2}\right) N'_{jr} + \left[\frac{k^3-(k-1)^3}{3} - \frac{(2k-1)}{2} i \right] M'_{jr} \right\} \right) \tag{B32a}$$

Let

$$\lambda \equiv \frac{B_0}{\omega^2 \delta^4 m_0} \tag{B34}$$

then the characteristic equation becomes

$$\left| \left[\beta_{ij}\right] - \lambda I \right| = 0 \tag{B35}$$

where I is the identity matrix and $\left[\beta_{ij}\right]$ is the dynamical matrix. In expanded form, equation (B35) becomes

$$\begin{vmatrix} \beta_{11}-\lambda & \beta_{12} & \cdots & \beta_{1n} \\ \beta_{21} & \beta_{22}-\lambda & \cdots & \beta_{2n} \\ \cdots & \cdots & \cdots & \cdots \\ \beta_{n1} & \beta_{n2} & \cdots & \beta_{nn}-\lambda \end{vmatrix} = 0 \tag{B35a}$$

where λ is a latent root of the matrix $\left[\beta_{ij}\right]$.

Coupled bending-torsion vibrations. - The deflections at the station i are given as before by equations (B19) and (B28). The loading functions q_t and q_b are changed, as follows:

$$\left.\begin{aligned} q_t(z) &= \omega^2 \left[I\,\theta(z) + S\,y(z) \right] \\ q_b(z) &= \omega^2 \left[S\,\theta(z) + m\,y(z) \right] \end{aligned}\right\} \tag{B36}$$

If these two equations are substituted into equations (B19) and (B28) and the integrations are performed as previously, the following relation is obtained:

$$\left.\begin{aligned}\theta_i &= \frac{\omega^2 m_0 \delta^4}{B_0} \sum_{j=1}^{n} \left(\Gamma \alpha_{ij}\, \theta_j + \epsilon \Gamma \gamma_{ij} \frac{y_j}{r_0} \right) \\ \frac{y_i}{r_0} &= \frac{\omega^2 m_0 \delta^4}{B_0} \sum_{j=1}^{n} \left(\delta_{ij}\, \theta_j + \beta_{ij} \frac{y_j}{r_0} \right)\end{aligned}\right\} \tag{B37}$$

where α_{ij} and β_{ij} are given in equations (B24) and (B32) and

$$\epsilon \equiv \frac{r_0^2}{r_{g_0}^2}$$

$$\Gamma \equiv \frac{1}{\delta^2} \frac{I_0 B_0}{C_0 m_0}$$

$$\gamma_{ij} \equiv \sum_{k=1}^{i} \frac{1}{C_k} \left[S_k\, N'_{jk} - (k-1) S_k\, M'_{jk} + \sum_{r=k+1}^{n} S_r\, M'_{jr} \right]$$

$$\delta_{ij} \equiv \sum_{k=1}^{i} \frac{1}{B_k} \left\{ S_k \left[i\, P_{jk} - Q_{jk} \right] + \sum_{r=k+1}^{n} S_r \left[\left(i-k+\tfrac{1}{2}\right) N_{jr} + \left(\frac{k^3-(k-1)^3}{3} - \frac{2k-1}{2}\, i \right) M_{jr} \right] \right\} \tag{B38}$$

where

$$P_{jk} \equiv \int_{k-1}^{k} \left[\frac{z^2}{2} - (k-1)z + \frac{1}{2}(k-1)^2 \right] f_j(z)\, dz$$

$$Q_{jk} \equiv \int_{k-1}^{k} \left[\frac{z^3}{6} - \frac{1}{2}(k-1)^2 z + \frac{1}{3}(k-1)^3 \right] f_j(z)\, dz$$

the determinantal equation therefore is

$$\left|\lambda I - \left[\eta_{ij}\right]\right| = 0$$

where $\left[\eta_{ij}\right]$ is the dynamical matrix, the elements of which are as indicated in equation (B37). $\left[\eta_{ij}\right]$ is seen to be a $2n \times 2n$ matrix.

APPENDIX C

QUADRATIC FORMULA FOR FIRST COUPLED MODE

If only the first vibrational mode is desired, it is possible to obtain this mode approximately by coupling together the fundamental uncoupled bending mode with the fundamental uncoupled torsional mode to obtain a simple quadratic equation for the first coupled frequency. This equation is valid when the coupling coefficient ϵ is constant along the beam. The differential equations obtained by coupling the fundamental uncoupled torsional mode with the fundamental uncoupled bending mode are:

$$\left.\begin{aligned} m\ddot{y} + S\ddot{\theta} + m\omega_b{}^2 y = 0 \\ S\ddot{y} + I\ddot{\theta} + I\omega_t{}^2\theta = 0 \end{aligned}\right\} \qquad (C1)$$

where

m mass per unit length of beam, function of z

S static mass unbalance, function of z

I mass moment of inertia about elastic axis, function of z

ω_b frequency of uncoupled fundamental bending mode

ω_t frequency of uncoupled fundamental torsional mode

$\cdot\cdot$ denotes differentiation twice with respect to time

These equations lead to a quadratic equation in the frequency ratio Ω, whose solution for the lowest frequency, provided ϵ is constant along the beam, is

$$\Omega \equiv \frac{\omega^2}{\omega_b{}^2} = \frac{1-\gamma}{2(1-\epsilon)}\left[1 - \sqrt{1 - \frac{4\gamma(1-\epsilon)}{(1-\gamma)^2}}\right] \qquad (C2)$$

where

Ω frequency ratio, $(\omega/\omega_b)^2$

γ uncoupled frequency ratio, $(\omega_t/\omega_b)^2$

ϵ coupling coefficient, $(r/r_g)^2$

This quadratic has been plotted in figure 4 for values of ϵ ranging from 0 to 1 and values of $\gamma = (\omega_t/\omega_b)^2$ from 1 to 100.

APPENDIX D

EXACT SOLUTION FOR COUPLED BENDING-TORSION VIBRATIONS OF UNIFORM CANTILEVER BEAM

The differential equations for the equilibrium of an element of a beam vibrating in coupled bending-torsion vibrations can be put in the following dimensionless form:

$$\left.\begin{aligned} \frac{d^4Y_1}{dx^4} &= \frac{ml^4}{B}\omega^2 Y_1 + \frac{ml^4}{B}\omega^2 Y_2 \\ \frac{d^2Y_2}{dx^2} &= -\epsilon \frac{Il^2}{C}\omega^2 Y_1 - \frac{Il^2}{C}\omega^2 Y_2 \end{aligned}\right\} \qquad (D1)$$

where

$$Y_1 \equiv y/r$$

$$Y_2 \equiv \theta$$

$$x \equiv \frac{\text{distance from root}}{l}$$

$$\epsilon = (r/r_g)^2$$

now

$$\omega_b^2 = \frac{c_4 B}{ml^4}$$

$$\omega_t^2 = c_5 \frac{C}{Il^2}$$

where

$$c_4 = 12.36$$

$$c_5 = 2.467$$

Equations (D1) become

$$\left.\begin{aligned} \frac{d^4Y_1}{dx^4} &= c_4\,\Omega(Y_1+Y_2) \\ \frac{d^2Y_2}{dx^2} &= -\epsilon\,\frac{c_5\Omega}{\gamma}Y_1 - \frac{c_5\Omega}{\gamma}Y_2 \end{aligned}\right\} \qquad \text{(D2)}$$

where

$$\Omega \equiv (\omega/\omega_b)^2$$

$$\gamma \equiv (\omega_t/\omega_b)^2$$

Let

$$\left.\begin{aligned} \frac{dY_1}{dx} &= Y_3 \\ \frac{dY_3}{dx} &= Y_4 \\ \frac{dY_4}{dx} &= Y_5 \\ \frac{dY_2}{dx} &= Y_6 \end{aligned}\right\} \qquad \text{(D3)}$$

Then

$$\left.\begin{aligned} \frac{dY_5}{dx} &= c_4\,\Omega(Y_1+Y_2) \\ \frac{dY_6}{dx} &= -\frac{c_5\Omega}{\gamma}(\epsilon Y_1+Y_2) \end{aligned}\right\}$$

Equations (D3) can be written as the single matrix equation

$$\frac{d}{dx}\begin{bmatrix} Y_1 \\ Y_2 \\ Y_3 \\ Y_4 \\ Y_5 \\ Y_6 \end{bmatrix} = \begin{bmatrix} 0 & 0 & 1 & 0 & 0 & 0 \\ 0 & 0 & 0 & 0 & 0 & 1 \\ 0 & 0 & 0 & 1 & 0 & 0 \\ 0 & 0 & 0 & 0 & 1 & 0 \\ c_4\Omega & c_4\Omega & 0 & 0 & 0 & 0 \\ \frac{-\epsilon c_5\Omega}{\gamma} & \frac{-c_5\Omega}{\gamma} & 0 & 0 & 0 & 0 \end{bmatrix} \begin{bmatrix} Y_1 \\ Y_2 \\ Y_3 \\ Y_4 \\ Y_5 \\ Y_6 \end{bmatrix} \tag{D4}$$

or

$$\frac{dY}{dx} = AY \tag{D4a}$$

where Y and A are the matrices indicated.

The solution to the matrix equation (D4) is given by

$$Y = e^{Ax} Y_0 \tag{D5}$$

where Y_0 is a column of arbitrary constants.

From the boundary conditions

$$\text{at } x = 0 \qquad Y_1 = Y_2 = Y_3 = 0$$

$$x = 1 \qquad Y_4 = Y_5 = Y_6 = 0$$

$$Y_0 = Y(0) = \begin{bmatrix} 0 \\ 0 \\ 0 \\ Y_4(0) \\ Y_5(0) \\ Y_6(0) \end{bmatrix}$$

If then Ω_{ij} is an element of the matrizant e^A, the boundary conditions give

$$\begin{vmatrix} \Omega_{44} & \Omega_{45} & \Omega_{46} \\ \Omega_{54} & \Omega_{55} & \Omega_{56} \\ \Omega_{64} & \Omega_{65} & \Omega_{66} \end{vmatrix} = 0 \qquad \text{(D6)}$$

Equation (D6) is the frequency equation. It has an infinite number of roots for ω.

In order to determine the elements Ω_{ij}, e^A must be evaluated. Use will be made of Sylvester's theorem (reference 13).

The λ matrix of A is

$$\begin{bmatrix} -\lambda & 0 & 1 & 0 & 0 & 0 \\ 0 & -\lambda & 0 & 0 & 0 & 1 \\ 0 & 0 & -\lambda & 1 & 0 & 0 \\ 0 & 0 & 0 & -\lambda & 1 & 0 \\ c_4\Omega & c_4\Omega & 0 & 0 & -\lambda & 0 \\ -\frac{c_5\Omega}{\gamma}\epsilon & -\frac{c_5\Omega}{\gamma} & 0 & 0 & 0 & -\lambda \end{bmatrix}$$

The characteristic equation $\Delta(\lambda) = 0$ is

$$\lambda^6 + \frac{c_5\Omega}{\gamma}\lambda^4 - c_4\Omega\lambda^2 - (1-\epsilon)\, c_4 c_5 \frac{\Omega^2}{\gamma} = 0 \qquad \text{(D7)}$$

Equation (D7) is a cubic equation in λ^2. Let the roots be

$$\lambda_1,\ -\lambda_1,\ \lambda_2,\ -\lambda_2,\ \lambda_3,\ -\lambda_3$$

Then by the confluent form of Sylvester's theorem

$$e^A = \sum_{i=1}^{r} \frac{1}{(\alpha_i - 1)!} \frac{d^{(\alpha_i - 1)}}{d\lambda^{(\alpha_i - 1)}} \left[\frac{e^{\lambda} F(\lambda)}{\prod_{k \neq i} (\lambda - \lambda_k)^{\alpha_k}} \right]_{\lambda = \lambda_i} \qquad \text{(D8)}$$

where $F(\lambda)$ is the adjoint matrix, r is the number of distinct roots, and α_i is the multiplicity of the i^{th} root.

If the roots are all distinct, this relation becomes

$$e^A = \sum_{i=1}^{3} \frac{e^{\lambda_i} F(\lambda_i) - e^{-\lambda_i} F(-\lambda_i)}{2\lambda_i \prod_{j \neq i} (\lambda_i - \lambda_j)(\lambda_i + \lambda_j)} \tag{D9}$$

where adjoint matrix $F(\lambda)$ is given by

$$F(\lambda) = -\begin{bmatrix}
\lambda^5 + \frac{c_5\Omega}{\gamma}\lambda^3 & c_4\Omega\lambda & \lambda^4 + \frac{c_5\Omega}{\gamma}\lambda^2 & \lambda^3 + \frac{c_5\Omega}{\gamma}\lambda & \lambda^2 + c_5\frac{\Omega}{\gamma} & c_4\Omega \\
-\epsilon c_5\frac{\Omega}{\gamma}\lambda^3 & \lambda^5 - c_4\Omega\lambda & -\epsilon\frac{c_5\Omega}{\gamma}\lambda^2 & -\epsilon\frac{c_5\Omega}{\gamma}\lambda & -\epsilon\frac{c_5\Omega}{\gamma} & \lambda^4 - c_4\Omega \\
c_4\Omega\lambda^2 + (1-\epsilon)c_4c_5\frac{\Omega^2}{\gamma} & c_4\Omega\lambda^2 & \lambda^5 + \frac{c_5\Omega}{\gamma}\lambda^3 & \lambda^4 + \frac{c_5\Omega}{\gamma}\lambda^2 & \lambda^3 + \frac{c_5\Omega}{\gamma}\lambda & c_4\Omega\lambda \\
c_4\Omega\lambda^3 + (1-\epsilon)c_4c_5\frac{\Omega^2}{\gamma}\lambda & c_4\Omega\lambda^3 & c_4\Omega\lambda^2 + (1-\epsilon)\frac{c_4c_5\Omega^2}{\gamma} & \lambda^5 + \frac{c_5\Omega}{\gamma}\lambda^3 & \lambda^4 + \frac{c_5\Omega}{\gamma}\lambda^2 & c_4\Omega\lambda^2 \\
c_4\Omega\lambda^4 + (1-\epsilon)c_4c_5\frac{\Omega^2}{\gamma}\lambda^2 & c_4\Omega\lambda^4 & c_4\Omega\lambda^3 + (1-\epsilon)\frac{c_4c_5\Omega^2}{\gamma}\lambda & c_4\Omega\lambda^2 + (1-\epsilon)\frac{c_4c_5}{\gamma}\Omega^2 & \lambda^5 + \frac{c_5\Omega}{\gamma}\lambda^3 & c_4\Omega\lambda^3 \\
\frac{\epsilon c_5\Omega}{\gamma}\lambda^4 & \frac{c_5\Omega}{\gamma}\lambda^4 + (1-\epsilon)\frac{c_4c_5\Omega^2}{\gamma} & -\epsilon\frac{c_5\Omega}{\gamma}\lambda^3 & -\epsilon\frac{c_5\Omega}{\gamma}\lambda^2 & -\epsilon\frac{c_5\Omega}{\gamma}\lambda & \lambda^5 - c_4\Omega\lambda
\end{bmatrix} \tag{D10}$$

From equations (D9) and (D10), the elements Ω_{ij} are seen to be given by

$$\left.\begin{aligned}
\Omega_{44} &= -\sum_{i=1}^{3} \frac{\lambda_i^4 + \frac{c_5\Omega}{\gamma}\lambda_i^2}{\prod_{j\neq i}(\lambda_i^2-\lambda_j^2)} \cosh \lambda_i \\
\Omega_{45} &= -\sum_{i=1}^{3} \frac{\lambda_i^4 + \frac{c_5\Omega}{\gamma}\lambda_i^2}{\lambda_i \prod_{j\neq i}(\lambda_i^2-\lambda_j^2)} \sinh \lambda_i \\
\Omega_{46} &= -\sum_{i=1}^{3} \frac{c_4\Omega\lambda_i^2}{\lambda_i \prod_{j\neq i}(\lambda_i^2-\lambda_j^2)} \sinh \lambda_i \\
\Omega_{54} &= -\sum_{i=1}^{3} \frac{c_4\Omega\lambda_i^2 + \frac{c_4c_5\Omega^2}{\gamma}(1-\epsilon)}{\lambda_i \prod_{j\neq i}(\lambda_i^2-\lambda_j^2)} \sinh \lambda_i \\
\Omega_{55} &= \Omega_{44} \\
\Omega_{56} &= -\sum_{i=1}^{3} \frac{c_4\Omega\lambda_i^2}{\prod_{j\neq i}(\lambda_i^2-\lambda_j^2)} \cosh \lambda_i \\
\Omega_{64} &= -\sum_{i=1}^{3} \frac{-\epsilon c_5\frac{\Omega}{\gamma}\lambda_i}{\prod_{j\neq i}(\lambda_i^2-\lambda_j^2)} \sinh \lambda_i \\
\Omega_{65} &= -\sum_{i=1}^{3} \frac{-\epsilon c_5\frac{\Omega}{\gamma}\lambda_i}{\lambda_i \prod_{j\neq i}(\lambda_i^2-\lambda_j^2)} \cosh \lambda_i \\
\Omega_{66} &= -\sum_{i=1}^{3} \frac{\lambda_i^4 - c_4\Omega}{\prod_{j\neq i}(\lambda_i^2-\lambda_j^2)} \cosh \lambda_i
\end{aligned}\right\} \quad (D11)$$

The value of the determinant in equation (D6) must be plotted against the frequency; the value of the frequency for which this determinant becomes zero is thereby obtained. This procedure involves first solving the cubic equation (D7) for each assumed value of frequency parameter and then calculating the elements of the determinant from equations (D11). The process is evidently long and laborious.

REFERENCES

1. Timoshenko, S.: Vibration Problems in Engineering. D. Van Nostrand Co., Inc., 2d ed., 1937.

2. Burgess, C. P.: The Frequencies of Cantilever Wings in Beam and Torsional Vibrations. NACA TN 746, 1940.

3. Boukidis, N. A., and Ruggiero, R. J.: An Iterative Method for Determining Dynamic Deflections and Frequencies. Jour. Aero. Sci., vol. 11, no. 4, Oct. 1944, pp. 319-328.

4. Duncan, W. J., and Collar, A. R.: A Method for the Solution of Oscillation Problems by Matrices. Phil. Mag. and Jour. Sci., ser. 7, vol. 17, no. 115, May 1934, pp. 865-909.

5. Houbolt, John C., and Anderson, Roger A.: Calculation of Uncoupled Modes and Frequencies in Bending or Torsion of Non-uniform Beams. NACA TN 1522, 1948.

6. Den Hartog, J. P.: Mechanical Vibrations. McGraw-Hill Book Co., Inc., 2d ed., 1940, p. 188.

7. Mykelstad, N. O.: Vibration Analysis. McGraw-Hill Book Co., Inc., 1944.

8. Billington, A. E.: The Vibrations of Stationary and Rotating Cantilevers with Special Reference to Turbine Blades. Reps. SM. 109 & E. 61, Div. Aero., Council Sci. Ind. Res. (Australia), Jan. 1948.

9. White, Walter T.: An Integral-Equation Approach to the Problems of Vibrating Beams. I. Jour. Franklin Inst., vol. 245, no. 1, Jan. 1948, pp. 25-36; pt. II, vol. 245, no. 2, Feb. 1948, pp. 117-133.

10. Fettis, Henry E.: The Calculation of Coupled Modes of Vibration by the Stodola Method. Jour. Aero. Sci., vol. 16, no. 5, May 1949, pp. 259-271.

11. Rauscher, Manfred: Station Functions and Air Density Variations in Flutter Analysis. Jour. Aero. Sci., vol. 16, no. 6, June 1949, pp. 345-354.

12. Benscoter, Stanley U., and Gossard, Myron L.: Matrix Methods for Calculating Cantilever-Beam Deflections. NACA TN 1827, 1949.

13. Frazer, R. A., Duncan, W. J., and Collar, A. R.: Elementary Matrices. Cambridge Univ. Press (London), 1938, pp. 78-85.

TABLE I - STATION NUMBERS

n = 1

	j \ k	1
M	1	$\frac{2}{3}$
N		$\frac{5}{12}$
P		$\frac{3}{20}$
Q		$\frac{7}{180}$
M'		$\frac{2}{5}$
N'		$\frac{13}{45}$
P'		$\frac{71}{630}$
Q'		$\frac{31}{1008}$

TABLE II - STATION NUMBERS

n = 2

	j \ k	1	2
M	1	$\frac{11}{12}$	$\frac{5}{12}$
N		$\frac{8}{15}$	$\frac{8}{15}$
P		0.183333	0.025000
Q		.046032	.029365
M'		.536364	.627273
N'		.367100	.851948
P'		.137933	.057955
Q'		.036616	.069733
M	2	$-\frac{13}{48}$	$\frac{29}{48}$
N		$-\frac{31}{240}$	$\frac{239}{240}$
P		-0.037500	0.143750
Q		-.008135	.181448
M'		-.060795	.448674
N'		-.034875	.758685
P'		-.011252	.118462
Q'		-.002614	.150415

TABLE III - STATION NUMBERS

n = 3

	j \ k	1	2	3
M	1	0.950000	0.450000	-0.050000
N		.545833	.587500	-.120833
P		.186310	.032143	-.005357
Q		.046577	.038244	-.011756
M'		.596268	.533205	-.097426
N'		.399646	.708205	-.239994
P'		.148013	.042560	-.012798
Q'		.038884	.050843	-.028318
M	2	-0.525000	0.725000	0.475000
N		-.241667	1.175000	1.091667
P		-.068452	.160714	.031548
Q		-.014583	.202083	.068750
M'		-.149356	.602896	.625418
N'		-.083406	.994860	1.475153
P'		-.026378	.143948	.057937
Q'		-.006034	.181698	.127659
M	3	0.235185	-0.153704	0.568519
N		.106019	-.231944	1.513426
P		.029563	-.023677	.139749
Q		.006222	-.028963	.316408
M'		.040630	-.072928	.445812
N'		.022325	-.111744	1.200133
P'		.006972	-.012081	.118007
Q'		.001579	-.014830	.267865

TABLE IV - STATION NUMBERS

n = 4

	j \ k	1	2	3	4
M	1	1.022222	0.429630	-0.051852	0.022222
N		.576455	.557937	-.127249	.076455
P		.194478	.029597	-.006581	.002612
Q		.048240	.035167	-.014547	.008359
M'		.623188	.511882	-.082891	.042276
N'		.413738	.676680	-.203719	.146954
P'		.152256	.039616	-.010651	.005795
Q'		.039818	.047267	-.023551	.018630
M	2	-0.647917	0.747917	0.518750	-0.085417
N		-.292857	1.207143	1.207143	-.292857
P		-.081920	.163021	.041295	-.009598
Q		-.017295	.204828	.090642	-.030688
M'		-.211987	.667412	.544025	-.112648
N'		-.116662	1.091462	1.269193	-.390585
P'		-.036502	.153469	.044508	-.015000
Q'		-.008281	.193310	.097745	-.048203
M	3	0.522222	-0.255556	0.633333	0.522222
N		.229365	-.381746	1.673810	1.729365
P		.062798	-.037401	.148512	.037202
Q		.013040	-.045624	.335791	.118397
M'		.122052	-.166738	.582158	.643846
N'		.065879	-.252823	1.545802	2.164827
P'		.020304	-.026235	.140822	.060554
Q'		.004551	-.032114	.318707	.194016
M	4	-0.221701	0.094850	-0.105961	0.543924
N		-.096544	.140724	-.267841	1.997206
P		-.026267	.013391	-.017322	.136803
Q		-.005428	.016301	-.038574	.446729
M'		-.035456	.042628	-.064723	.438962
N'		-.019023	.064205	-.164169	1.622066
P'		-.005836	.006481	-.010869	.117037
Q'		-.001303	.007917	-.024222	.382752

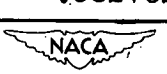

TABLE V - STATION NUMBERS

n = 5

	j \ k	1	2	3	4	5
M	1	1.097991	0.408755	-0.040898	0.019866	-0.013120
N		.608222	.527493	-.100112	.069159	-.058445
P		.202887	.026908	-.005074	.002776	-.001627
Q		.049943	.031910	-.011210	.008927	-.006836
M'		.649902	.492141	-.070298	.034939	-.024007
N'		.427616	.647530	-.172488	.121519	-.107639
P'		.156411	.036908	-.008903	.004824	-.003375
Q'		.040729	.043977	-.019678	.015509	-.014228
M	2	-0.839550	0.799339	0.493783	-0.089550	0.049339
N		-.373049	1.282044	1.145470	-.310549	.219544
P		-.103119	.169599	.037952	-.011949	.006007
Q		-.021583	.212792	.083245	-.038398	.025243
M'		-.255330	.699256	.523828	-.099723	.058134
N'		-.139170	1.138472	1.219101	-.345551	.260447
P'		-.043239	.157833	.041704	-.013166	.008078
Q'		-.009758	.198610	.091532	-.042299	.034055
M	3	0.762798	-0.313591	0.651687	0.575298	-0.126091
N		.329315	-.465823	1.718204	1.923065	-.559573
P		.089079	-.044602	.150488	.049347	-.014691
Q		.018334	-.054326	.340126	.157843	-.061693
M'		.197103	-.228783	.633812	.573549	-.137821
N'		.105126	-.344915	1.674943	1.916360	-.616234
P'		.032115	-.034985	.148520	.048803	-.018600
Q'		.007151	-.042759	.335798	.156076	-.078385
M	4	-0.548214	0.187897	-0.159325	0.576786	0.562897
N		-.233780	.276637	-.400446	2.109970	2.432887
P		-.062665	.025479	-.024868	.140460	.042295
Q		-.012809	.030950	-.055302	.458397	.177006
M'		-.117990	.117132	-.136452	.557359	.664560
N'		-.062435	.175188	-.344108	2.041363	2.901646
P'		-.018958	.017186	-.021868	.137234	.063512
Q'		-.004201	.020954	-.048664	.447980	.267043
M	5	0.214238	-0.069026	0.050904	-0.080137	0.525349
N		.090928	-.101352	.127410	-.283759	2.458336
P		.024289	-.009225	.007667	-.013645	.134478
Q		.004952	-.011196	.017031	-.044065	.573757
M'		.033722	-.031711	.032307	-.056459	.432107
N'		.017789	-.047311	.081140	-.200039	2.030260
P'		.005389	-.004593	.005002	-.009675	.116059
Q'		.001192	-.005596	.011120	-.031249	.495663

TABLE VI - STATION NUMBERS

n = 6

	j \ k	1	2	3	4	5	6
M	1	1.172073	0.391101	-0.032371	0.013323	-0.010149	0.008879
N		.638800	.501856	-.078978	.046300	-.045644	.048522
P		.210893	.024685	-.003894	.001823	-.001498	.001143
Q		.051551	.029221	-.008595	.005860	-.006322	.005949
M'		.676394	.474177	-.059129	.026582	-.018685	.015649
N'		.441269	.621067	-.144759	.092370	-.083901	.085903
P'		.160476	.034473	-.007337	.003631	-.002691	.002241
Q'		.041616	.041021	-.016206	.011674	-.011350	.011694
M	2	-1.066598	0.853106	0.468124	-0.070505	0.044513	-0.035782
N		-.466718	1.360105	1.081893	-.244062	.199948	-.195451
P		-.127634	.176358	.034411	-.009203	.006452	-.004561
Q		-.026505	.220969	.075401	-.029565	.027216	-.023740
M'		-.303948	.731991	.503742	-.085145	.049793	-.038661
N'		-.164215	1.186681	1.169252	-.294736	.223322	-.212149
P'		-.050692	.162263	.038896	-.011103	.007043	-.005503
Q'		-.011384	.203987	.085309	-.035665	.029701	-.028708
M	3	1.150584	-0.404200	0.693794	0.546418	-0.133366	0.089627
N		.489124	-.597296	1.822457	1.822457	-.597296	.489124
P		.130870	-.055956	.156259	.045293	-.018484	.011225
Q		.026719	-.068060	.352909	.144808	-.077925	.058410
M'		.267118	-.275585	.662165	.553477	-.126314	.083246
N'		.141177	-.413819	1.745286	1.846431	-.564890	.456509
P'		.042839	-.041308	.152473	.045980	-.017100	.011713
Q'		.009490	-.050434	.344556	.146998	-.072063	.061097
M	4	-0.930965	0.273028	-0.194854	0.592473	0.624591	-0.171416
N		-.390902	.399897	-.488124	2.163786	2.720209	-.933437
P		-.103635	.036020	-.029594	.142229	.056698	-.020561
Q		-.021011	.043690	-.065761	.464052	.238215	-.106938
M'		-.210538	.182630	-.180822	.598464	.604424	-.166643
N'		-.110263	.271857	-.454522	2.185427	2.628772	-.912352
P'		-.033225	.026154	-.028221	.143453	.053359	-.022768
Q'		-.007320	.031846	-.062753	.468015	.224100	-.118729
M	5	0.581796	-0.156399	0.092907	-0.111954	0.537351	0.599157
N		.242612	-.228221	.231501	-.394888	2.509279	3.194001
P		.063996	-.020218	.013474	-.018261	.134578	.046991
Q		.012925	-.024496	.029896	-.058920	.574036	.243745
M'		.120308	-.097119	.081568	-.110987	.535339	.685021
N'		.062735	-.144101	.204039	-.391731	2.499695	3.678582
P'		.018841	-.013674	.012212	-.018226	.133988	.066470
Q'		.004140	-.016634	.027119	-.058815	.571521	.345986
M	6	-0.209220	0.054246	-0.030239	0.031561	-0.064035	0.510543
N		-.086982	.079042	-.075223	.110987	-.291427	2.902746
P		-.022893	.006957	-.004323	.004969	-.011243	.132560
Q		-.004616	.008425	-.009587	.016022	-.047575	.698254
M'		-.033141	.025961	-.020586	.024431	-.049677	.425817
N'		-.017248	.038471	-.051417	.085977	-.225999	2.427820
P'		-.005173	.003631	-.003042	.003877	-.008676	.115150
Q'		-.001135	.004415	-.006753	.012502	-.036708	.606979

TABLE VII - STATION NUMBERS

n = 7

	j \ k	1	2	3	4	5	6	7
M	1	1.243487	0.376396	-0.026266	0.009112	-0.005896	0.006025	-0.006513
N		.667840	.480602	-.063889	.031590	-.026481	.033195	-.042160
P		.218415	.022882	-.003069	.001211	-.000853	.000925	-.000863
Q		.053049	.027042	-.006769	.003890	-.003599	.004829	-.005357
M'		.702228	.458303	-.050122	.019989	-.012820	.011370	-.011099
N'		.454474	.597757	-.122429	.069352	-.057533	.062529	-.072080
P'		.164382	.032358	-.006088	.002679	-.001831	.001689	-.001614
Q'		.042465	.038456	-.013441	.008611	-.007724	.008815	-.010037
M	2	-1.321299	0.905437	0.446479	-0.055674	0.029812	-0.027896	0.028701
N		-.570270	1.435730	1.028397	-.192270	.133730	-.153603	.185730
P		-.154452	.182773	.031489	-.007052	.004233	-.004239	.003780
Q		-.031847	.228718	.068932	-.022639	.017853	-.022136	.023463
M'		-.357636	.764868	.485193	-.071706	.038132	-.031029	.028988
N'		-.191650	1.234950	1.123273	-.247832	.170920	-.170555	.188216
P'		-.058807	.166641	.036328	-.009168	.005346	-.004565	.004199
Q'		-.013146	.209297	.079621	-.029438	.022542	-.023823	.026110
M	3	1.672922	-0.511106	0.737737	0.516672	-0.104856	0.081487	-0.077078
N		.701415	-.751768	1.931045	1.718603	-.468955	.448232	-.498585
P		.185835	-.069049	.162183	.040990	-.014225	.012162	-.010056
Q		.037666	-.083877	.366024	.130958	-.059956	.063490	-.062408
M'		.355047	-.329159	.692136	.532099	-.108454	.073511	-.063669
N'		.186093	-.492459	1.819566	1.771836	-.484684	.403671	-.413268
P'		.056122	-.048434	.156613	.042913	-.014528	.010624	-.009166
Q'		.012374	-.059075	.353730	.137128	-.061218	.055439	-.056987
M	4	-1.605312	0.409927	-0.250374	0.629063	0.592219	-0.182666	0.144688
N		-.664780	.597643	-.625274	2.291470	2.574726	-1.002357	.935220
P		-.174510	.052757	-.037056	.147488	.051989	-.026098	.018551
Q		-.035122	.063907	-.082279	.480975	.218352	-.136173	.115110
M'		-.317567	.247432	-.216700	.623577	.584350	-.157315	.115706
N'		-.164912	.366953	-.543417	2.273022	2.538692	-.861833	.750618
P'		-.049381	.034761	-.033166	.147041	.050504	-.021773	.016464
Q'		-.010826	.042284	-.073708	.479557	.212061	-.113560	.102355
M	5	1.129029	-0.264373	0.134585	-0.136596	0.551252	0.668960	-0.220971
N		.464325	-.384008	.334325	-.480675	2.570992	3.589325	-1.425675
P		.121269	-.033334	.019010	-.021700	.136202	.063551	-.027154
Q		.024312	-.040333	.042147	-.069981	.580855	.330701	-.168426
M'		.234133	-.168109	.122950	-.143020	.568583	.634247	-.197770
N'		.120971	-.248408	.306705	-.503685	2.649577	3.397336	-1.281188
P'		.036084	-.023166	.017983	-.022914	.139081	.057851	-.027322
Q'		.007887	-.028149	.039907	-.073907	.593022	.300912	-.169818
M	6	-0.617807	0.137401	-0.064103	0.054068	-0.084474	0.507772	0.632193
N		-.252961	.199169	-.158887	.189539	-.383331	2.883613	4.007039
P		-.065852	.017129	-.008878	.008211	-.014243	.130010	.051386
Q		-.013170	.020712	-.019672	.026453	-.060230	.684756	.318021
M'		-.125078	.086131	-.058376	.057414	-.092005	.516450	.704705
N'		-.064447	.127049	-.145336	.201491	-.417397	2.931074	4.491463
P'		-.019183	.011759	-.008393	.008826	-.015450	.131144	.069349
Q'		-.004186	.014281	-.018616	.028441	-.065330	.690659	.430362
M	7	0.205449	-0.044613	0.020059	-0.010652	0.021382	-0.053078	0.498306
N		.083943	-.064008	.049675	-.055505	.096798	-.295079	3.334065
P		.021819	-.005533	.002756	-.002373	.003481	-.009551	.130932
Q		.004358	-.006689	.006106	-.007644	.014713	-.049981	.820708
M'		.033023	-.022307	.014642	-.013579	.018939	-.044219	.420133
N'		.016993	-.032878	.036425	-.047602	.085721	-.245636	2.816717
P'		.005053	-.003033	.002091	-.002060	.003074	-.007854	.114318
Q'		.001102	-.003682	.004637	-.006638	.012992	-.041094	.716958

TABLE VIII - STATION NUMBERS

n = 8

	j \ k	1	2	3	4	5	6	7	8
M	1	1.312192	0.364019	-0.021829	0.006490	-0.003545	0.003081	-0.003931	0.005039
N		.695399	.462793	-.052953	.022453	-.015893	.016958	-.025621	.037691
P		.225483	.021401	-.002485	.000839	-.000499	.000484	-.000622	.000684
Q		.054447	.025255	-.005476	.002694	-.002103	.002422	-.003869	.004929
M'		.727233	.444367	-.043004	.015242	-.008698	.007082	-.007522	.008334
N'		.467152	.577362	-.104816	.052799	-.038988	.038933	-.048943	.062492
P'		.168111	.030533	-.005119	.002003	-.001220	.001045	-.001145	.001228
Q'		.043271	.036245	-.011294	.006433	-.005146	.005456	-.007123	.008863
M	2	-1.600390	0.955663	0.428499	-0.045077	0.020351	-0.016189	0.019610	-0.024337
N		-.682210	1.507998	.984086	-.155335	.091123	-.089039	.127790	-.182002
P		-.183160	.188781	.029123	-.005550	.002808	-.002412	.003082	-.003289
Q		-.037524	.235968	.063696	-.017807	.011838	-.012593	.019183	-.023705
M'		-.415706	.797175	.468735	-.060778	.028715	-.021414	.021627	-.023284
N'		-.221089	1.282229	1.082551	-.209723	.128559	-.117660	.140686	-.174560
P'		-.067464	.170868	.034087	-.007611	.003953	-.003129	.003272	-.003421
Q'		-.015018	.214419	.074659	-.024428	.016664	-.016330	.020358	-.024694
M	3	2.337500	-0.630523	0.780389	0.491625	-0.082648	0.054514	-0.060500	0.071477
N		.967933	-.923581	2.036155	1.631308	-.368956	.299530	-.394067	.534419
P		.254178	-.083331	.167794	.037442	-.010886	.007975	-.009418	.009602
Q		.051181	-.101109	.378439	.119546	-.045861	.041626	-.058605	.069206
M'		.462586	-.388839	.722423	.512112	-.091426	.056607	-.052469	.054058
N'		.240602	-.579786	1.894495	1.702145	-.408100	.310711	-.341167	.405216
P'		.072148	-.056240	.160734	.040069	-.012016	.008120	-.007864	.007911
Q'		.015838	-.068533	.362854	.127977	-.050617	.042369	-.048918	.057107
M	4	-2.630070	0.593584	-0.315718	0.667195	0.558819	-0.143453	0.132430	-0.143916
N		-1.075644	.861856	-.786292	2.424356	2.424356	-.786292	.861856	-1.075644
P		-.279850	.074709	-.045646	.152881	.046981	-.020073	.020253	-.019152
Q		-.055949	.090392	-.101283	.498324	.197214	-.104712	.126011	-.138032
M'		-.466670	.329868	-.258293	.650770	.561588	-.135711	.104892	-.100193
N'		-.240468	.487559	-.646305	2.367821	2.436346	-.743106	.681473	-.750848
P'		-.071591	.045534	-.038818	.150902	.047150	-.018614	.015449	-.014572
Q'		-.015627	.055337	-.086223	.491981	.197950	-.097075	.096084	-.105178
M	5	2.192995	-0.454018	0.201514	-0.175130	0.584107	0.633389	-0.237005	0.215982
N		.890699	-.656778	.499217	-.614926	2.718847	3.393592	-1.539301	1.613222
P		.230544	-.055975	.027793	-.027134	.141097	.058226	-.034728	.028253
Q		.045912	-.067648	.061577	-.087460	.601511	.302906	-.215987	.203600
M'		.389428	-.253524	.165704	-.170613	.591124	.614158	-.191506	.155413
N'		.199636	-.373346	.412443	-.599857	2.750891	3.287044	-1.241724	1.164103
P'		.059201	-.034316	.023783	-.026822	.142374	.054969	-.027027	.022340
Q'		.012882	-.041657	.052749	-.086477	.606915	.285874	-.168026	.161236
M	6	-1.350286	0.265559	-0.108064	0.078152	-0.102878	0.520374	0.709714	-0.274441
N		-.546005	.383370	-.267117	.273370	-.466005	2.952258	4.523995	-2.046630
P		-.140865	.032367	-.014611	.011568	-.016907	.131525	.070024	-.034431
Q		-.027983	.039093	-.032351	.037251	-.071468	.692634	.434540	-.248035
M'		-.263362	.163432	-.098083	.084195	-.115917	.543778	.662638	-.230699
N'		-.134575	.240192	-.243600	.294907	-.525024	3.081687	4.216400	-1.725908
P'		-.039810	.021885	-.013810	.012656	-.019020	.135367	.062213	-.032195
Q'		-.008646	.026552	-.030611	.040765	-.080395	.712714	.385904	-.232314
M	7	0.654484	-0.124395	0.048081	-0.031856	0.034801	-0.066829	0.484484	0.662747
N		.263837	-.179348	.118705	-.111252	.157170	-.370670	3.239551	4.867795
P		.067914	-.015052	.006430	-.004626	.005472	-.011570	.126311	.055545
Q		.013468	-.018172	.014232	-.014889	.023114	-.060517	.791745	.399381
M'		.130945	-.079057	.045388	-.036054	.041862	-.077799	.500211	.723527
N'		.066783	-.116059	.112606	-.126105	.189085	-.431248	3.341811	5.337321
P'		.019727	-.010524	.006331	-.005328	.006593	-.013324	.128649	.072134
Q'		.004280	-.012763	.014029	-.017155	.027846	-.069680	.806281	.519815
M	8	-0.202414	0.037821	-0.014268	0.009104	-0.009307	0.015388	-0.045167	0.487926
N		-.081470	.054494	-.035205	.031774	-.041992	.085181	-.296574	3.754721
P		-.020947	.004560	-.001898	.001312	-.001443	.002573	-.008294	.129520
Q		-.004150	.005504	-.004201	.004221	-.006093	.013452	-.051711	.941457
M'		-.033107	.019722	-.011093	.008527	-.009326	.015058	-.039785	.414996
N'		-.016869	.028937	-.027507	.029809	-.042089	.083310	-.260993	3.198326
P'		-.004979	.002618	-.001541	.001252	-.001450	.002493	-.007173	.113558
Q'		-.001080	.003174	-.003414	.004029	-.006122	.013034	-.044710	.825790

TABLE IX - COMPARISON OF RESULTS

Number of Stations	Torsion			Bending			Coupled		
	$\omega_1\sqrt{\frac{I_0 l^2}{C_0}}$	$\omega_2\sqrt{\frac{I_0 l^2}{C_0}}$	$\omega_3\sqrt{\frac{I_0 l^2}{C_0}}$	$\omega_1\sqrt{\frac{m_0 l^4}{B_0}}$	$\omega_2\sqrt{\frac{m_0 l^4}{B_0}}$	$\omega_3\sqrt{\frac{m_0 l^4}{B_0}}$	$\omega_1\sqrt{\frac{m_0 l^4}{B_0}}$	$\omega_2\sqrt{\frac{m_0 l^4}{B_0}}$	$\omega_3\sqrt{\frac{m_0 l^4}{B_0}}$
Station-Function Method									
1	1.549			3.493			3.46		
2	1.571	4.526		3.516	21.71		3.48	19.7	
3	1.571	4.689	7.502	3.516	22.04	60.20	3.48	20.6	48.2
Weighted influence coefficients									
2	1.575	5.39		3.56	15.63				
4	1.571	4.73		3.52	22.80				
Exact theoretical value									
	1.571	4.712	7.854	3.516	22.04	61.70	3.49	20.6	49.1

TABLE X - STATIONS REQUIRED FOR SATISFACTORY ACCURACY

Method	Torsion			Bending		
	$\omega_1\sqrt{\frac{I_0 l^2}{C_0}}$	$\omega_2\sqrt{\frac{I_0 l^2}{C_0}}$	$\omega_3\sqrt{\frac{I_0 l^2}{C_0}}$	$\omega_1\sqrt{\frac{m_0 l^4}{B_0}}$	$\omega_2\sqrt{\frac{m_0 l^4}{B_0}}$	$\omega_3\sqrt{\frac{m_0 l^4}{B_0}}$
Station functions	1	3	4	1	2	3
Weighted influence coefficients	2	4		3	6	

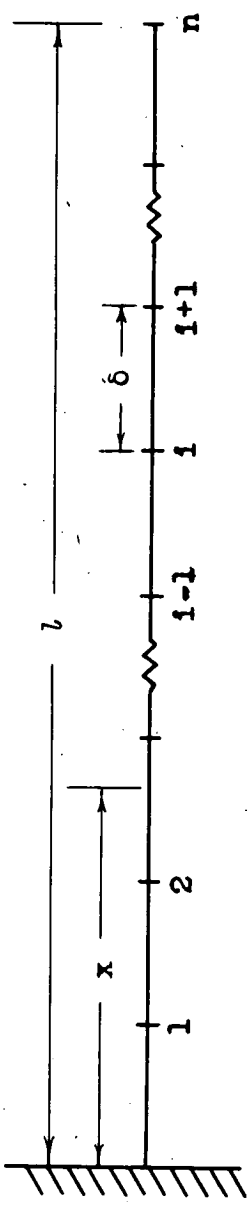

Figure 1. - Cantilever beam with n stations.

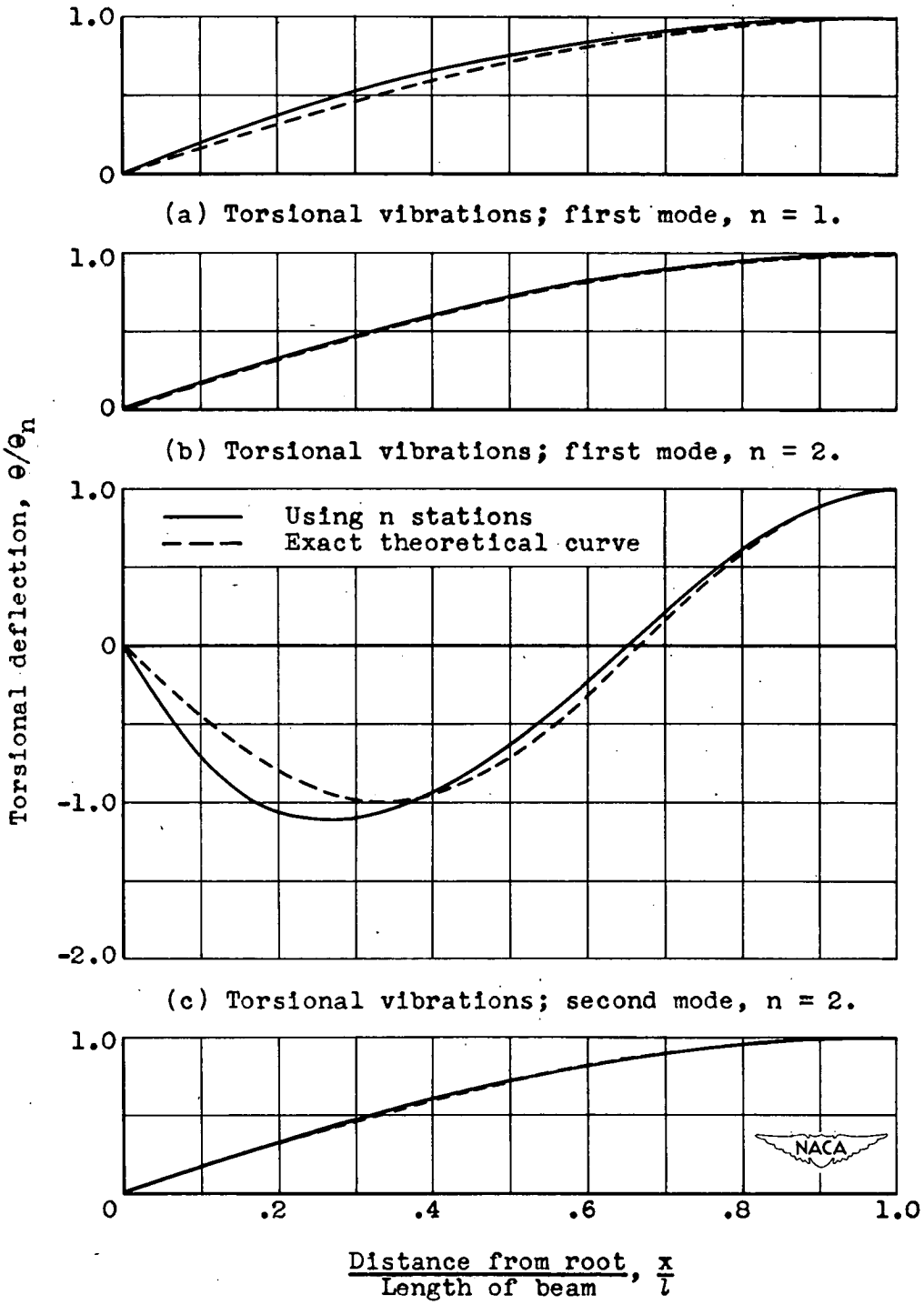

Figure 2. - Comparison of theoretical mode shapes with mode shapes obtained by taking n stations along the beam for torsional vibrations.

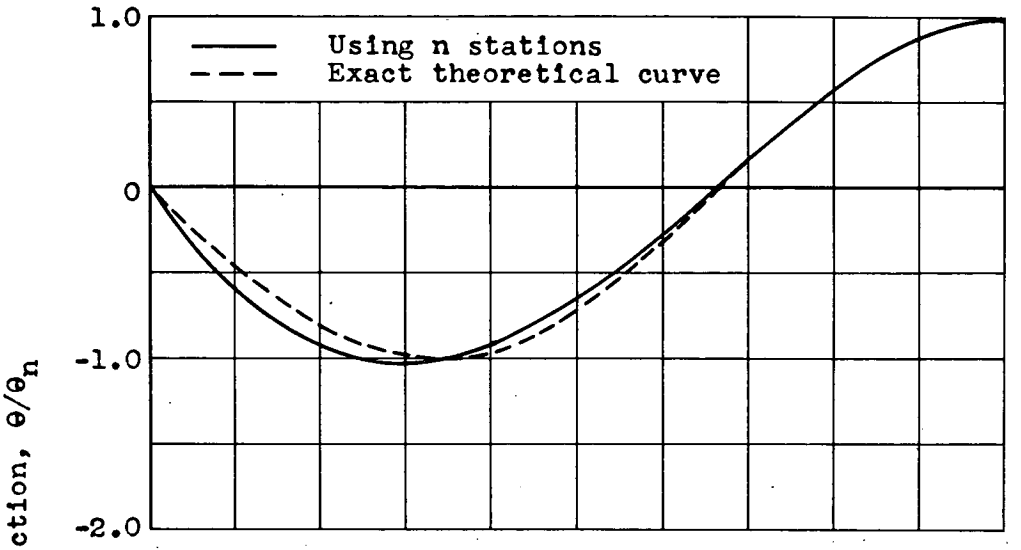

(e) Torsional vibrations; second mode, n = 3.

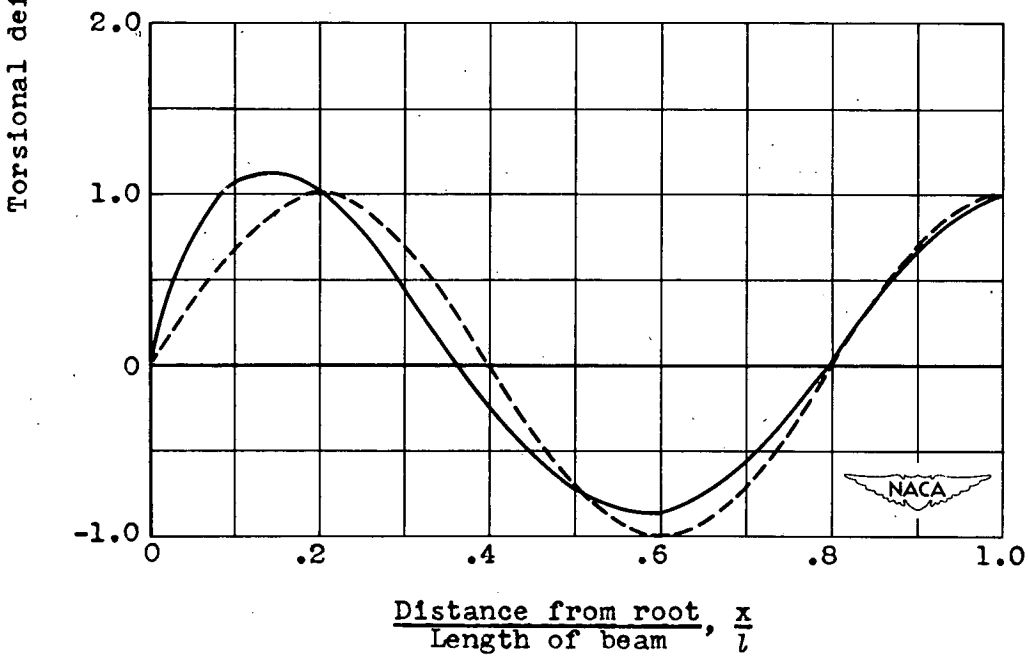

(f) Torsional vibrations; third mode, n = 3.

Figure 2. - Concluded. Comparison of theoretical mode shapes with mode shapes obtained by taking n stations along the beam for torsional vibrations.

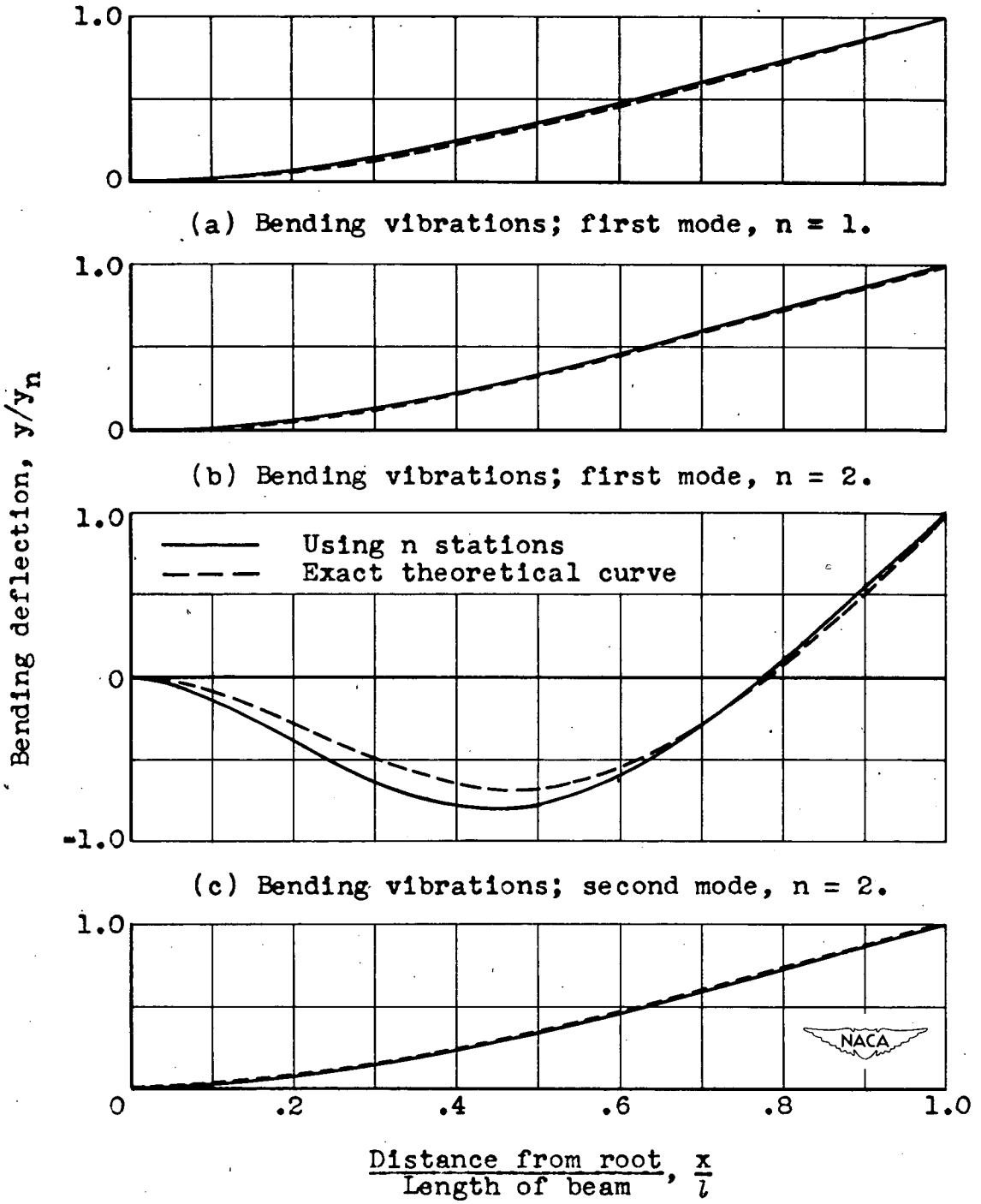

Figure 3. - Comparison of theoretical mode shapes with mode shapes obtained by taking n stations along the beam for bending vibrations.

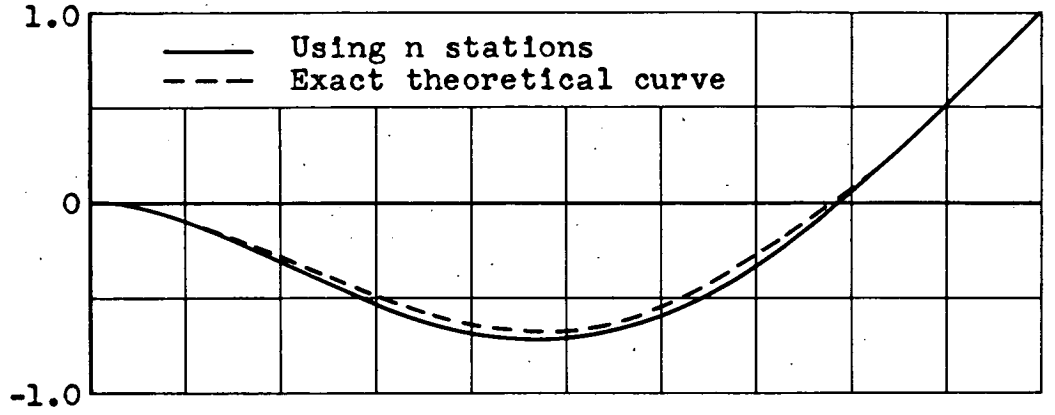

(e) Bending vibrations; second mode, n = 3.

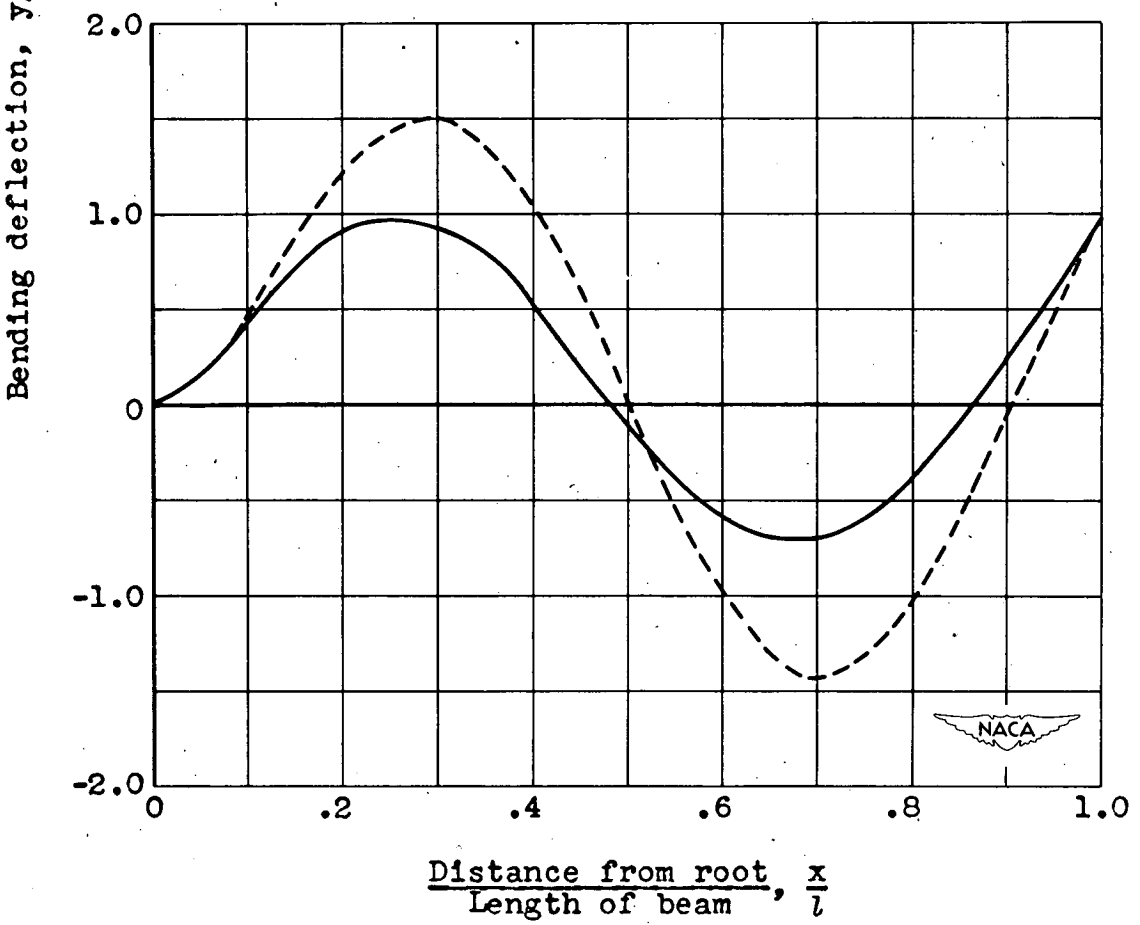

(f) Bending vibrations; third mode, n = 3.

Figure 3. - Concluded. Comparison of theoretical mode shapes with mode shapes obtained by taking n stations along the beam for bending vibrations.

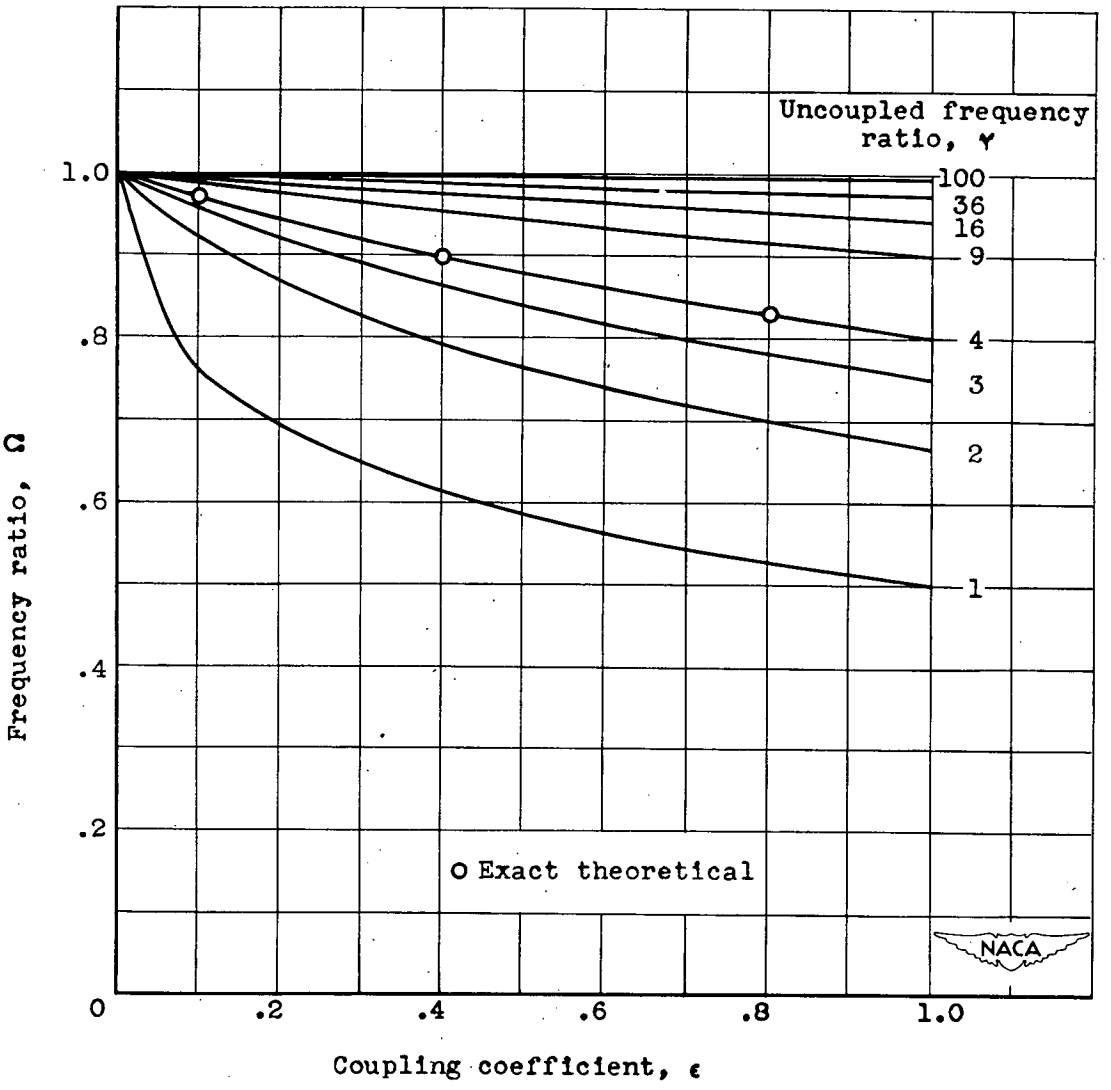

Figure 4. - Variation of frequency ratio Ω with coupling coefficient ϵ for several values of uncoupled frequency ratio γ.